Hungarian Academy of Sciences
Research Centre for Natural Sciences

Yearbook

2012

Institute of Technical Physics and Materials Science

http://www.ttk.mta.hu/
http://www.mfa.kfki.hu/

Hungarian Academy of Sciences

Research Centre for Natural Sciences

Institute of Technical Physics and Materials Science

Director: Prof. István Bársony, corr. member of HAS

Address: Konkoly-Thege Miklós út 29-33,
H-1121 Budapest, Hungary
Postal: P.O.Box 49, H-1525 Budapest, Hungary
Phone: +36-1-392 2225
Fax: +36-1-392 2226
E-mail: info@ttk.mta.hu, info@mfa.kfki.hu
URL: http://www.ttk.mta.hu/
http://www.mfa.kfki.hu/

MTA TTK MFA Yearbook 2012

Editors: Miklós Menyhárd and Csaba S. Daróczi
Published by: MTA TTK MFA, Budapest, Hungary, 2013

CONTENT

DIRECTOR'S FOREWORD

Enforced reshuffling… this is the most adequate expression for the activities of the year.

2012 was a year of accommodation in the 650-strong organisation of the Research Centre for Natural Sciences (RCNS) of the HAS. Since both the director general and the director of administration of HAS RCNS were appointed from the former Chemical Research Centre of HAS, obviously, their customs and administrative rules were imposed upon the three formerly independent member institutes at their respective sites. Besides the operation at four separate locations in Budapest, major difficulties manifested themselves as *large divergences in research culture, management habits, level of organisation, discipline and the service for researchers* in these formerly independent institutions. In case of MFA, regarding automation and efficiency of organisation of the administration in service of the researchers it meant, unfortunately, several big steps backward, compared to the formerly autonomous arrangements of accounting, bookkeeping, contracting and ordering, etc.

Following a decision of the HAS management MFA had to start 2012 with a reduced upper limit of staff of 122 employees, relying on the centralised administration within the Research Centre. The subsidy cuts, the reorganisation, and the financing of the central administration led to a critical situation; the amount for operational support dropped from *522 MFt (ca. 1.9 M€) in the previous year to a mere 377 MFt (ca. 1.4 M€)*, which did not even cover the loan-expenditures at MFA. Nevertheless, thanks to the revenues from research projects not yet settled and closed in 2012, the Institute registered a total turnover of 1200 MFt (ca. 4.3 M€), roughly the same amount as the year before.

MFA is not among the five member institutes of TTK scheduled to move into the new research facility, called MTA Q2, at the joint campus of the Budapest University of Technology and Economics and the Roland Eötvös Science University. Under the newly appointed young and energetic TTK leadership from the beginning of 2013, this means a prevailing administrative remote control for MFA, since the facilities at the Csillebérc KFKI Campus will continue to be used even in the long term.

As a **multidisciplinary system-integrator** MFA follows its proven research strategy, and conducts both *exploratory research* on the properties *of nanoscale structures and architectures of functional materials* as well as the *creative exploitation* of the obtained results *in integrated micro- and nanosystems*. The achievements of MFA can thus be measured beyond scientometric parameters on the submitted patent applications, the support for higher education provided through M.Sc. and Ph.D. training, by the industrial utilisation of scientific results, and by advisory activities.

The highest financial burden for the 5000m^2 institute - operating under the quality assurance system ISO 9001:2008 at the KFKI Campus in Csillebérc - is the *running,*

maintenance and continuous development of its large infrastructure for experimental materials research. This comprises everything from clean laboratories to large analytical facilities laboratories, of which *four are dedicated national scale Strategic Research Infrastructures*. One of them, for spectroscopic ellipsometry, is an Accredited Analytic Laboratory.

The severe financial conditions were further aggravated by the *CERN@Wigner investment*, affecting the electron microscopy lab's operation. This was effectively the last straw, forcing the institute to reconsider and reshuffle its research themes and relocate a number of its laboratories. Following the decision *to stop the process development activities for thin film solar cells*, the vacated laboratory-space became free for other research purposes. The *completion of thermal isolation and renovation of our main building* in 2012 made the relocation of the electron microscopy laboratories and the whole Thin Film Physics Department feasible and desirable. The respective costs were and will be covered by the Wigner compensation (50 MFt) as well as a renovation subsidy (34 MFt) and a dedicated support (30 MFt) granted by HAS for this structural reshuffling.

Accompanied by an extraordinary scrapping of unusable equipment and furniture, eight large preparative and analytical laboratories were relocated, including some of the clean-room and measurement facilities of the Microtechnology Department and moving the complete Thin Film Department. As a result, *the occupied floor space was reduced by 20%*, while the standard of the renovated laboratories and 11 working cabinets was raised considerably. The electrical wiring, air conditioning utilities, and closed-loop cooling were completely renovated, which will lead to further lowering of running costs. *This was particularly important since even after the commissioning of the new Q2 facility MFA will operate separately with reduced costs at the present location.* Although the finalisation of work will still require a few more months in 2013, the improvement of working conditions is already felt by now.

The internal organisation of MFA remained unchanged in 2012, albeit some of the administrative and technical responsibilities had to be transferred due to retirement of some colleagues. The scientific program was carried out in six research departments led by the same key persons as in the previous year.

In 2012 *five EU FP7 projects, and an ENIAC2 project* were conducted at MFA, one new Ph.D. degree was obtained, and **33 Ph.D. research projects were supervised**. Seven MFA postdocs were on leave in leading foreign research institutions worldwide. *The high number of* ***student projects*** *at the institute:* ***TDK (14), B.Sc. (30), and M.Sc. (27)*** *is a proof of the growing attractivity of MFA*, despite the long geographic distances from the universities.

The very successful initiative of the Institute, the summer camp for college students was again organised with 24 youngsters aged 17, coming from the whole Carpathian Basin. Also the Open Day of the institute was a well-visited event drawing over 140 members of the public.

Again we had reason to be proud of some excellent achievements and distinctions of our colleagues.

Zoltán Juhász obtained the Hungarian Gold Cross of Merit; *József Gyulai* became Doctor h. c. of the University of Miskolc; *László Péter Biró* was nominated for

corresponding membership of HAS, *György Radnóczi* received the Grand Prize of the Scientific Department of Physics of HAS, *Géza Ódor* was named Outstanding Reviewer of APS, *György Kádár, Péter Arató* and *György Kozmann* became professors emeritus, *Levente Tapasztó, András Deák* and *Anita Pongrácz* obtained the „Young Researcher Award of TTK".

The 2012 recipients of the MFA prize for young researcher were *Róbert Erdélyi* and *Péter Vancsó*, in the researcher category the MFA Prize went to *Levente Tapasztó* and *András Deák*. Three of our retiring colleagues were awarded the MFA Prize for Excellent Research Support, *Ira Ferenczy*, *Vera Somogyi* and *László Honty* for their decade long service. One Ph.D. degree was granted to *Orsolya Tapasztó* and several more are in the pipeline. Also two further Bolyai Grants were given to MFA researchers.

A big recognition of the scientific-excellence and also financial success of the institute is the first „Lendület Grant of HAS" won by *Róbert Horváth* to establish his own research group at MFA!

In summary, the director, starting his third term as head of the Institute, can report that MFA is prepared to adjust to the quickly changing research environment and hopes to receive the required organisatorial freedom for the realisation of its plans in the interests of materials science and R&D in Hungary.

Budapest, February 2013

István Bársony
director, corr. member of HAS

GENERAL INFORMATION

Organization of RCNS (TTK)

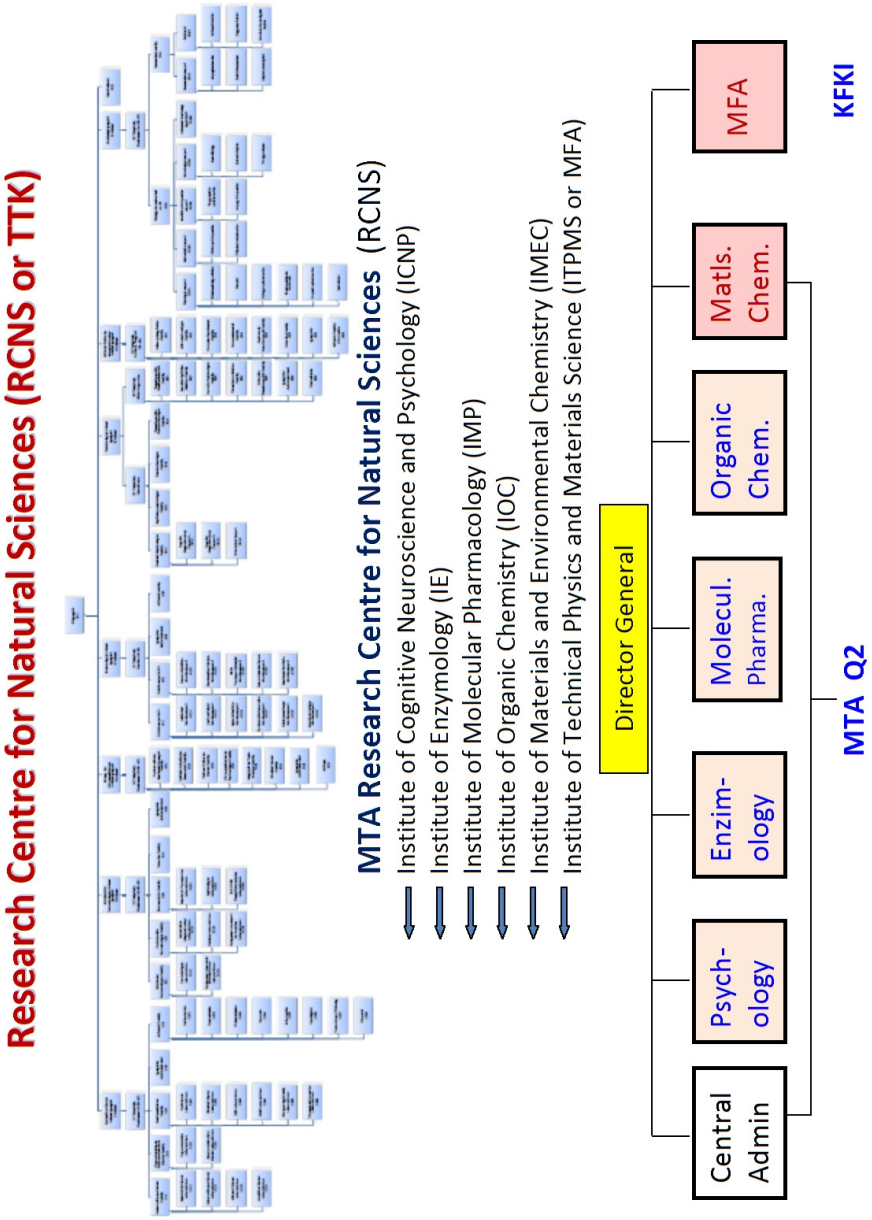

Organization of MFA

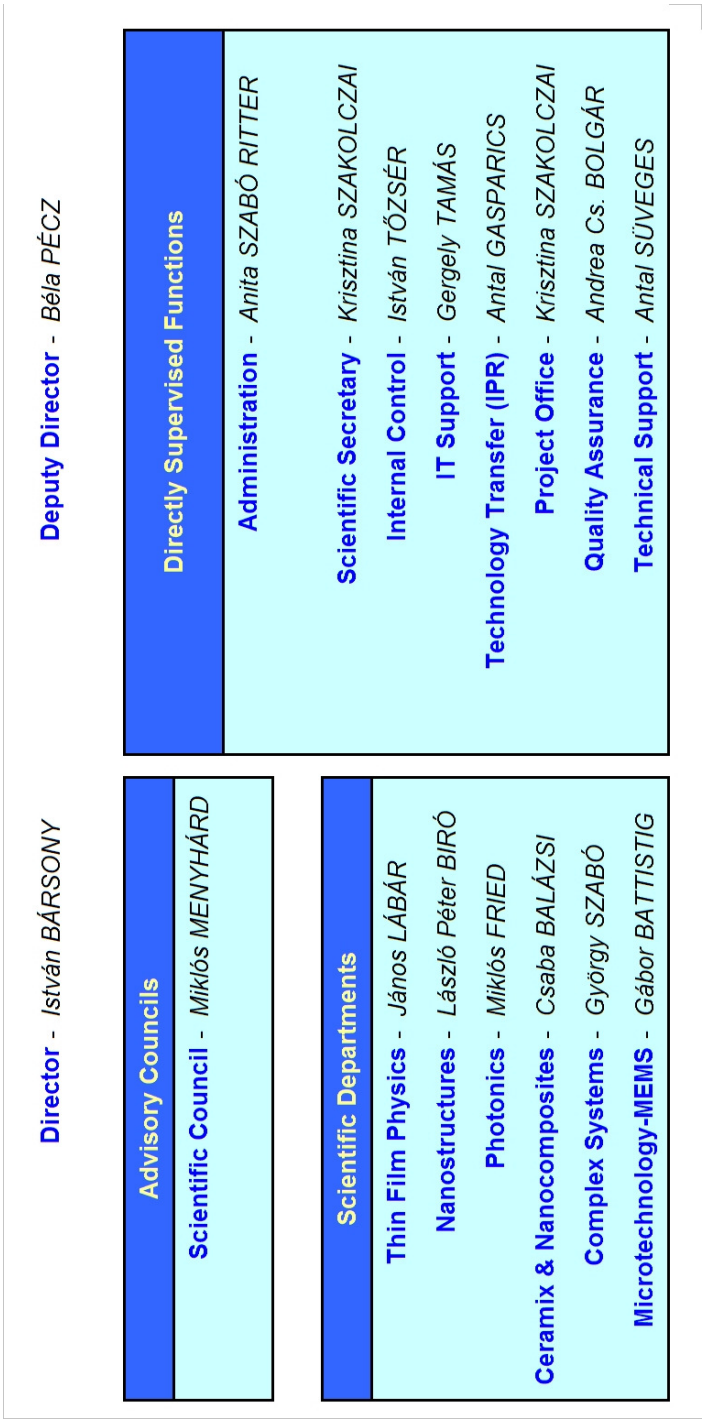

Key Financial Figures of MFA

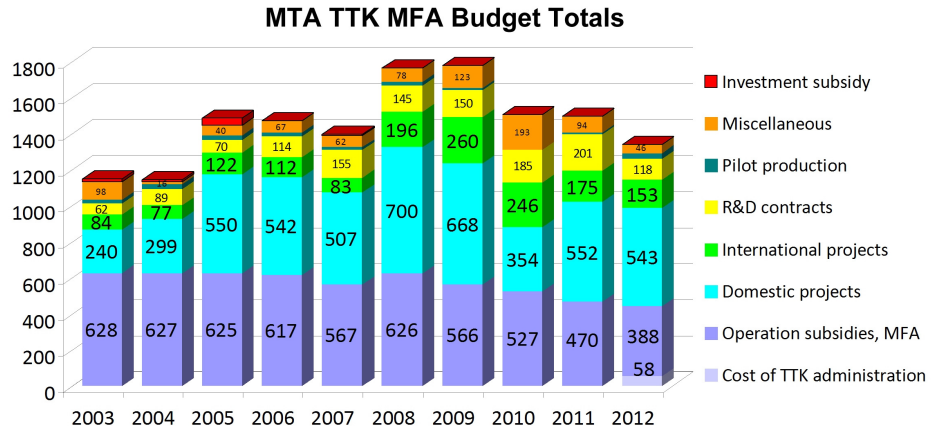

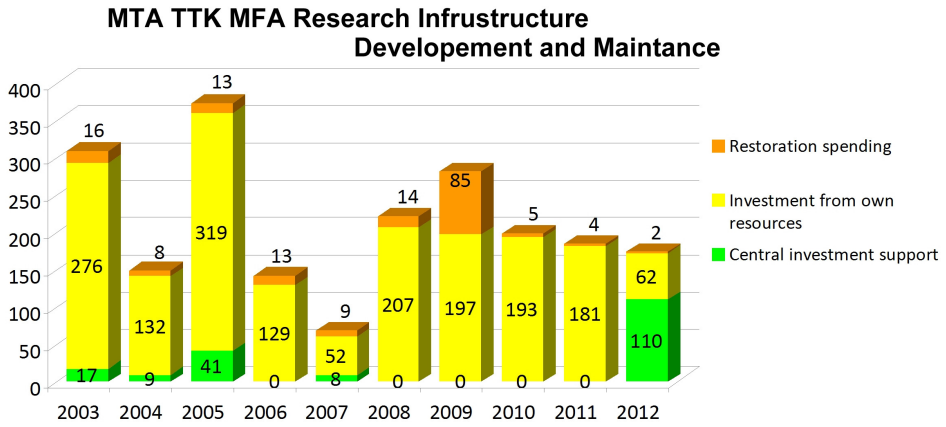

Publications & Citations of MFA

According to the Thomson-Reuters ISI "Web of Knowledge" database, the institute has maintained the average publication activity of around 100 peer reviewed scientific journal papers per year.

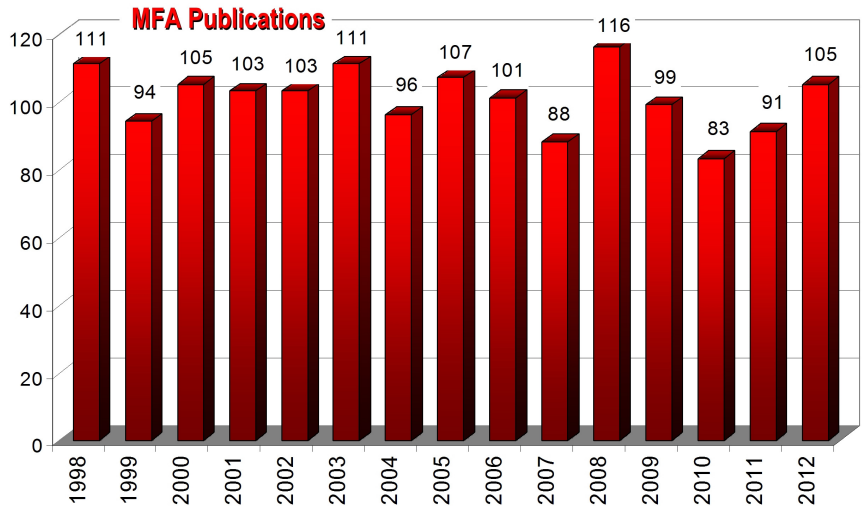

The complete publication list of MFA in 2012 – with considerably more titles than listed by the ISI Web of Science –is included at the end of this yearbook.
A good measure of the recognition of MFA's scientific activity is the **h-index value of 62**, and the steady growth of the number of independent citations over the years.

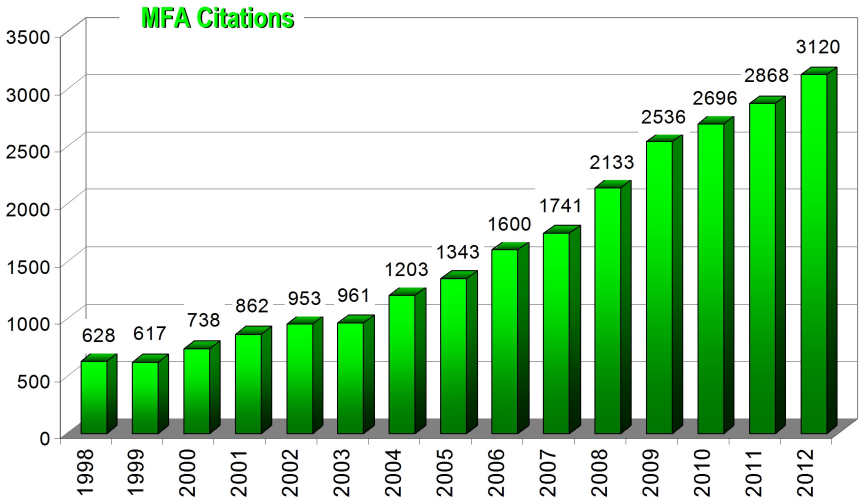

Prizes, distinctions, degrees

	**JUHÁSZ, Zoltán**	Gold Cross of the Merit of the Hungary
	**GYULAI, József**	Doctor Honoris Causa (University of Miskolc)
	**BIRÓ, László Péter**	nominated for corresponding membership of HAS
	**RADNÓCZI, György**	Grand Prize of Physics by the Department of Physical Sciences of HAS
	**LÁBÁR, János**	Schmid Rezső Prize of The Roland Eötvös Physical Society -ELFT
	**KÁDÁR, György**	Professor Emeritus of the Hungarian Academy of Sciences
	**ARATÓ, Péter**	Professor Emeritus Instituti
	**KOZMANN, György**	Professor Emeritus Instituti
	**ÓDOR, Géza**	APS outstanding reviewer

	**TAPASZTÓ, Levente**	MFA Prize (Researcher); TTK Young Researcher Prize
	**DEÁK, András**	MFA Prize (Researcher); TTK Young Researcher Prize, shared
	**PONGRÁCZ, Anita**	TTK Young Researcher Prize, shared
	**ERDÉLYI, Róbert**	MFA Prize (Ph.D. student)
	**VANCSÓ, Péter**	MFA Prize (Ph.D. student)
	**FERENCZY, Ferencné**	MFA Prize for Excellent Research Support
	**HONTY, László**	MFA Prize for Excellent Research Support
	**SOMOGYI, Istvánné**	MFA Prize for Excellent Research Support

HIGHLIGHTS

Integrated Solid State Nanopores for Biochemical Sensing

P. Fürjes, Z. Fekete, A. L. Tóth, L. Illés, R. E. Gyurcsányi (BME), and I. Bársony

Complex micro- and nanodevices become increasingly relevant for mechanical, chemical and biochemical sensing and control applications. Innovative biosensing principles proposed open up new prospects in medical applications by the development of robust, user-friendly and cost-effective in-vitro diagnostic platforms. Novel bioanalytical systems, however, are expected to integrate the nanoscale transducers with interface chemistry, and bio-receptors as well as the sample preparation microfluidics, read-out electrodes in complex Lab-on-a-Chip devices.
Chemically modified, nanonopore based sensors can be used for the detection of specific biomolecules by transport modulation, determined by molecule binding in the pores [R. E. Gyurcsányi: Trac-Trends In Analytical Chemistry 27 (7), 2008, 627-639]. In spite of the principally extreme sensitivity of the method, reliability and reproducibility of nanoscale fabrication processes are not proven so far. The final goal is to develop a nanopore based multi-parametric biosensing platform for label-free detection of blood marker proteins of cardiovascular symptoms.
The characterized test structures were fabricated by the combination of silicon micromachining and nanofabrication processes. The supporting membrane materials allowed the fabrication of low-stress mechanical structures. Functional layer surfaces in the nanopores were altered in order to provide proper conditions for the application of receptor immobilization techniques, i.e. nanopores were “drilled” in both bare Silicon-Nitride and Gold coated Silicon-Nitride layers, respectively.

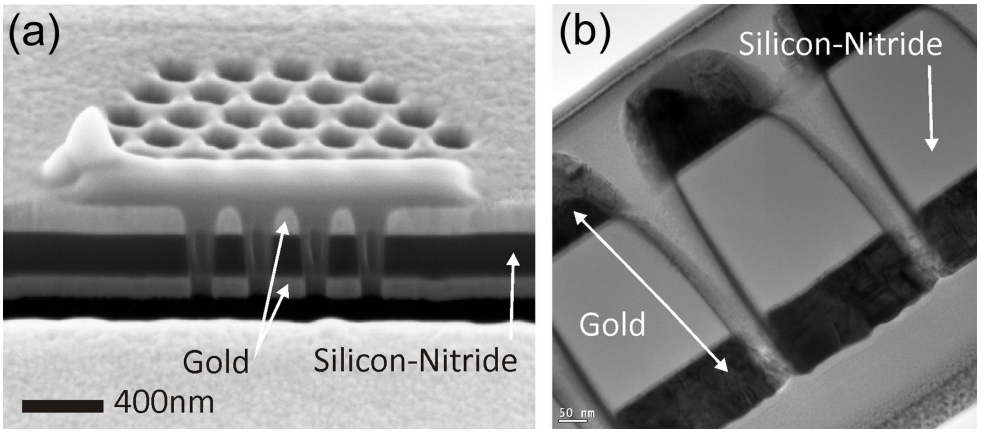

Figure 1. *(a, left): Nanopore array in a Gold / Silicon-Nitride / Gold multilayer structure drilled by Focussed Ion Beam Milling (SEM image),and (b, right): a typical pore cross section (TEM image).*

The solid state nanopores were formed by focused accelerated Ga^+ ions by applying different milling currents. The resulting nanopore membrane and geometry is shown in the SEM micrograph of Fig. 1. In order to establish a reliable fabrication process the FIB drilling was characterized regarding the accuracy of the pore geometry engineering, particularly the uniformity of pore diameter to be tuned by using appropriate fabrication parameters (milling time and ion-current) for the different material combinations.

The nanopore membranes were integrated into an electrochemically addressable fluidic system, consisting of both, sample channels and electrodes. The fluidic vias, the channel system and the multilayer membrane structure were machined in Si by 3D MEMS processes including multistep Deep Reactive Ion Etching (DRIE), and wafer level anodic bonding to the glass microfluidics. The final fluidic chips (Fig. 2(a)) consisting nanopore membranes and vertical vias (Fig. 2(b)) were mounted onto a fluidic connection platform (Fig. 2(c)), designed and realized by Micronit Microfluidics. The integrated microfluidics for nanopore sensing was characterized in terms of contingent shunting and proper sealing using impedance spectroscopy, supporting the necessity of 3D passivation of the microchip for improved sensitivity. Deposited aluminum-oxide and titanium-oxide passivation layers significantly improved the impedance stability of the integrated electrochemical cell.

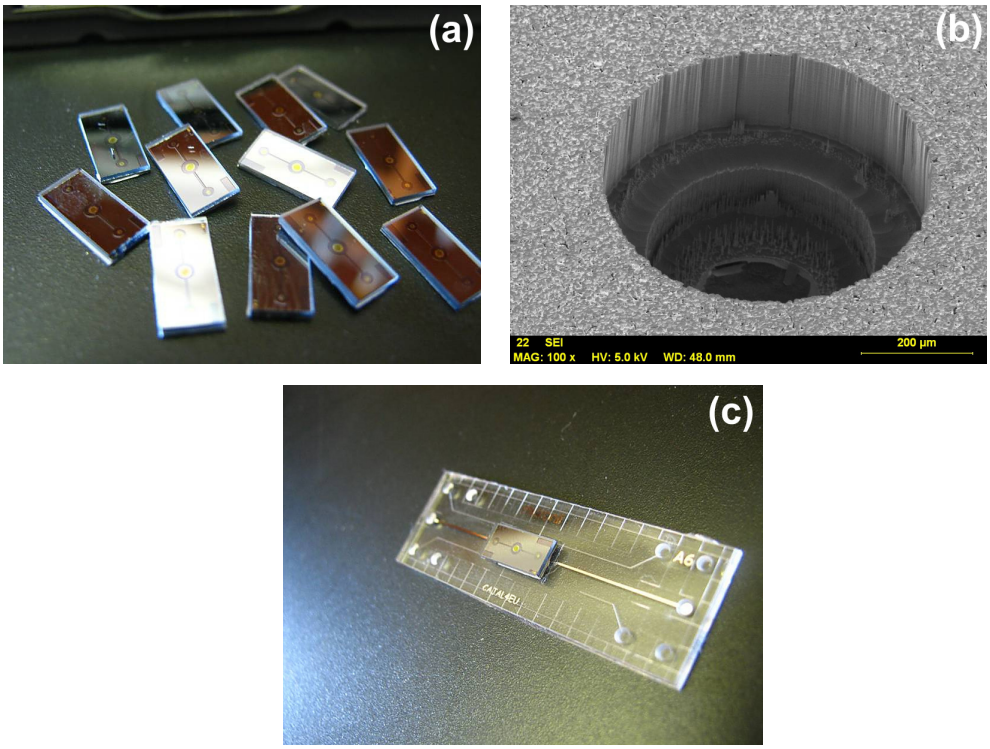

Figure 2. *The assembled microfluidic nanopore chips (a), with vertical fluidic vias (b), and the mounting onto the flow cell for addressing the nanopores (c).*

Deposition of aluminum-oxide, and titanium-oxide thin films considerably improved the impedance stability of the electrochemical cell, which allowed the exact tracking of the membrane impedance vs. pore diameter, according to Fig. 3.

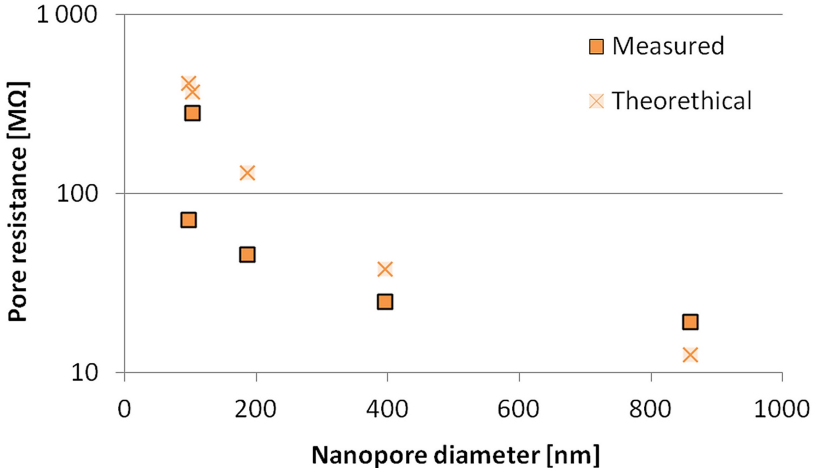

Figure 3. *The ohmic membrane impedance vs. nanopore diameter measured in KCl elektrolyte of 0.02M concentration. The theoretical values were obtained from the Hall-model.*

Conclusions

FIB milling of micromachined membranes was characterized to establish a reliable nanopore fabrication technology for nanoscale bio-transducers. The obtained pore geometries were analyzed to define optimal milling parameters, and statistical limitations for pore diameter accuracy, caused by uncertainties e.g. in beam convergence in nanoscale processes. The integrability of the nanoscale sensor process was proven by the development of a silicon-based microsystem consisting of fluidic and electronic interface, microfluidic components. According to preliminary measurements, the microsystem is a good candidate for the detection of low concentration proteins in blood samples.

Acknowledgements

The partial support of the ENIAC JTI and the National Innovation Office (NIH) via CAJAL4EU project, the Hungarian National Research Fund (OTKA) via NF69262 and the János Bolyai fellowship of the Hungarian Academy of Sciences are gratefully acknowledged. The support of Magda Erős in MEMS fabrication and of György Sáfrán in TEM imaging is appreciated.

Strain-engineering the electronic structure of graphene through sub-nanometer-wavelength structural ripples

(Korea-Hungary Joint Laboratory for Nanosciences, OTKA PD 8442)

L. Tapasztó, T. Dumitrica (Univ. Minnesota), S. J. Kim (KRISS, Korea),
P. Nemes-Incze, C. Hwang (KRISS, Korea), and L. P. Biró

Understanding how the mechanical behavior of materials deviates at the nanoscale from the macroscopically established concepts is a key challenge of particular importance for graphene, given the complex interplay between its nanoscale morphology and electronic properties. When the local curvature of the graphene sheet is of the nanometer scale the electronic structure is substantially modified. To implement the nanoscale periodic rippling of graphene, one can employ the strain engineering of nanometer scale suspended graphene membranes. Such suspended graphene nanomembranes naturally form during the chemical vapor deposition (CVD) growth of graphene on Cu (111) single crystals. At the growth temperature of graphene (1000°C) trench-like vacancy islands with well-defined widths of about 5nm appear in the Cu substrate (Fig. 1(a)). Upon cooling down the sample to room temperature the Cu substrate contracts, while the overgrown graphene layer tries to expand according to its negative thermal expansion coefficient. Consequently, where graphene is in direct contact, i.e. pinned to the Cu substrate it is subjected to a strong compressive strain. However, in those areas where the graphene is suspended above the nanotrenches it is allowed to relax some amount of the compressive strain through out-of-plane deformation (rippling).

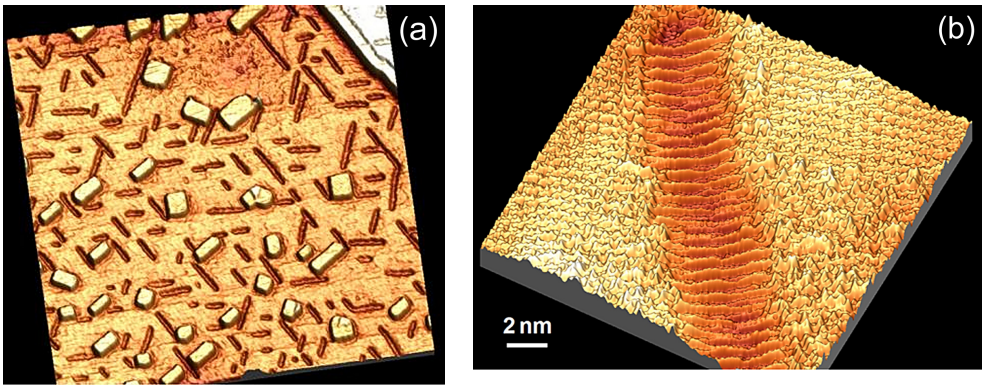

Figure 1. *(a): STM image (300x300 nm) of a reconstructed Cu(111) surface continuously covered with graphene. (b): High resolution STM image of a nanotrench revealing nanoscale periodic rippling of the graphene membrane suspended over the trench.*

The atomic resolution topographic STM images reveal the honeycomb lattice of graphene all over the sample surface. High-resolution STM measurements, of the graphene membrane over the trenches reveal a highly regular periodic oscillation, with a wavelength of ~0.7 nm and modulation of ~0.1 nm superposed on the honeycomb atomic lattice of graphene (Fig. 1(b)).

Using the continuum mechanical formulas a rippling wavelength of λ_{theor} = 4.2 nm and an amplitude of A_{theor} = 2.6 Å has been obtained, which is in striking discrepancy with our measurements (λ_{exp} = 0.7 nm, A_{exp} = 0.5 Å). The inability of the phenomenological continuum model to describe the peculiar sub-nanometer rippling observed in our experiments, prompted us to perform accurate microscopic-level simulations. We studied the rippling of freestanding graphene nanoribbons with fixed armchair edges by means of conjugate gradient relaxation simulations and a density functional-based tight binding interatomic potential, which describes explicitly the σ and π C-C bonding of graphene.

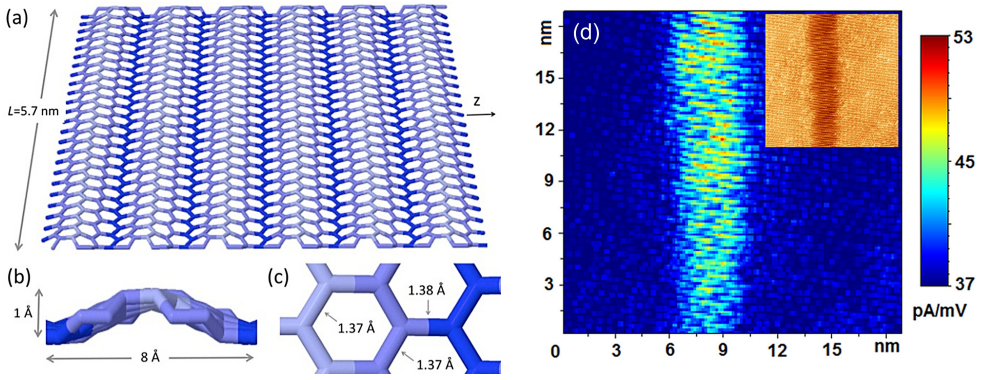

Figure 2. *(a): Simulation of a 5.7 nm wide graphene nanoribbon subjected to 5% in-plane compression, revealing a periodic rippling morphology of 0.8 nm wavelength and (b): 1 Å modulation; (c): Details of the C-C bond lengths; (d): Local electronic density of states map on graphene nanoripples.*

In contrast to the continuum model, we found that the microscopic approach can regain sub-nanometer rippling (Fig. 2(a)) and thus confirms our interpretation of the STM observations. The striking discrepancy with the continuum mechanical model predictions is a manifestation of the breakdown of the continuum mechanics for the nanoscale rippling of graphene. We found that in the monolayer, the resistance to bending involves the π-orbital misalignment between adjacent pairs of C atoms, and can be completely decoupled from its in-plane σ bond deformations [153].

We have also performed spatially resolved tunneling spectroscopy measurements to verify how the nanoscale structural ripples affect the local electronic properties of graphene. The spectroscopy map reveals the periodic modulation of the local density of electronic states (LDOS) on the nanorippled region (Fig. 2(d)). This evidences that nanoscale structural ripples substantially affect the local electronic structure of graphene giving rise to one-dimensional electronic superlattices.

The ability of graphene to ripple down to sub-nanometer wavelengths can be exploited in strain-engineering graphene based nanoelectronic and NEMS devices beyond the boundaries set by continuum mechanics.

PUBLIC OUTREACH

Nanobus

The MFA-built Nanobus co-sponsored by General Electrics Hungary continued the roadshows in 2012, a.o. in the XIIth district of the capital. Director Iván Hütter of GE and the Mayor of the Hegyvidék district, Zoltán Pokorni opened the interactive demonstrations, revealing the interesting properties and features of nanoobjects to children of different age-groups. (MTI photos).

MFA Summer School

Our traditional **MFA Summer School** was organized already the 5th time for the selected 24 high school students (in the 15-17 age group) coming from all over the Carpathian Basin. The school provides exceptional one week long working opportunity in scientific environment on different subjects, under enthusiastic tutorial guidance throughout the week, involving from young Ph.D. students to emeritus professors of the institute! It is hard to select the best applicants, this year's "student researchers". On the first day they got a complete overview of the laboratories involved in the project, then everybody started to work on his/her subject. At the end of the week everyone delivered a short summary presentation about the work done and the results obtained in front of MFA's scientific community.

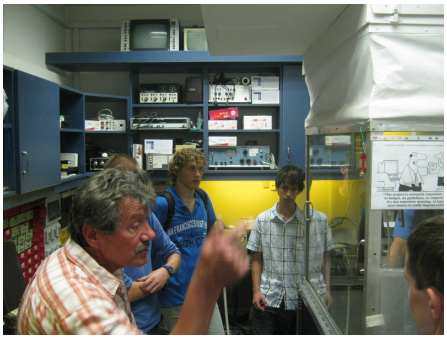

But our summer school is not just about the work ☺! We have many kinds of sports, music and social programs, including countless number of excursions (day and night) to the beautiful town (Budapest), and the surrounding forests and hills. (We could even identify some spots of the Sun using one of the smaller telescopes at the Research Institute for Astronomy.)
The program of the working week is very packed, we know, but everybody can sleep up on the next week, can't he ☺? We find the summer school not just exciting but effective as well - at least we are regularly contacted with our former students, when they are studying at the university, to latch on to the science at higher level.

MFA Open Day

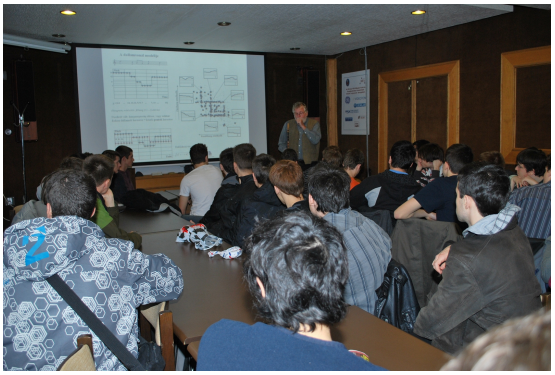

Our regular **Open Day** in November offered again 150-200 visitors, a.o. interested tax payers the chance for getting acquainted with the research at MFA. For this occasion we offered guided laboratory tours and popular scientific presentations on quantum physics, game theory computer simulations, and on evolutionary music analysis.

Industrial collaboration

Industrial associations, from the Far-East, like the Korean Trade Association represented in Hungary by Mr. Young-Suk Kim are increasingly interested in collaboration and technology-licencing from our institute.

The information day organised at the Central Building of the HAS was opened by his excellency the Ambassador of the Republic of Korea in Budapest, Mr. Kwan-Pyo Nam and the President of the HAS, Prof. József Pálinkás.

CERN@Wigner data-center at the KFKI Campus

The construction of the CERN@Wigner data-center at the KFKI Campus forced us to vacant 450m^2 technology-space by scrapping some outdated facilities, and decommission the over pressure-vessel with the evaporator for liquid nitrogen, having served the semiconductor processing line for over 40 years.

Life and achievements

As an important event of the year an interview-book about the life and achievements of our former director, *Prof. József Gyulai* was published.

From 2012 he serves as Chairman of the Curatorial Gremium (sitting second from right) awarding the *Dénes Gábor Prize* at an annual ceremony hosted by the President of the Hungarian Parliament, *László Kövér* (MTI photo).

SOCIAL EVENTS

Farewell party

After having sucessfully directed the financial administration of the Research Institute for Technical Physics and Matarials Science (MFA) of the Hungarian Academy of Sciences for over 14 years, following the reorganisation of MFA as a member institute of MTA TTK, **Ms. Vera Somogyi** left the institute, just like a number of other colleagues on the picture. This was the occasion, where the former colleagues of the administration under her direction came together to thank and wishing their director good health and happy retirement.

MFA Sports Day

Well, this is really about sporting - at least in the case of the youngest ones…

While the adults are looking forward some more serious things ☺…

Regardless the rather poor treat corresponding to the critical finances in 2012, the MFA-Sports Day remained the main team-building event of the year! Very well visited by active and retired co-workers as well as their families, we enjoyed in good weather cooking, sport contests, children programs and all kind of activities, but mostly the opportunity of being together in an informal company.

Christmas Celebration

The other popular event is the Christmas Celebration, an occasion to summarise the year's events, achievements and disclose the next year's plans. This is the time of handing over the MFA Prize to the colleagues having excelled in the previous year, like *Levente Tapasztó* (down, left) and *András Deák* (down, right) in 2012.

SCIENTIFIC REPORTS

Nanostructures Department

Head: Prof. László Péter BIRÓ, D.Sc.

Research Staff

- Zsolt Endre HORVÁTH, Ph.D., Deputy Head of Department
- Prof. József GYULAI, Member of the HAS (Professor Emeritus)
- Antal Adolf KOÓS, Ph.D. (on leave)
- Géza István MÁRK, Ph.D.
- Zoltán OSVÁTH, Ph.D. (on leave till September 2012)
- Levente TAPASZTÓ, Ph.D.
- Krisztián KERTÉSZ, Ph.D.
- Enikő HORVÁTH, Ph.D. (maternity/on leave)
- Zofia VÉRTESY, Ph.D.

Ph.D. students / Diploma workers

- Gergely DOBRIK, Ph.D. student
- Gábor MAGDA, Ph.D. student
- Péter NEMES-INCZE, Ph.D. student
- Péter Lajos NEUMANN, Ph.D. student (on leave)
- Bernadeth PATAKI, Ph.D. student
- István TAMÁSKA, Ph.D. student
- Péter VANCSÓ, Ph.D. student
- Vince OBRECZÁN, diploma worker
- Gábor PISZTER, diploma worker

Technical Staff

- Zoltánné SÁRKÁNY, technician

The Nanostructures Department has an almost two decades expertise in the production and characterization of various nanostructures. In recent years in the focus of work were various carbon nanostructures (CNTs, graphene and few-layer graphite) their nanoarchitectures, bioinspired photonic nanoarchitectures and applications of these nano-objects in various fields in nanotechnology, nanoelectronics, sensorics and environmental protection. The most relevant results in 2012 are detailed below:

We observed or the first time the breakdown of continuum mechanic for graphene, and the evidence of nanoripples with a periodicity of 0.7 nm. The rippling affects the electronic structure too.

We revealed for the first time several important characteristics of grain boundaries (GBs) in CVD graphene: opposite to HOPG, or graphite generated by other high temperature procedures, CVD graphene exhibits a significant degree of structural disorder which strongly affects the electronic properties of the GBs. In particular, the double-coordinated C atoms, occurring in the GBs have the most marked effect by inducing localized states in the vicinity of the Fermi energy.

We showed for the first time that both, the coloration and the nanoarchitecture are responsible for the color of blue Lycaenid butterflies are species specific and allow the automated species discrimination.

For more details, please feel free to visit the web page of the Nanostructures Department (link: http://www.nanotechnology.hu/)

Disordered grain boundaries of graphene grown by chemical vapour deposition

(KHJLN 2010K000980, OTKA PD 84244 and K 101599. TÉT_10-1-2011-0752 and ANR-BLAN-SIMI10-LS-100617-12-01 grants)

P. Nemes–Incze, P. Vancsó, Z. Osváth, G. I. Márk, X. Jin (KRISS, Korea), Y.S. Kim (KRISS, Korea), C. Hwang (KRISS, Korea), Ph. Lambin (FUNDP, Belgium), C. Chapelier (SPSMS), L. P. Biró

Graphene prepared by chemical vapor deposition (CVD) on metal surfaces, especially copper [C. Hwang et al., J. Phys. Chem. C 115, 22369–22374, 2011] is becoming a material with significance in applications [S. Bae et al., Nat. Nanotechnol. 5, 574–578, 2010]. Perturbations of the two dimensional carbon lattice of graphene such as grain boundaries (GB) [154] have significant influence on the properties of CVD graphene, from charge transport to mechanical compliance. Revealing the structure of GBs can go a long way to better understand the properties and behavior of CVD graphene and through this, enable the tailoring of GB properties. The physical properties of graphene GBs are usually computed by modeling them as periodic dislocation cores composed of non-hexagonal units, mostly pentagons and heptagons [O. V. Yazyev, S. G. Louie, Phys. Rev. B 81, 195420, 2010]. We have studied the atomic and electronic structure of GBs in graphene prepared by chemical vapor deposition (CVD), comparing STM topography and spectroscopy data with ab-initio density functional (VASP) calculations. Our STM measurements show that localized states near the Dirac point, so called “midgap states”, dominate the local density of states (LDOS) of GBs.

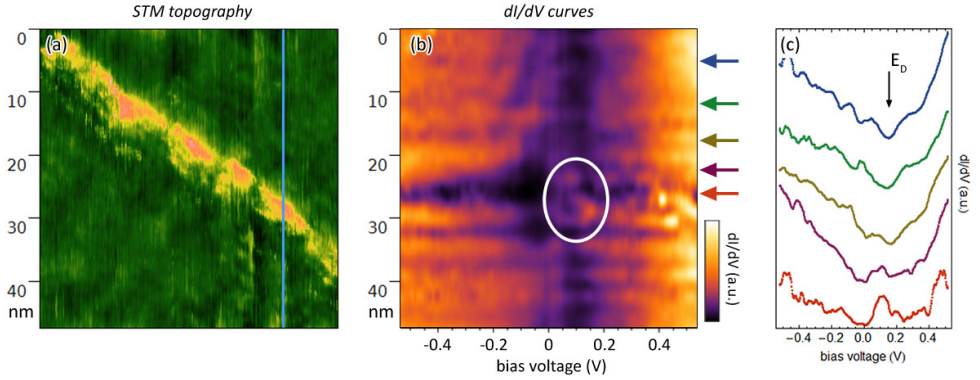

Figure 1. (a) STM topography image of a GB. A line of dI/dV spectra was measured across the GB in the position shown by the blue line. (b) Color plot of the line of dI/dV spectra across the GB. White ellipse shows the localized states close to the Dirac point. (c) Selected dI/dV spectra from positions shown by appropriately colored arrows in (b).

Fig. 1. shows an STM topography image of a GB in graphene grown on a copper surface. By measuring successive dI/dV curves along the blue line shown in Fig. 1(a) we can trace the evolution of the sample LDOS as the STM tip approaches the GB.

Far away from the GB we can observe the typical "V" shaped dI/dV characteristic of graphene. The minimum of the dI/dV corresponds to the Dirac point of graphene where the DOS vanishes. At the GB we can observe the appearance of an LDOS peak close to 0 bias voltage, near the LDOS minimum (red curve in Fig. 1(c)).
In graphene a strong localized state appears close to the Dirac point if the lattice has defects with more atoms on one sublattice than the other, for example a zigzag edge [Y. Kobayashi, K. Fukui, T. Enoki, K. Kusakabe, Y. Kaburagi, Phys. Rev. B 71, 193406, 2005] or edges and cracks with zigzag edged components [M. A. H. Vozmediano, M. P. López-Sancho, T. Stauber, F. Guinea, Phys. Rev. B 72, 155121, 2005]. Furthermore, vacancies and di-vacancies have a very similar signature. Since in the pentagon-heptagon dislocation core model of GBs we can not account for the ubiquitous presence of such "midgap states", observed in our measurements, we have extended this model to include disorder in the form of two-coordinated carbon atoms.

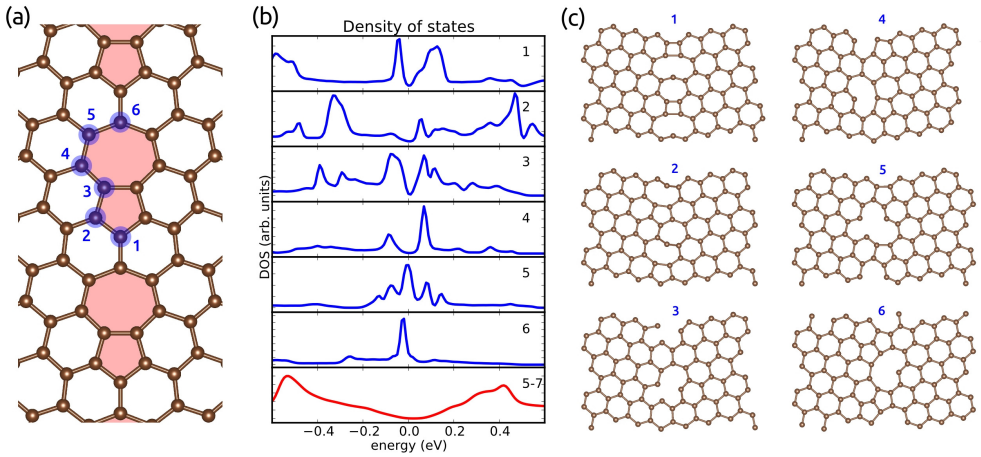

Figure 2. *(a) GB constructed from 5-7 membered carbon rings, with a mismatch angle of 21.8°. (The removed carbon atoms are numbered.) (b) DOS of the unperturbed 5-7 boundary (red) and of the 6 disordered structures produced by inducing vacancies in the 5-7 GB (blue). (The Fermi level is at 0 eV.) (c) Atomic positions of the 6 disordered GBs.*

Fig. 2(a) shows a graphene GB with a similar mismatch angle as the one presented in Fig. 1. This GB is made up of pairs of 5-7 membered carbon rings. The calculated DOS of this structure does not show "midgap states" (red curve in Fig. 2(b)). To introduce disorder in this structure we have systematically removed carbon atoms at all possible positions in the unit cell used for calculations. The resulting six GB atomic structures can be seen in Fig. 2(c). All of these structures contain two-coordinated carbon atoms, while the calculated DOS reproduces the low energy states observed in STM measurements. We expect that inter-valley scattering at these defect sites is a leading influence on charge transport phenomena. For example it can contribute to weak localization in the case of inter-grain transport [Q. Yu et al., Nat. Mater. 10, 443–449, 2011] and may destroy the high transparency [O. V Yazyev, S. G. Louie, Nat. Mater. 9, 806–809, 2010] of certain dislocation core configurations to charge carriers.

Color change of Blue butterfly wing scales in an air-vapor ambient

(OTKA PD 83483)

K. Kertész, G. Piszter, E. Jakab (CNS, Hungary), Zs. Bálint (HNHM, Hungary), Z. Vértesy, and L. P. Biró

Dielectric nanoarchitectures composed of materials with different enough optical properties and with a characteristic length scale of a few hundreds nanometers can interact strongly with visible light. These nanocomposites exhibit a photonic band gap for certain photon energies (wavelength region), this means that a proper structure with a suitable length scale and sufficient refractive index contrast between the two materials building up the nanostructure, may exhibit colour even in the absence of chemical pigments. Such colours are called structural colours. Structural colours can also occur in the living world, most frequently in arthropods. It was shown recently that butterfly wings coloured by PBG type material might exhibit measurable colour changes that allow the discrimination of different volatiles. The optical response of such nanoarchitectures on chemical changes in the environment is determined by the spectral change of the reflected light, and depends on the composition of the ambient atmosphere and on the nanostructure characteristics. The vapour enters in the structure, and capillary condensation is taking place in the pores.

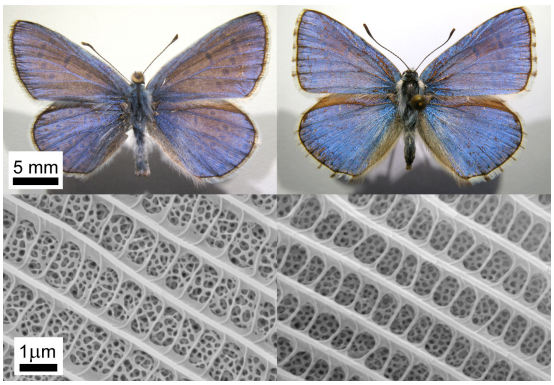

Figure 1. *The violet Polyommatus icarus (left) and the sky-blue Polyommatus bellargus (right) imago and scanning electron microscope image of a wing scale.*

We carried out reflectance measurements on closely related Blue lycaenid butterfly males possessing so called “pepper-pot” type photonic nanoarchitecture in their scales covering their dorsal wing surfaces. Experiments were carried out changing the concentration and nature of test vapours while monitoring the spectral variations in time. All the tests were done with the sample temperature set at, and below the room temperature. One complete cycle of measurement contains 10 s of vapour flow followed by 50 s of synthetic air flow, repeated 5 times with increasing the vapour concentration in 20% steps (Fig. 2a). In two wavelength ranges a region of 30 nm width is selected and the integrated reflectance value in the selected range is presented as a time dependent signal in Fig. 2b for ethanol, and Fig. 3. for water vapour.

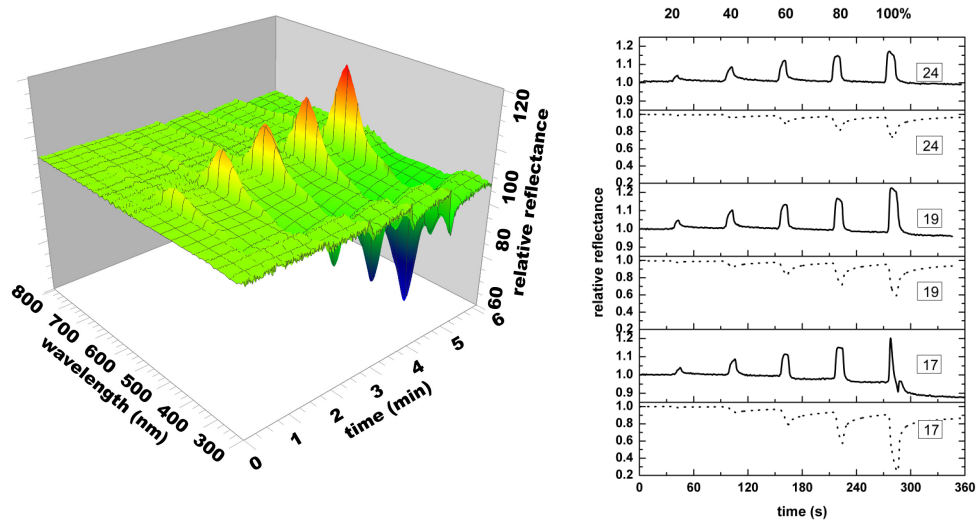

Figure 2. *Optical reflectance variation in time of Polyommatus icarus when the wing in synthetic air was used as reference (100%) (left). Normalised minima (dots) and maxima (continuous) of the integrated response signal variation in time in selected spectral ranges (480 – 510 nm for maxima, and 300 – 330 for minima) at 17, 19 and 24°C (right).*

The signal intensity is linear with the vapour concentration, and is increasing with the decrease of the sample temperature. Surpassing peaks appear at 17°C and 100% volatile concentration, and could be attributed to the hysteresis of the capillary condensation.

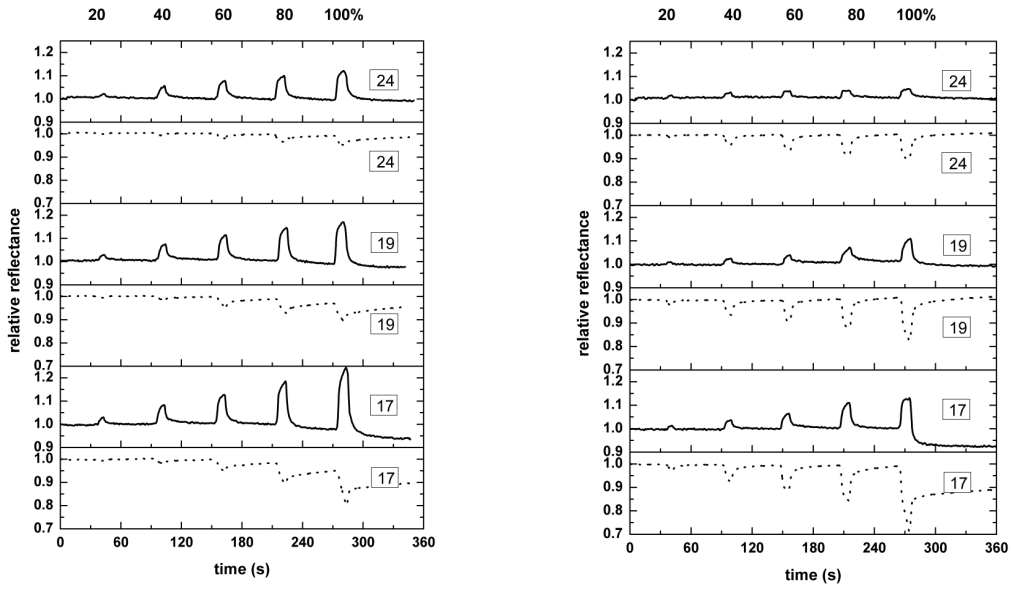

Figure 3. *Polyommatus icarus (left), and bellargus (right) response for water vapours. (See Fig. 2 for details.)*

Polarized light microscopy of chemical-vapor-deposition-grown graphene on copper

(KHJLN 2010K000980, OTKA PD 8424, OTKA K101599)

K. Kertész, A. A. Koós (Oxford Univ., UK), A. T. Murdock (Oxford Univ., UK), Z. Vértesy, P. Nemes-Incze, P. J. Szabó (BME), Z. E. Horváth, L. Tapasztó, C. Hwang (KRISS, Korea), N. Grobert (Oxford Univ.), and L. P. Biró

Due to the very promising electronic, mechanical, and optical properties, graphene has continuously been the focus of attention since it was first produced by mechanical cleavage. However, for practical applications, large area graphene must be produced at low cost, on large areas and with good quality. To achieve industrially viable prices, chemical vapor deposition (CVD) technique in conjunction with polycrystalline Cu substrates is perhaps the best candidate to achieve these demands. This process yields polycrystalline graphene material, i.e., a patchwork of randomly grown crystallites fused together. Another factor influencing material quality may be associated with nanowrinkles attributed to the step formation in the Cu substrate during graphene growth. Optical characterization methods are extremely useful in order to investigate the orientation of individual Cu grains, their characteristic step structure, and the graphene overlayer grown on them. Unlike scanning electron microscopy (SEM) and EBSD, they are contamination-free and easy to use.

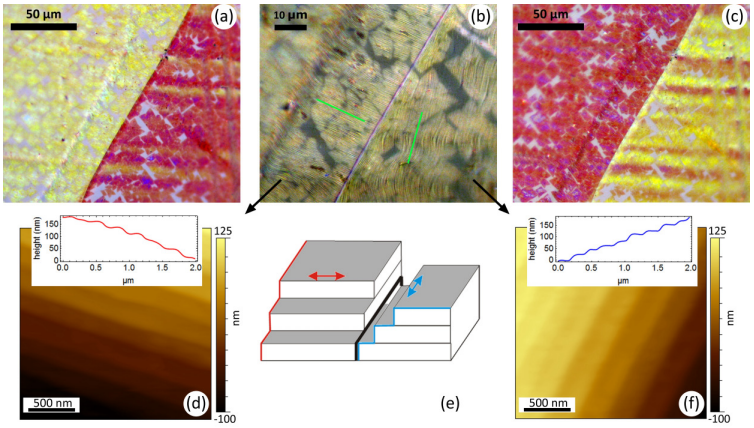

Figure 1. *Neighboring Cu grains with yellow/violet coloration and their characteristic step structure as revealed by PM and AFM images. (a), (c) yellow/violet and violet/yellow coloration at (90+Δ°) and (90- Δ°) setting of the analyzer; (b) high resolution PM image with rigorously crossed polarizer and analyzer. Note the parallel steps in each grain. Green lines indicate the average step edge direction; (d), (f) contact mode AFM image of the two grains; (e) schematic presentations of the step structure in the two grains, the shaded faces are roughly parallel with the surface of the Cu foil.*

In this work, we used linearly polarized light in order to reveal the grain structure of the Cu substrate, and the orientation of the characteristic step structure formed during graphene growth on the Cu crystallite facets with different Miller indices. Examining

the samples with polarized light microscopy (PM) and offsetting the analyzer a few degrees from the rigorously crossed position with the polarizer, the graphene crystallites covering the Cu substrate appeared yellow or violet contrasting the homogeneous gray of the Cu substrate (Fig. 1). On the basis of spectrogoniometric and microspectrometric measurements we attribute these colors to the selective coupling of the polarized light with the graphene over the stepped surface of the Cu crystallites.

Studies of an individual graphene flake in high resolution using PM (Figs. 2(a) and 2(b)), topographic C-AFM (Fig. 2(c)), friction force measurements (Fig. 2(d)), CT-AFM, and SEM, revealed that the violet or yellow coloration is not observed in those regions where the Cu surface is smooth. While PM clearly showed that in these regions the color is coincident with that of the Cu background (Fig. 2(a)), the AFM and SEM data convincingly showed that the graphene layer is present in these regions as well.

The linearly polarized light can have two distinct orientations with respect to the face of the Cu steps, which is in a plane at right angles with the plane of the Cu foil itself (see, Fig. 1(e), not shaded face), this will be called the "normal" face of the step, while the face parallel with the plane of the sample (shaded face) will be called the "parallel" face of the step. Light with the E parallel with the normal face may be coupled into the graphene membrane covering the normal face of the step. It will be reflected/scattered at the bottom of the step under angles close to the incidence angle so that a significant fraction will enter the microscope objective.

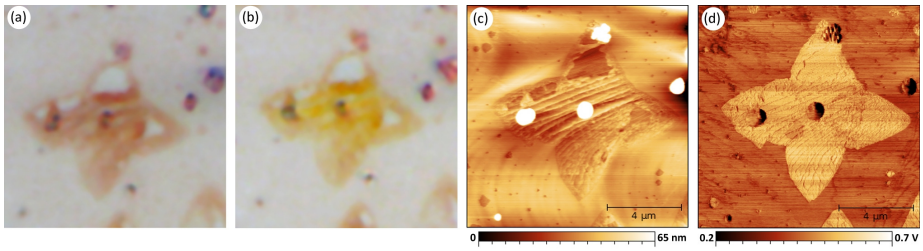

Figure 2. *PM and AFM images of an individual graphene flake. (a) PM image in violet and (b) yellow orientation, note certain regions where no color is observed. The same grey coloration can be observed as for the Cu background; (c) topographic C-AFM image; (d) FF-AFM image, note the characteristic difference between graphene and Cu.*

On the contrary, the light with E perpendicular to the normal face of the step will be scattered close to angles normal to this step face so that most of it will be lost and not captured by the microscope objective. These processes will be responsible for the "additional" light in the spectral range of 400–650 nm, causing the yellow color when the plane of polarization is parallel with the normal face of the step. The lack of the light scattered so that it cannot enter the microscope objective will cause the violet color when the plane of polarization is normal to the normal step face.

Polarized light microscopy proved to be a useful tool in the fast, large area, and contamination free investigation of the characteristic step structure developed on polycrystalline Cu used as a substrate for CVD graphene [80].

Electronic transport through graphene grain boundaries

(OTKA NKTH101599, KHJLN 2010K000980)

P. Vancsó, G. I. Márk, Ph. Lambin (FUNDP, Belgium), Y.-S. Kim (KRISS, Korea)
C. Hwang (KRISS, Korea) and L. P. Biró

Grain boundaries (GBs) in graphene have substantial effects on the outstanding electronic and transport properties of the perfect graphene lattice. By using wave-packet dynamical simulations we investigated the spreading of electronic wave packets through different types of periodical GBs. The electrons are injected from a simulated scanning tunnelling microscope (STM) tip, which is situated above one of the grains, far from the GB line (Fig. 1 a,b), then their time evolution is followed while crossing through the GB.

The first structure we analyzed was an experimentally observed periodical pentagon-heptagon (5-7) GB. Our simulations show a rich variety of transport phenomena, including beam splitting and states localized on the GB (Figs. 1 c,d). The energy dependent wavefunctions were calculated from the time dependent wavefunctions with t→E Fourier transformation. Localized states energy positions in the calculations correspond to the DOS maximums of the structure.

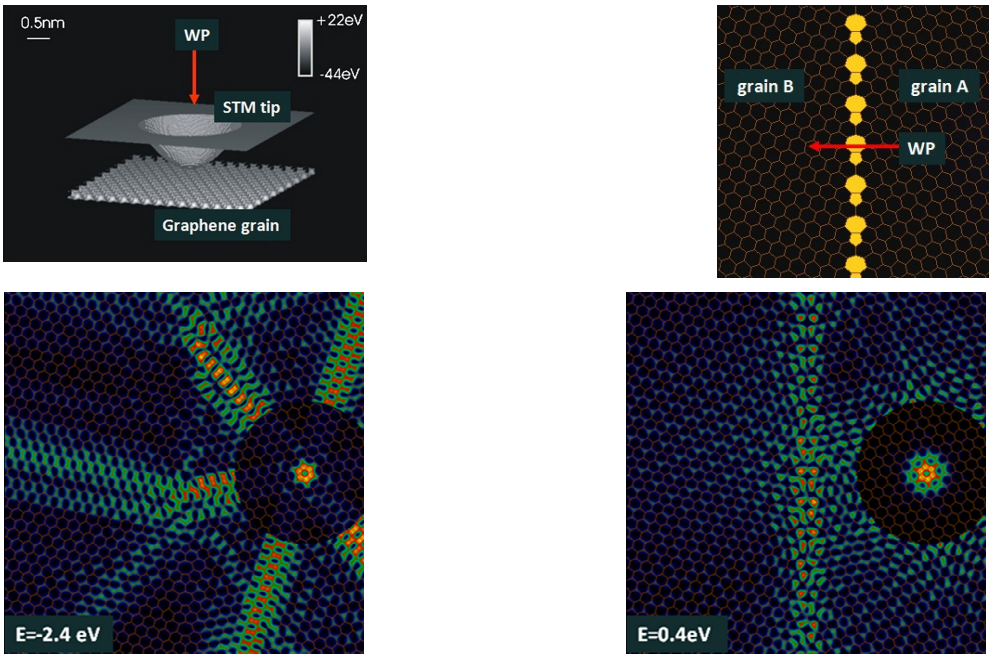

Figure 1. *(a) Model geometry of the STM tip - graphene system shown by the -2.7 eV equipotential surface of the potential (top left), (b) Strucutre of a pentagon-heptagon GB (top right). (c,d)Probability density on the graphene sheet with the grain boundary for selected energies shown as a colour coded 2D (XY) sections. Different colours scale were used in the near- and far regions (inside and outside of the circle). The STM tip is located above the center of the cirlce.*

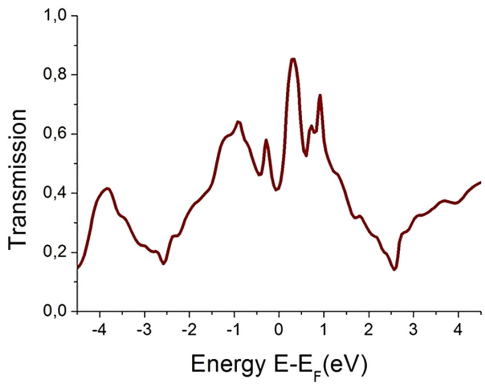

Figure 2. *Transmission probabilities of the WP calculated for the 5-7 GB. Low and high energy (±2.5eV) minimums come from the misorientation angle of the two grains.*

We performed energy dependent transmission calculations based on the calculated probability density wave functions (Fig. 2). The result shows that in those energy positions where the GB structure has high DOS values transmission is increased according to Landauer transport theory. Furthermore, we observed a geometrical effect based on the mismatch angles of the two grains, which reduce the transmission at the low and high-energy regions (±2.5eV). At these energies, the equal energy curves of the graphene dispersion relation are warped into hexagons (trigonal warping), causing anisotropic spread of electrons along the zig-zag directions (Fig 1.c). Due to the different orientation angles of the grains, transmission values are suppressed.

We also studied an exotic GB where the misorientation angle is zero. This extended defect contains pentagons and octagons (Fig. 3 b inset) and has a metallic behavior. Our simulations show that despite of the same orientation the transmission value is decreased above the Fermi energy at 2.6eV (Fig. 3b). The origin of this phenomenon was found in the detailed analysis of the electronic structure, where the LDOS have an electron-hole asymmetry on the GB. These simulations allowed us to separate geometrical- and electronic structure effects in various GB configurations.

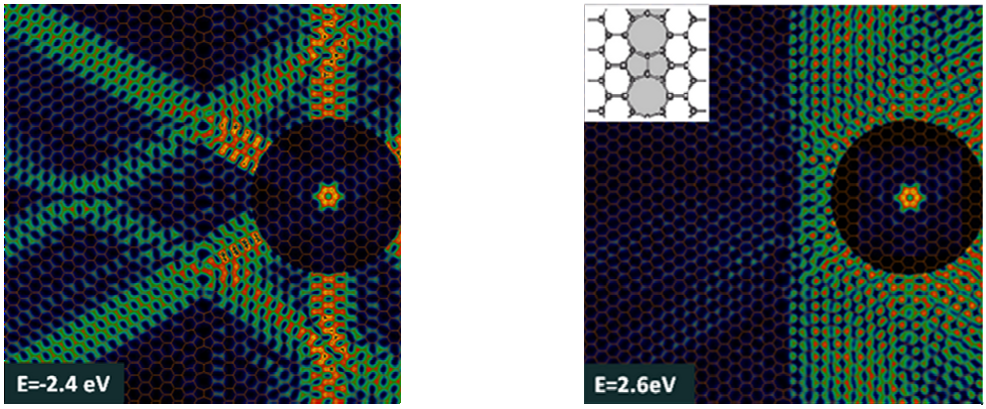

Figure 3. *Electron-hole assymmetry in the transmission of a periodical pentagon-octogon extended defect. (a),(b) Probability density on the graphene sheet with the extended defect for high and low energy regions shown as a color coded 2D (XY) sections. The inset show the geometry of the 5-8-5 extended defect.*

Forming electronic waveguides from graphene grain boundaries

(KHJLN 2010K000980, OTKA K101599)

G. I. Márk, P. Vancsó, Ph. Lambin (FUNDP, Belgium), Ch. Hwang (KRISS, Korea), and L. P. Biró

Electromagnetic waveguides have important applications in modern technology, e.g. the fiber optic cables in telecommunications. Similar structures – sometimes also called nanowires – can be designed for electron waves and will become essential building elements of nanoelectronic circuits. One of the promising candidates to do so is graphene. The presence of grain boundaries (GBs), however, affects the propagation of charge carriers in graphene. Electron mobility of CVD graphene – which is known to contain a large number of GBs – can be considerably smaller than that for cleaved graphene. Conductivity of the defect region can either increase or decrease compared to graphene, depending on the atomic structure of the defect. Using quantum mechanical dynamics based simulation, we investigated the spreading of electronic wave packets on graphene containing various configurations of GBs. Our simulations demonstrated that reflection and refraction phenomena occur in the charge spreading on graphene by a line defect. The waveguide effect is investigated by placing a simulated metallic scanning tunneling microscope (STM) tip above the nanoribbon between two GBs (Fig.1). A Gaussian wave packet is injected into the graphene sheet from the tip and its time development is calculated by wave packet dynamics.

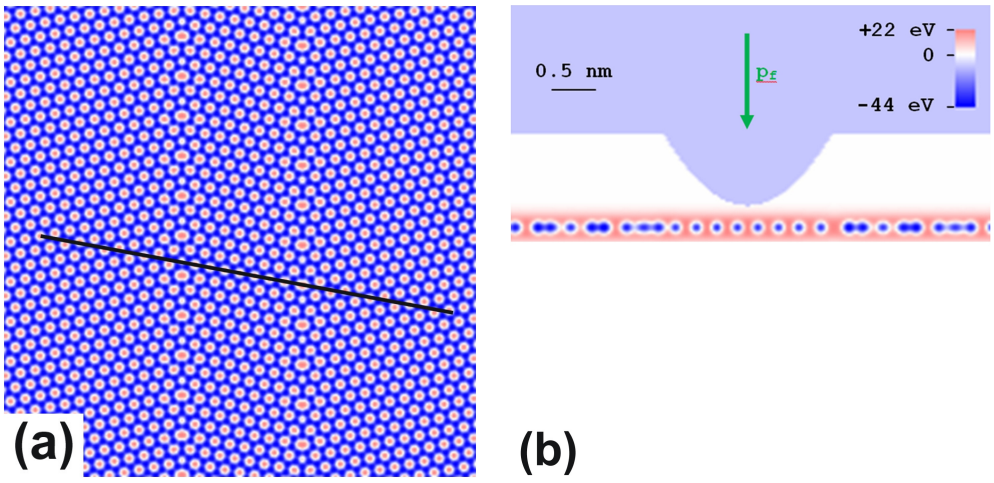

Figure 1. *Model geometry. (a) 2D cross section of the potential at the graphene plane, shown by color coding. White is the zero potential, blue (red) colors show the negative (positive) values, respectively, see the color bar in (b). (b) 2D cross section of the potential perpendicular to the graphene plane, taken along the black line in (a). The vertical green arrow shows the momentum of the incoming wave packet.*

The graphene sheet was modeled by a local one-electron pseudo-potential matching the ab-initio band structure of graphene. The 38.9° GBs are formed by a linear chain of abutting pentagons and heptagons separated by one row of hexagons, relaxed by a molecular mechanics potential. The tip is taken as a hyperboloid of 0.5 nm apex radius and 15° aperture angle. In order to study the behavior of the different energy components of the WP, we calculated the energy-dependent wave function by utilizing a t→E Fourier transformation. Fig. 2 shows the energy-dependent probability density for two selected energy values. At $E=E_F+0.8eV$ localized states are seen at the GBs. Emergence of states localized on the GB opens up the possibility for using graphene GBs as interconnects in all-carbon nanoelectronic circuits. At $E= E_F+2.9$ eV the probability density is confined to the nanostripe between the GBs, hence this structure acts as an electronic waveguide at this energy. This energy value corresponds to the DOS peak of graphene at $E=E_F\pm\gamma$ where γ is the tight-binding C-C hopping matrix element.

In summary, our simulation shows the possibility of creating nanoscale waveguides and nanowires for charge carriers on the graphene surface by a controlled formation of grain boundaries. For most of the energy values the charge carriers cross the grain boundaries, suffering reflection and refraction. At certain selected energies, however, the electrons are channeled into the grain boundary line, creating extended localized states. There are specific energy values where the two grains boundaries behave as a waveguide: the electron density is confined between them. These effects may have a great significance in the theory of graphene nanoelectronic circuits.

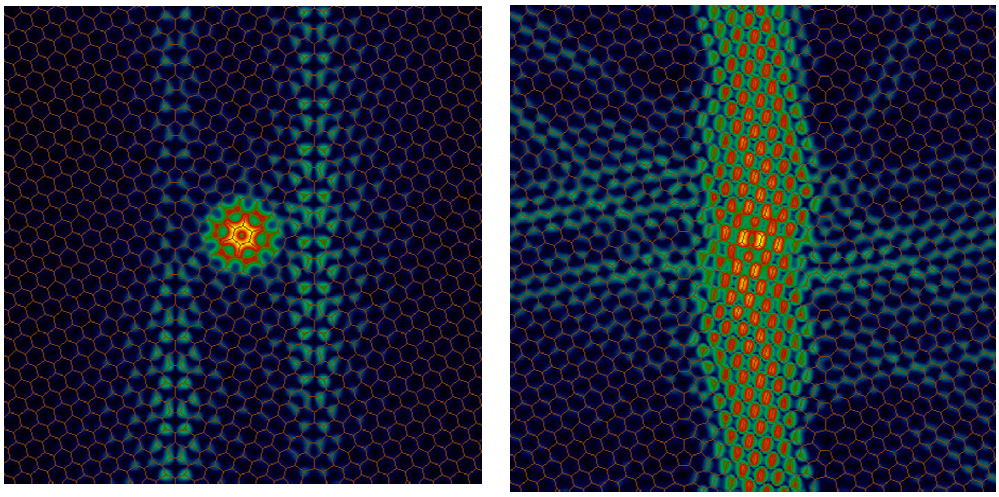

Figure 2. *Probability density on the graphene sheet with the two grain boundaries for selected energies (E_F+0.8eV and E_F+2.9eV) shown as color-coded 2D sections. The black color corresponds to the zero density, and the bright yellow to the maximum density. The graphene network is shown by thin orange lines.*

Characterization of the electrical percolation paths in injection moulded MWNT/polycarbonate composite parts

(CONTACT FP7-People-ITN-2008, 238363)

B. Kiss-Pataki, Z. E. Horváth, J. Tiusanen (Promolding BV, Netherland),
Daniel Vlasveld (Promolding BV, Netherland)

Mapping of local electrical properties at the nano scale of the electrically conductive, MWNT loaded composites can strongly contribute to the understanding of their final electrical properties and the optimization of the processing conditions of the materials serving in more appropriate tailoring of conductive products. The microstructure of plastic parts is the consequence of thermomechanical changes imposed to the host polymer by the processing conditions, which induce stresses by combination of shear, elongational flow and cooling.

Six injection moulding settings with different injection speeds and melt temperatures of polycarbonate (PC) with 3 weight percent (w%) multi-walled carbon nanotube (MWNT) content were studied in order to study the effect of processing parameters on the final material properties. The injection moulded pieces presented a difference of orders of magnitude in electrical volume resistivities; therefore their investigation by microscopic methods from macro to nano scale was performed to evaluate the state of dispersion of the filler. The investigated samples had the filler 99.9% evenly distributed at the macro scale. Transmission electron microscopy (TEM, Fig. 1) and scanning electron microscopy (SEM, Fig. 2) results could not offer sufficient information about the electrical transport of MWNTs in the polycarbonate matrix, they can not directly distinguish between the isolated nanotubes and the ones connected to the conductive network.

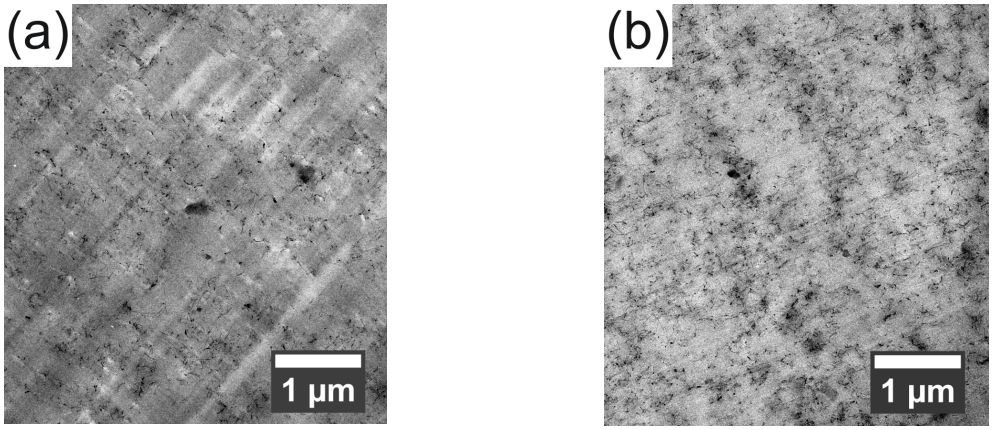

Figure 1. *TEM images of 3% MWNT/PC composites injection moulded with 42 mm/s injection velocity,* ***a:*** *at 280 ℃, having a volume resistivity of 6000 Ωcm;* ***b:*** *at 320 ℃, having a volume resistivity of 23 Ωcm. Individual MWNTs and loose clusters with neat polymer islands are present in both cases but with visible differences.*

Conductive atomic force microscopy (C-AFM, Fig. 3) investigation was performed on the samples, and a relation was found between the electrical volume resistivity of the parts and their nano-scale conductive properties measured.

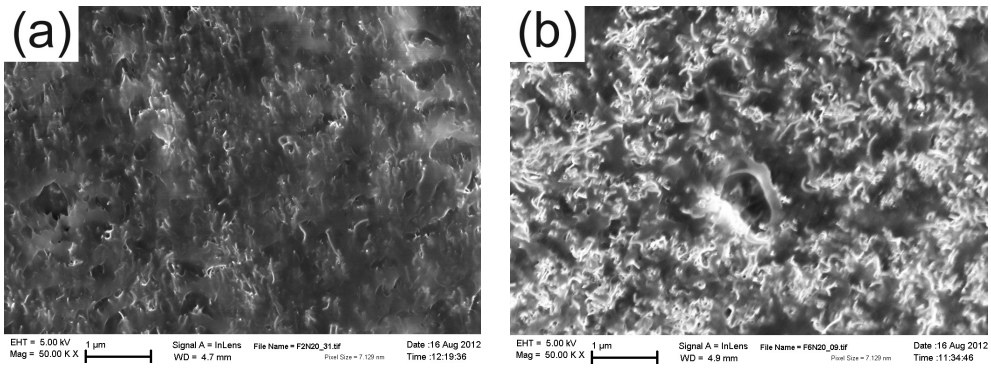

Figure 2. *SEM images of 3% MWNT/PC composite injection moulded with 42 mm/s injection velocity,* ***a:*** *at 280 ℃, having a volume resistivity of 6000 Ωcm;* ***b:*** *at 320 ℃, having a volume resistivity of 23 Ωcm. More cavities are visible, less nanotubes are covered with polymer in case of the lower resistivity sample.*

We found that the electrical volume resistivity decreases with the increasing amount of electrically percolating paths, as well as with decreasing distance between the conductive spots. Especially in case of the 2 presented samples, the comparison of the TEM and C-AFM images clearly show that the proportion of the isolated MWCNTs and clusters is definitely higher in case of the high resistivity sample.

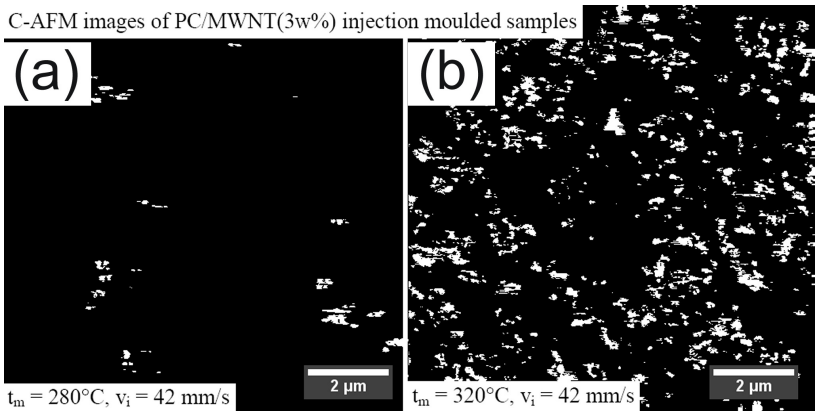

Figure 3. *Conductive atomic force microscopy images of the side parts of a Polycarbonate nanocomposite containing 3% CNT.*

C-AFM technique has been shown to complement effectively the electron microscopic methods in case of composites with conductive nanofillers, offering a tool to visualize in nanometric resolution a section of the conductive paths responsible for the macroscopic conduction of the material.

Photonics Department

Head: Miklós FRIED, D.Sc.

Research Staff

- Péter PETRIK, Ph.D., Head of Ellipsometry Laboratory·
- Miklós SERÉNYI, D.Sc., Head of Semiconductor Photonics Laboratory
- János BALÁZS, Ph.D. (part-time)
- Antal GASPARICS, Ph.D.
- Norbert NAGY, Ph.D.
- András HÁMORI, dr. Univ.
- Róbert HORVÁTH, Ph.D.
- Csaba MAJOR, Ph.D.
- György JUHÁSZ, dr. Univ.
- Zsolt LACZIK, Ph.D. (on leave)
- Tivadar LOHNER, C.Sc.
- György KÁDÁR, D.Sc.
- Sándor KURUNCZI, Ph.D.
- János MAKAI, C.Sc. (part-time)
- Olivér POLGÁR, Ph.D.
- Miklós RÁCZ, Ph.D. (part-time)
- Ferenc RIESZ, C.Sc.
- Gábor VÉRTESY, D.Sc.
- Péter TÖRÖK, D.Sc. (on leave)

Ph.D. students / Diploma workers

- Péter KOZMA, Ph.D.
- Dániel PATKÓ, Ph.D. student
- Emil AGÓCS, Ph.D. student
- Bálint FODOR, Ph.D. student
- Norbert ORGOVÁN, Ph.D. student
- Judit NÁDOR, Ph.D. student
- Krisztina JUHÁSZ, Ph.D. student
- Rita SALÁNKI, Ph.D. student

Technical Staff

- Rózsa Mária JANKÓNÉ, technician
- Beatrix PÉTER, bio-engineer

The Department, with other departments of MFA, was involved in the NANOMAGDYE (EU FP7) project with the aim to develop tailored biocompatible magneto-optical nanosystems and to apply them in medical practice. The task of the Department was to fabricate a magneto-optical probe for oncology imaging. A dual magneto-optical probe was built, which is able to simultaneously detect the dye and the magnetic nanoparticles in future surgical applications. Company EURORAD designed and realized the final prototype of the dual opto-magnetic detection system comprising the detection head (probe including magnetic sensor and optical detection in a single surgical housing) and the electronic module. The system proved to be accurate concerning both the localization of the probe within the displayed image as well as the identification of hot and cold areas in the test objects. After the project closing, EURORAD ordered 3 more magnetic sensor heads from MFA.

Magnetic Adaptive Testing (MAT) is a recently developed nondestructive magnetic measurement method, which is based on systematic measurement and evaluation of minor magnetic hysteresis loops. Very good correlation was found between the optimally chosen MAT parameters and the neutron radiation fluence of nuclear reactor structural materials. MAT seems to be an advantageous method to replacing the destructive test measurements by nondestructive magnetic measurements.

Grating Coupled Interferometry (GCI) using high quality waveguides with two incoupling and one outcoupling grating areas was introduced to increase and precisely control the sensing length of the device; and to make the sensor design suitable for plate-based multiplexing. In contrast to other interferometric arrangements, the sensor chips are interrogated with a single expanded laser beam illuminating both incoupling gratings simultaneously. In order to obtain the interference signal, only half of the beam is phase modulated using a laterally divided two-cell liquid crystal modulator. The developed highly symmetrical arrangement of the interferometric arms increases the stability and at the same time offers straightforward integration of parallel sensing channels. The sensitivity of the instrument for bulk refractive index was proven being below 10^{-7}. The high phase resolution allows the detection of surface adsorbed molecule densities below 1 pg/mm^2 without using any labeling or on-chip referencing.
MFA was involved in a multidisciplinary research project (including photonics, microfluidics, biochemistry and materials science) called P3SENS (www.p3sens-project.eu) which is funded by EU. This Pan-European cooperation aims to develop high-performance, multichannel optical biosensors for the early detection of brain diseases (for instance, to prevent the occurrence of ischemic damage as a result of stroke) from human blood. Among many other tasks MFA functionalizes the photonic biochips with appropriate surface chemistry and tests the receptor performances by a high-resolution label-free optical biosensor methods.
MFA have started a „Lendület" project: „Advanced label-free biosensors for proteins and cells" financed by the Hungarian Academy of Sciences.
We are involved in a "National technology development" project: „Equipment development for industrial size thin film optical mapping" and an ENIAC JU project: "E450EDL European 450mm Equipment Demo Line".

Magnetic characterization of neutron irradiated reactor steel material

(OTKA A08 CK80173)

G. Vértesy

Inspection of neutron-irradiation-generated degradation is a very important task in nuclear energetics. In ferromagnetic materials, such as nuclear reactor pressure vessel steel, fortunately, a change in their magnetic properties escorts the structural degradation. In this work the applicability of a novel magnetic nondestructive method (Magnetic Adaptive Testing, MAT), which is based on systematic measurement and evaluation of minor magnetic hysteresis loops, is shown for inspection of neutron irradiation embrittlement in nuclear reactor pressure vessel steel. Three series of samples, made of JRQ, 15H2MFA and 10ChMFT (weld) type steels were measured by MAT. The samples were irradiated by E>1 MeV energy neutrons with neutron fluence of 1.58×10^{19} – 1.19×10^{20} n/cm^2. Regular, monotonously increasing correlation was found between the optimally chosen MAT degradation functions and the neutron fluence, in all three types of the materials. Shift of the ductile-brittle transition temperature, ΔDBTT, independently determined as a function of neutron fluence for the 15H2MFA material, was also employed. A sensitive, linear correlation was found between the ΔDBTT and values of the MAT degradation functions. Based on these results, MAT is considered to be a promising complementary tool. It may serve in future, perhaps, even for replacement of the destructive tests within the surveillance programs, which are presently used for inspection of neutron irradiation generated embrittlement of nuclear reactor pressure vessel steel.

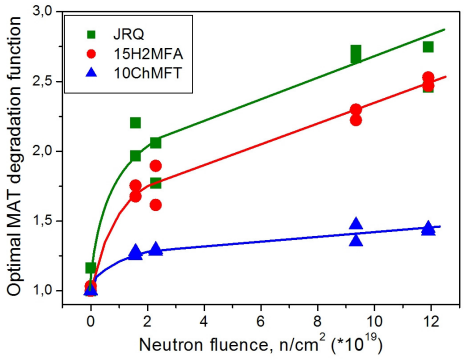

Figure 1. *The optimally chosen MAT degradation functions and the corresponding sensitivity map for the JRQ, 15H2MFA and 10ChMFT samples.*

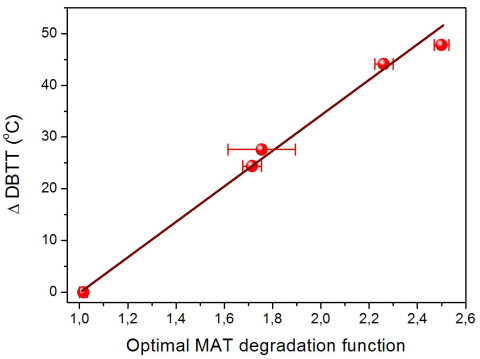

Figure 2. *Shift of the ductile-brittle transition temperature, ΔDBTT, due to neutron irradiation of the 15H2MFA reactor steel within the range of fluence up to $1.2*10^{19}$n/cm^2, in dependence on measured values of the optimal MAT degradation function.*

Makyoh topography

F. Riesz, and J. P. Makai

Makyoh topography (MT) is an optical tool for the qualitative flatness testing of specular surfaces, based on the defocused detection of a collimated light beam reflected from the tested surface. By inserting a square grid into the path of the illuminating beam, the height map can be calculated by integrating the gradients obtained from the distortion of the grid's reflected image (quantitative extension).

In the past year, activities were concentrated mainly on applications.

The flatness of Si substrates and the stress of thin films deposited onto them have been assessed for the company Mirrotron Ltd. for neutron optics applications.

The substrate morphology and deformation of 3C-SiC layers deposited on Si substrates by hot-wall epitaxy at IMEM–CNR (Parma, Italy) were also studied. Substrate-related texture and inhomogeneous curvature along the gas flow direction, correlating with the layer thickness variations, were observed.
For in-house research, Makyoh topography was used to assess sample deformation and surface/interface defects for process optimization of wafer bonding technology of various structures. Fig. 1 shows two examples. The left image shows rough morphology, numerous surface defects and a clear trace of the bonding tool on a glass substrate subjected to bonding. On the right image, corrugation of a polymer/glass microfluidic structure is visible.

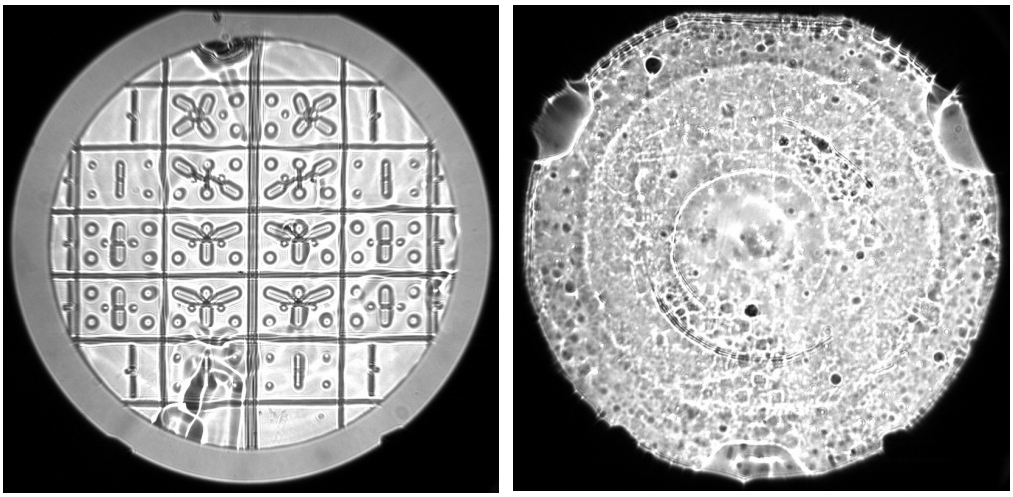

Figure 1. *Examples of Makyoh-topography assesment of wafer bonding technology: images of glass substrate subjected to bonding (left) and a polymer/glass structure for microfluidic applications (right).*

MeV Energy N^+-Implanted Planar Optical Waveguides in Er-Doped Tungsten-Tellurite Glass Operating at 1.55 micron

(OTKA K68688, K101223)

I. Bányász (Wigner), S. Berneschi (IFAC-CNR), M. Bettinelli (IFAC-CNR), M. Brenci (IFAC-CNR), M. Fried, N. Q. Khanh, T. Lohner, G. Nunzi-Conti (IFAC-CNR), S. Pelli (IFAC-CNR), P. Petrik, G. C. Righini (IFAC-CNR), A. Speghini (IFAC-CNR), A. Watterich (Wigner), and Zs. Zolnai

Ion beam technique is among the best methods for optical waveguide fabrication in crystalline and amorphous materials. It has better controllability and reproducibility than other techniques. The first articles reporting fabrication of waveguides by light ions ion implantation appeared between the end of 1960's and early 1980's.

Tellurite glasses have gained a widespread attention because of their potential as hosts of rare-earth elements for the development of fiber and integrated optical amplifiers and lasers covering all main telecommunication bands

We have recently reported fabrication of channel waveguides in an Er-doped tungsten-tellurite (Er:Te) glass via implantation of 1.5-3.5 MeV N^+ ions to result in waveguide operation in the 1550-nm telecommunication band.

Structure of the ion implanted planar waveguides is determined mainly by the energy and fluence of the implanted ions. Full-cascade SRIM (Stopping and Range of Ions in Matter) simulations were performed and compared with spectroscopic ellipsometric (SE) investigations to estimate the ion and damage depth distributions in the target, Fig. 1. Maximum of the collision events (vacancy production) distribution roughly coincides with that of the ion distribution, but it extends considerably toward sample surface. Center of the barrier layer is slightly beyond the projected range, while its width increases with the implanted fluence, as expected.

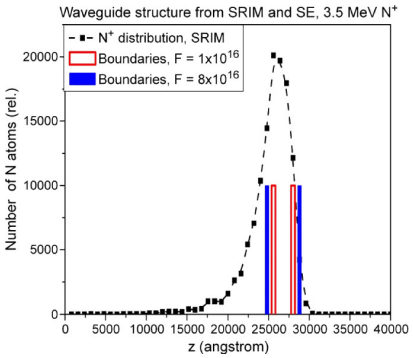

Figure 1. *SRIM simulation and SE fit of the waveguide structure.*

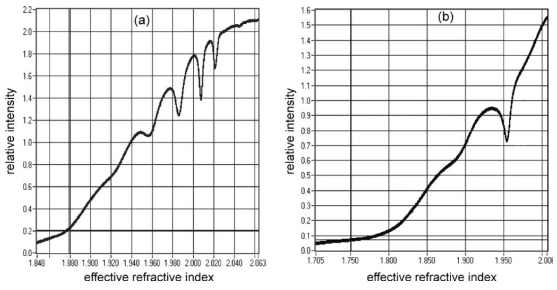

Figure 2. *M-line spectra of waveguide. Fluence = 8x10^{16} ions/cm^2, E = 3:5 MeV. (a) at 635 nm and (b) at 1550 nm.*

Functionality of the waveguides was tested by m-line (dark-line) spectroscopy and prism coupling technique. The accuracy is around $1x10^{-4}$ and $5x10^{-4}$ for measuring the

effective refractive index (n_{eff}) and bulk refractive index, respectively. Four guiding modes were detected at 635 nm in the waveguide (Fig. 2.). To analyze how the implantation parameters influence the characteristics of the waveguides, we have carried out numerical fits based on the m-lines measurements. The waveguide has been considered a 3-layer step structure and the leaky nature of the waveguide has been neglected, using the barrier layer as the substrate of the waveguide.

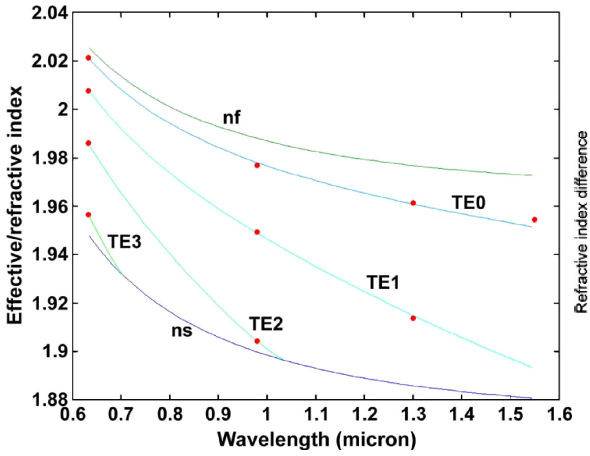

Figure 3. *Reconstruction of the refractive index of the guiding and barrier layers as a function of the wavelength. Sample irradiated with 8x10^{16} ions/cm^2 Calculated effective indices of the modes are also shown.*

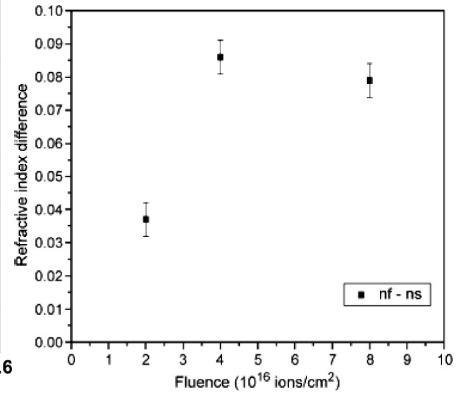

Figure 4. *Refractive index difference of the guiding and barrier layers versus fluence at 635 nm.*

The availability of data at several wavelengths (635, 980, 1310, and 1550 nm) has allowed us to obtain an accurate data processing. Assuming a Sellmeier-like law: $n^2 = 1 + \lambda^2/(A^2 + B^2)$ and using it in the fitting process, it was possible to obtain the thickness of the guiding layer and the parameters A and B for the guiding and the barrier layers in a broad wavelength range.

The fitting process allowed us to model through the A and B parameters the wavelength dependent refractive index of both the guiding (nf) and barrier layers (ns), see in Fig. 3. Moreover, the effective indices of the modes were calculated with the values of the numerical regression results and the same assumptions were used in the fitting process. The agreement between the experimental data (dots in Fig. 3) and the calculated effective indices is very good. Thickness of the guiding layer was assessed to be 2.2 micrometer, in agreement with SRIM simulations and spectroscopic ellipsometry (SE) measurements.

High modulation was found, up to 0.08 of the refractive index of the implanted waveguides in this material (Fig. 4).

Optical characterization of materials for optoelectronics and biosensorics

(OTKA K81842, NKTH PVMET_08, OTKA PD73084, EU FP7 P3SENS)

P. Petrik, E. Agócs, B. Fodor, M. Janosov (ELTE), A. Németh, S. Kurunczi, M. Fried, R. Horváth, Gy. Juhász, O. Polgár, Cs. Major, and P. Kozma

Optical characterization and modeling of ultra thin protein and optoelectronic reference layers is of large importance in a broad range of organic and solid state applications from sensors through printed electronics to photovoltaics. Metrologies are mainly used and developed independently, however cross checking and validation using reference method is crucial for the reliable characterizations and model developments. In the Ellipsometry Laboratory of MFA optical models and evaluation methods have been developed for the reliable measurement of Ga-doped ZnO films (Fig. 1), atomic layer deposited Al_2O_3 films (Fig. 2) as well as several organic layer systems such as flagellar filaments or polymer layers for the study of their degradation. In the investigations it has been pointed out that taking into account the surface (nanoroughness, contamination like water of hydrocarbon) and interface layers is of crucial importance. Applying these modeling steps correctly, the reference dielectric functions of ZnO (as shown in Fig. 1) and Al_2O_3 can be obtained correctly.

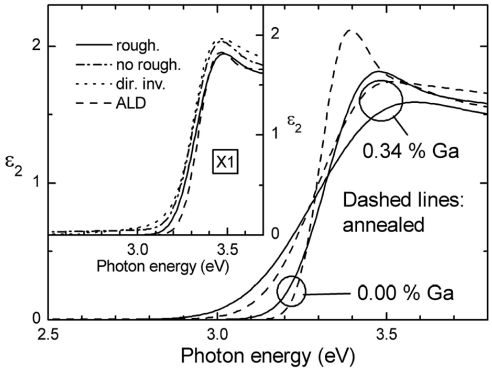

Figure 1. *Imaginary part of the dielectric function of sputtered Ga-doped ZnO films measured by ellipsometry arount the band gap. Large sensitivity on the Ga content and importance of taking into account the surface nanoroughness are emphasized.*

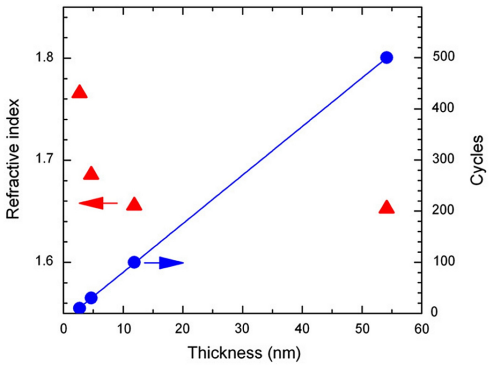

Figure 2. *Refractive index (triangles, using a one-layer model) and number of atomic layer deposition cycles (circles, showing a good linearity) of Al_2O_3 as a fungtion of the thickness measured by ellipsometry.*

Development of metrology tools based on electrical and optical techniques for in-line and laboratory qualification of thin film solar cells

(NKTH PVMET_08)

B. Fodor, P. Petrik, Cs. Major, Gy. Juhász, Zs. Zolnai, N. Nagy, and M. Fried

The aim of this project (coordinated by *Semilab, Inc.*) is to develop an equipment and measurement technology family, which is capable to perform electrical and optical measurements for in-line and laboratory qualification of thin film solar cells. MFA's task in the project was to render spectroscopic ellipsometry (SE) capable for this task. We have developed optical models for different (artificially) roughened surfaces. Model surface: Periodic (2D) nanostructures by electron-lithography.

Using rotating compensator spectroscopic ellipsometry, the complete Muller-matrix spectrum is measurable. The non-zero off-diagonal spectra show that a significant diffraction is observable when the wavelength is in the order of the periodicity of the structure studied (Fig. 1).

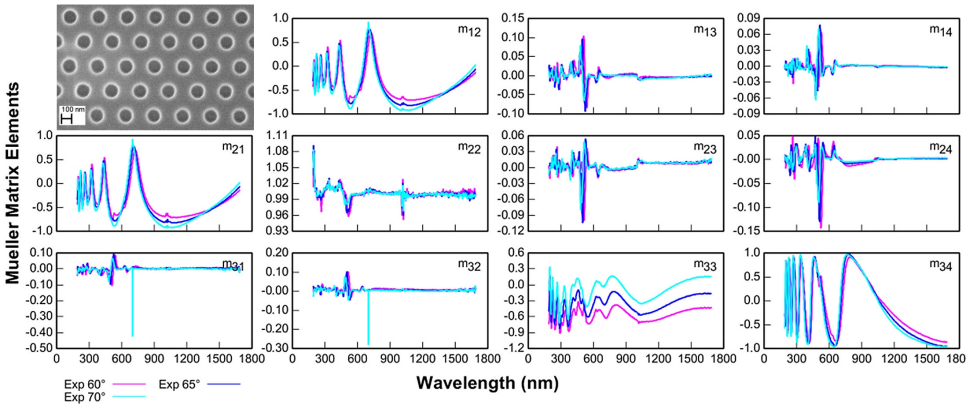

Figure 1. *The complete Muller-matrix spectrum, measured by a rotating compensator spectroscopic ellipsometer. The non-zero off-diagonal spectra show that a significant diffraction is observable when the wavelength is in the order of the periodicity of the structure studied. (Insert at upper-left: Periodic (2D) nanostructures created by electron-lithography).*

Polyethylene imine-based receptor immobilization for label free bioassays

(„Lendület" Grant of HAS, OTKA K81842 and EU FP7 P3SENS)

S. Kurunczi, K. Juhász, D. Patkó, N. Orgován, and R. Horváth

Polyethylene imine (PEI) based immobilization of antibodies was described and the concept was proved on the label free assay of C-Reactive Protein (CRP). This novel immobilization method was composed of a hyperbranched PEI layer, which was deposited at a high pH (9.5) on the sensor surface. The free amino groups of PEI were derivatized with neutravidin by Biotin N-hydroxysuccinimide ester and the biotinylated anti-CRP antibody immobilized on this layer (Fig. 1). Direct binding assay of recombinant CRP was successfully performed in the low µg/ml concentrations using a label free optical waveguide biosensor (Fig. 2).

An advantageous property of such PEI layer is the flexibility and hydrophilicity of these extended molecule loops. The PEI layer can be further developed as a competitive method for immobilization, having the advantage of simplicity (possibly requires 1-2 steps), having relatively low cost using aqueous solutions, and there is no need for thermal curing (in contrast with the case for silane chemistry), neither plasma treatment.

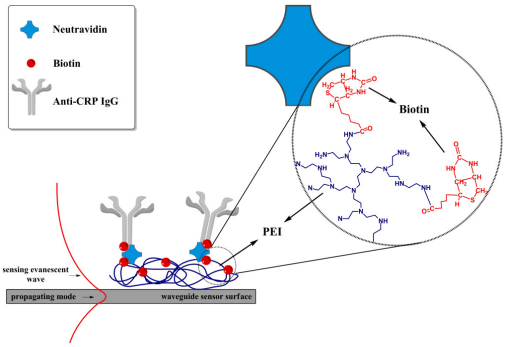

Figure 1. *Schematic of the proposed immobilization layer.*

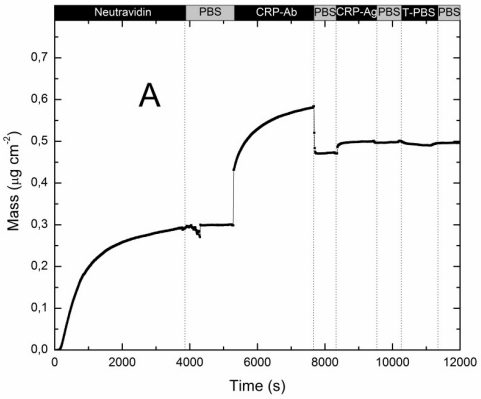

Figure 2. *CRP measurement on OWLS chip using the PEI-based immobilization (10 µg/ml CRP).*

Single beam grating coupled interferometry

(FP7 OPTIBIO, OTKA PD73084, „Lendület" Grant of HAS, TÁMOP-4.2.2/B-10/1-2010-0025)

D. Patkó, K. Cottier (Creoptix GmbH), A. Hámori, and R. Horváth

There is an increasing need for cost-effective, reliable and high-resolution measurements of biological and chemical processes in the health, biotechnology and military areas. Measuring biomolecular or cellular interactions at the nanometer length scale also opens up several challenging applications in basic biological, chemical and biophysical research with significant industrial relevance. It is especially useful when the processes and interactions are monitored without the need of any fluorescent or radioactive labeling; by following, for example, refractive index variations. The Grating Coupled Interferometry (GCI) using high quality waveguides with two incoupling and one outcoupling grating areas is introduced to increase and precisely control the sensing length of the device; and to make the sensor design suitable for plate-based multiplexing. In contrast to other interferometric arrangements, the sensor chips are interrogated with a single expanded laser beam illuminating both incoupling gratings simultaneously. In order to obtain the interference signal, only half of the beam is phase modulated using a laterally divided two-cell liquid crystal modulator. The developed highly symmetrical arrangement of the interferometric arms increases the stability and at the same time offers straightforward integration of parallel sensing channels. It was concluded that the sensor is capable of monitoring RI variations below 10^{-7} and protein surface coverage sensitivity of 0.1 pg/mm^2 was demonstrated [126].

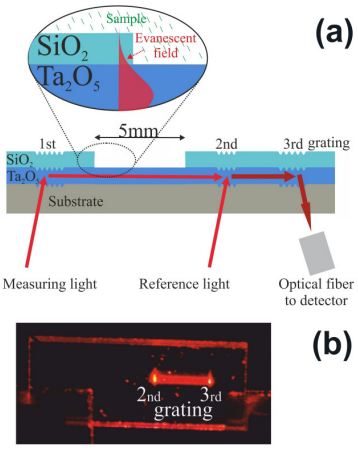

Figure 1. *(a) Cross section of the waveguide sensor, (b) Photo of the waveguide chip with mode propagation.*

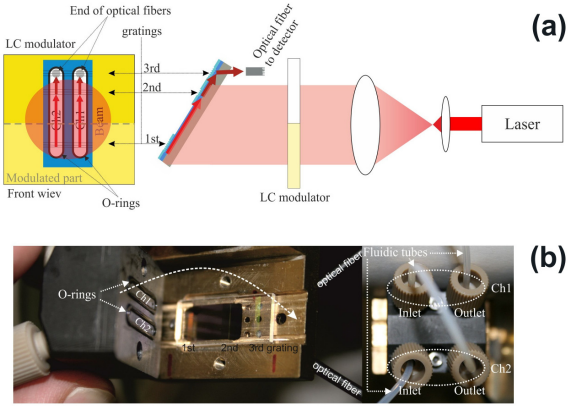

Figure 2. *(a) Schematic drawing of the optical setup. (b) Photos of the waveguide sensor chip holder and cuvette.*

From nano-voids to nano blisters in hydrogenated a-Si

M. Serényi, and C. Frigeri (CNR- IMEM, Italy)

Like in other amorphous materials, nano-voids are usually present in a-Si. Since they are empty spaces they bring about density reduction that can change the refractive index, electronic defect states and inhomogeneous stress distribution if filled with H or if they form Si-H platelets. The voids are most crucial if they are large enough to accommodate H molecules. Hydrogen may desorb as H_2 with the consequent reconstruction of dangling bonds and Si-Si weak bonds. Here we report on the generation of surface nano-blisters from nano-voids in hydrogenated a-Si layers grown by RF sputtering followed by annealing. It is argued that the generation is assisted by changes of the H bonding configuration caused by the annealing.

The set of IR spectra of Fig. 1 shows the typical shape of the stretching mode absorption as a function of the annealing time t as observed for all the samples. By Gaussian deconvolution two peaks can be identified at ~2000 and ~2100 cm^{-1}, respectively. The ~2000 cm^{-1} vibration is due to isolated Si-H mono-hydride bonds while the ~2100 cm^{-1} vibration is due to $(Si\text{-}H)_n$ clusters and polymers, such as $Si\text{-}H_2$ di-hydrides or chains of them $(Si\text{-}H_2)_n$. Fig. 1 shows that, upon annealing, the mono-hydride bonds break and their density decreases while the poly-hydride density increases and becomes even greater than the one of the mono-hydrides. The total integrated area, i.e., the total H concentration of bonded H, decreases with increasing t which indicates that annealing caused the break of some bonds of H to Si. The polymers decorating the walls of the voids (Fig. 2) and are expected to easily liberate their H into the voids themselves where H atoms may react to form molecular H_2. The blisters have thus developed from nanoscopic voids, decorated by $(Si\text{-}H_2)_n$ complexes, $n \geq 1$, which have increased their volume because of the increase of the inside pressure due to the thermal expansion of the H_2 gas upon annealing.

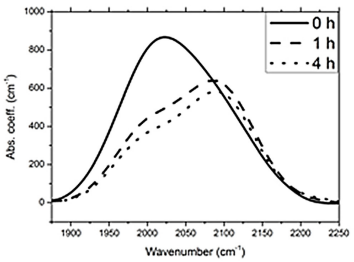

Figure 1. *IR absorption spectra in the stretching mode range for an a-Si layer hydrogenated at 1.5 ml/min non-annealed (solid curve) and annealed at 350 °C for 1 h (dash curve) and 4 h (dot curve).*

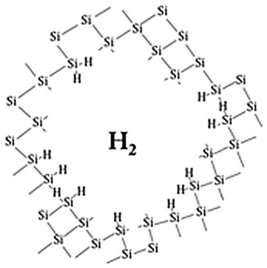

Figure 2. *Schematics of the bonding configuration of H to Si in a void. Si-H_2 di-hydrides and Si-H mono-hydrides can be present. It is assumed that some annealing has been applied and that hydrogen has already formed molecular hydrogen, H_2 .*

Microtechnology Department

Head: Gábor BATTISTIG, Ph.D.

Research Staff

- István BÁRSONY, Member of HAS
- László DÓZSA, Ph.D.
- Csaba DÜCSŐ, Ph.D.
- Péter FÜRJES, Ph.D.
- Zoltán HAJNAL, Ph.D.
- Zoltán LÁBADI, Ph.D.
- György MOLNÁR, Ph.D.
- Anita PONGRÁCZ, Ph.D.
- Vilmos RAKOVICS, Ph.D.
- Zsolt ZOLNAI, Ph.D.
- Andrea Edit PAP, Ph.D.
- Antalné ÁDÁM, M.Sc. (part time)
- Albert KARACS, M.Sc. (part time)
- Ákos NEMCSICS, Ph.D. (part time)
- Gábor PETŐ, D.Sc. Prof. Emeritus
- Béla SZENTPÁLI, Ph.D. (part time)
- Éva VÁZSONYI, M.Sc. (part time)

Ph.D. students / Diploma workers

- Zsófia BAJI, Ph.D. student
- Ferenc BIRÓ, Ph.D.student
- Zoltán FEKETE, Ph.D. student
- Tamás KÁRPÁTI, Ph.D. student
- Gergely MÁRTON, Ph.D.student
- Gergely HUSZKA (PPKE ITK) B.Sc. diploma w.
- Ferenc TOLNER (BME VIK) B.Sc. diploma w.
- Tamás PARDY (PPKE ITK) M.Sc. diploma w.

Technical Staff

- János FERENCZ, engineer
- Róbert HODOVÁN, engineer
- Csaba LÁZÁR, engineer
- András LŐRINCZ, engineer
- Ákos MAJOROS, engineer
- István RÉTI, engineer
- Erika TUNYOGI, engineer
- Katalin VERESNÉ-VÖRÖS, engineer
- Imre SZABÓ, engineer, dr. Univ. (part time)

- György ALTMANN, technician
- Gabriella BIRÓ, technician
- Sándor CSARNAI, technician
- Tibor CSARNAI, technician
- Magdolna ERŐS, technician
- Attila NAGY, technician
- Károlyné PÁJER, technician
- Csilla ARIAS-SOTONÉ FARAGÓ, technician
- Magda VARGA, technician

The main task of the Microtechnology Department is the research, development and system integration of physical, chemical/biochemical sensors and systems:

- Micro- electromechanical systems (MEMS) and MEMS related technologies, with special emphasis on development 3D microstructures;
- Development and functional testing of different MEMS based gas, chemical, 3D force, thermal, biology related sensors and sensor systems;
- Development of micro- and nanofluidic components and systems;
- Development and applications of near IR light emitting diodes and detectors;

Fundamental research on:

- Sensing principles;
- Novel materials and nanostructures;
- Novel 3D fabrication techniques;
- Ion-solid interaction for supporting MEMS development.

Device and material characterizations widely used in our projects:

- Ion beam analysis methods;
- IR and Raman scattering;
- Scanning Microprobes;
- Optical and Electron Microscopy, SEM, TEM, EDX;
- Spectroscopic Ellipsometry;
- Electrical characterisations;
- Microfluidic and biofunctional characterisation.

The Microtechnology Department of MFA runs the 300m^2 clean lab (Class 100-10000) with the complete Si-CMOS technology together with a mask shop, unique in Hungary. The technology base of the clean lab has been further improved in the recent years. The facility allows us to prepare layers, structures and devices on 3" and 4" Si and glass wafers with 1-micrometer line-width.

Main technologies available in the Microtechnology lab also for our partners and customers:

- High temperature annealing, diffusion and oxidation;
- Rapid Thermal Treatment;
- Low Pressure Chemical Vapor Deposition of poly-Si, SiO_2 and Si_3N_4 layers;
- Low Temperature Chemical Vapor Deposition;
- Ion implantation;
- Thin film depositions – Electron beam evaporation, DC and RF Sputtering;
- Atomic Layer Deposition;
- Deep Reactive Ion Etching;

- Photolithography with back-side alignment and Nanoimprinting;
- Wafer Bonding;
- Wet chemical treatments;
- Electro-chemical porous Silicon formation;
- Molecular Beam Epitaxy of III-V compound semiconductors;
- Mask design, laser pattern generator and laser writer;
- Polymer (PDMS, SU8, Polyimide) structuring by photolithography and micromoulding techniques;
- Materials and structural characterizations;
- Electrical and functional characterizations.

For detailed information please visit us at our web-site or contact through E-mail: dragon@mfa.ttk.hu, http://www.mems.hu/

MEMS (BIOMEMS) devices

Pellistor type gas sensor module

- **Pellistor type gas sensors** for multi-parallel flammable gas detection
- **Taguchi type gas sensors**
- **Microbolometers**
- **Thermopiles** for temperature monitoring
- **Thermopile antennas** for detection THz range radiation
- **Surface Acoustic Wave (SAW) filters**

- **Capacitive pressure sensors**
- **Calorimetric flow sensors**
- **Vectorial force and tactile sensors** for automotive, robotic and medical applications

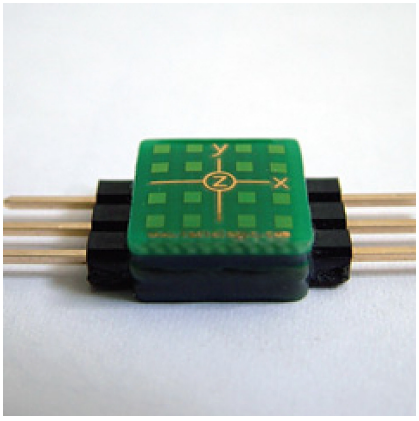

Vectorial force sensor

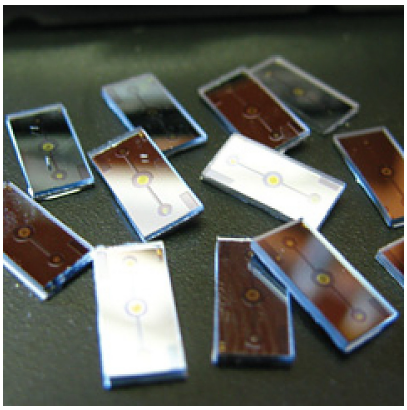

Nanopore biochemical sensors

- **Nanopore based biochemical sensors** for multi-parametric biomarker detection
- **Lab-on-a-Chip systems** for biomedical sample preparation

- **Cortical brain electrodes** for in-vivo monitoring local neural activity
- **Deep brain probes**with integrated drug delivery channels

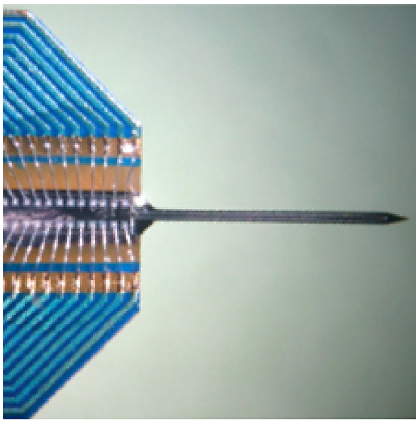

Cortical brain electrode

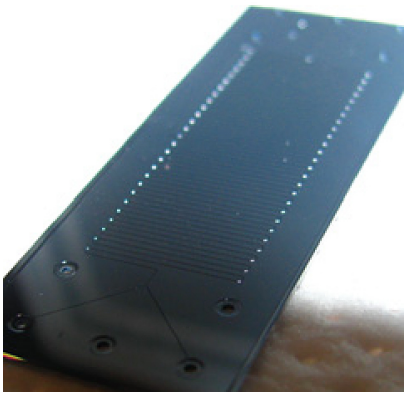

Microfluidic chip

- **Micro and Nanofluidics**
  Design, modelling and fabrication micro- and nanofluidic components and systems in Silicon, glass and polymer materials for biomedical applications

Competences

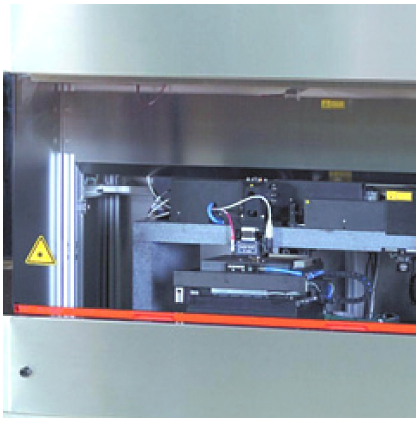

Mask Shop

- 1 µm resolution
- Laser Pattern Generator
- Chromium masks (4-7 inch)
- Direct wafer writing (3-6 inch)

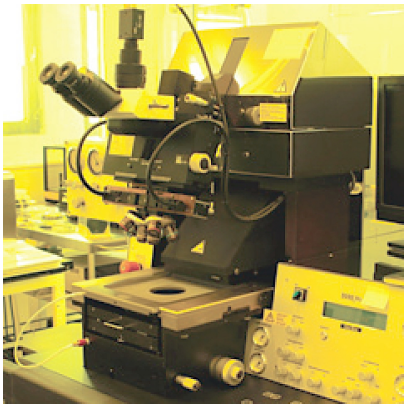

Photolithography

- 1 µm resolution
- Substractive patterning
- Lift-off patterning
- High aspect ratio SU-8 photorezist
- Double side alignment
- Pre-bond wafer alignment

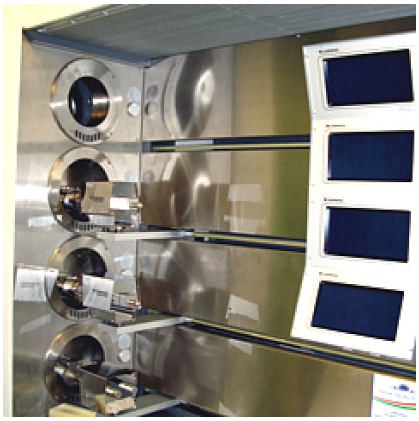

Thin film depositions - Chemical

- Low Pressure Chemical Vapor Deposition on
- (poly-Si, Silicon-Nitride)
- Low Temperature Oxide
- Atmospheric CVD (SiOx, PSG)
- Atomic Layer Deposition (ZnO, Al_2O_3, TiO_2)

Thin film depositions – Physical

- Electron beam vacuum evaporation (Al, Au, Ti, Cr)
- DC magnetron and RF sputtering (AlSi, Pt, Ti, AlSiCu, FeNi, Si, TiN, TiO_2, W)

CMOS related technologies

- Ion implantation
  energy: 20-120 keV
  dose: 10^{12} - 10^{16} ion/cm^2
- Semiconductor doping
- Surface treatment (B, BF_2, P, Ne, Ar)

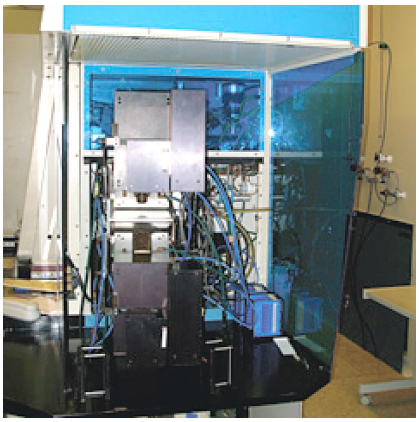

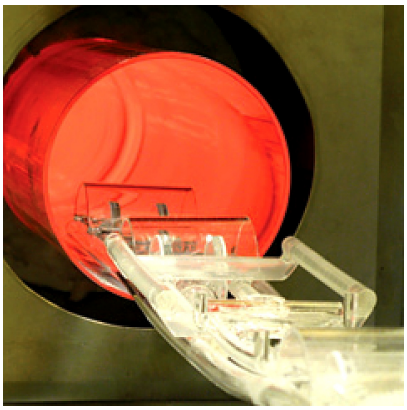

High temperature processes

- Max. 1150°C, N_2, O_2, Ar, N_2+H_2
- Thermal oxidation
- Dopant activation
- Drive-in diffusion
- Sintering contacts
- Rapid Thermal Annealing

Wet chemical processes

- Cleaning (standard CMOS)
- SiO_2, Si_3N_4, SiN_x, poly-Si, Al, Cr etching
- Sacrificial layer etching (SiO_2)
- Anisotropic alkaline etching of Si
- Electrochemical formation: porous Si, Al_2O_3
- Electrochemical Etch Stop of Si
- Sol-gel layers: TiO_2, SnO_2, SiO_2

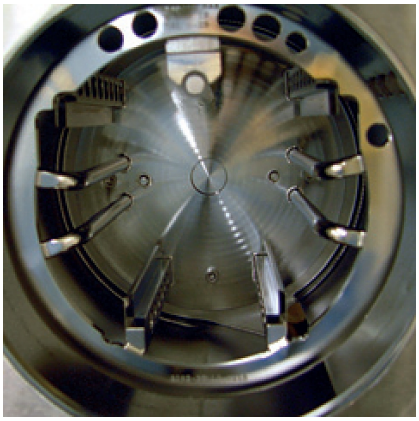

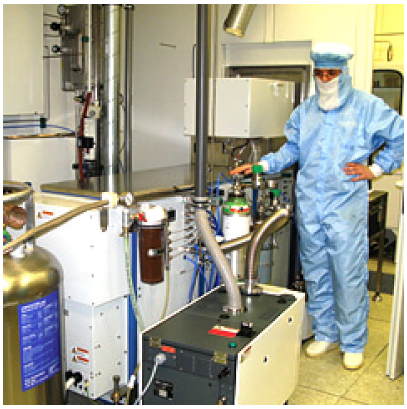

Dry chemical processes

- Plasma cleaning and treatments (O_2, Ar)
- Isotrop Silicon etching
- High Aspect Ratio Silicon etching
- ICP DRIE: Bosch, Cryo processes
- Dielectric (SiO_2, Si_3N_4, SiN_x) layer etching

Polymer technology

- PDMS micromoulding
- SU-8 photoresist (10-150 µm)
- Bonding
- Surface modification

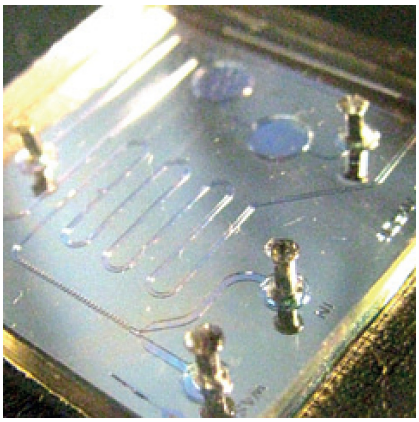

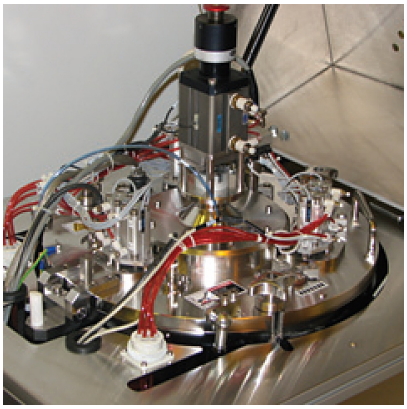

System integration – Packaging

- Wafer bonding: thermocompression, anodic and intermediate layer bonding
- Wafer dicing
- Wire bonding (Al, Au: 25 µm)
- Custom made special packaging

Simulation

- Technology and process simulation
- Monte-Carlo process simulation
- Device simulation
- Spice circuit modelling
- Finite Element Modelling: thermal, mechanical, electrical, fluid dynamics and coupled modeling

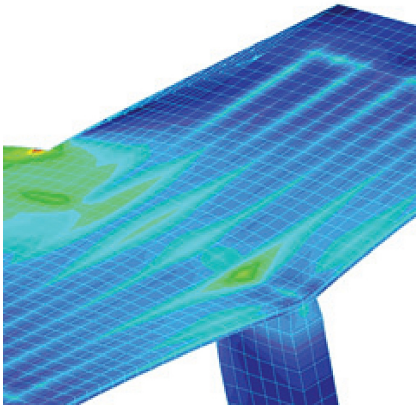

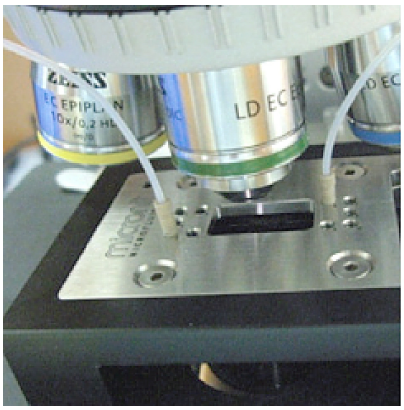

Characterisation

- Electrical characterisation
- Surface profiling
- SEM, TEM, AFM, EDS
- Functional tests: mechanical, chemical, biochemical, fluidical

From MEMS to BIOMEMS

The scientific orientation of the MEMS Laboratory of MTA TTK MFA has been significantly changed in the last period. Besides the developments in the field of silicon micromachining, reliable technology–knowledge and infrastructural background has been concentrated around the micro- and nanofluidical, bioanalytical and medical diagnostic research topics – based on several projects. The group – consisting of postdoc researchers, Ph.D. and gradual students – is able to efficiently support the scientific research of national and foreign partners, the development at industrial partners or the education in the partner universities well beyond its own scientific topics.

Motivation

The application of complex micro- and nanofabricated structures as sensing transducers becomes more important in the field of mechanical, chemical and biochemical sensors. As a result of novel and innovative biosensing principles new possibilities are being proposed in medical applications. These bioanalytical systems are expected to integrate the micro and nanoscale transducers with sample preparation microfluidic systems also composing Lab-on-a-Chip devices.
To fulfil the general requirements the microfluidic system must provide reliable sample transport, considering the final sensitivity of the diagnostic device. To make the sample preparation process more simple and comfortable from the point of the customers the integration of the main sample preparation steps in a microfluidic system is a clear demand. The aims:

- Development of reliable and robust micro- and nanofabrication technologies to realize structures.
- Revealing and establishing physical phenomena considering in the micro- and nanoscale systems, and utilizing them in novel bioanalitical, micro and nanofluidical devices.

Effects of the Focused Ion Beam parameters on nanopore milling in solid state membranes

(ENIAC JTI CAJAL4EU, OTKA NF69262, János Bolyai Fellowship)

P. Fürjes, Z. Fekete, L. Illés, A. L. Tóth, G. Battistig, and R. E. Gyurcsányi (BME)

This work describes a reliable nanofabrication technology of solid-state nanopore arrays. The geometric parameters of pores are achieved and optimized according to the requirements of bioanalytical applications regarding conformation and size of the characteristic proteins in clinical diagnostics. Different structural configurations and material compositions of the nanopore structures were developed and characterized according to the variable biofunctionalisation strategies. The geometry of the

fabricated pores were analysed as the statistical function of the focused ion beam milling parameters.
The chemically modified nanonopore based sensors can be applied to the detection of specific biomolecules through transport modulation determined by molecule binding in pores. In spite of the extraordinary sensitivity of the principle, reliability and reproducibility of nanoscale fabrication processes are not adequately elaborated so far.
The characterized test structures were fabricated by the combination of silicon micromachining and subsequent nanofabrication processes. The composition of supporting membrane materials was selected such that low-stress mechanical structures are achieved. Functional layers of the nanopores were altered in order to provide proper surfaces for the possible receptor immobilization techniques. Accordingly, nanopores were drilled in both non-passivated and perfluoro-alkyl passivated silicon-nitride and gold layers respectively (Fig. 1).

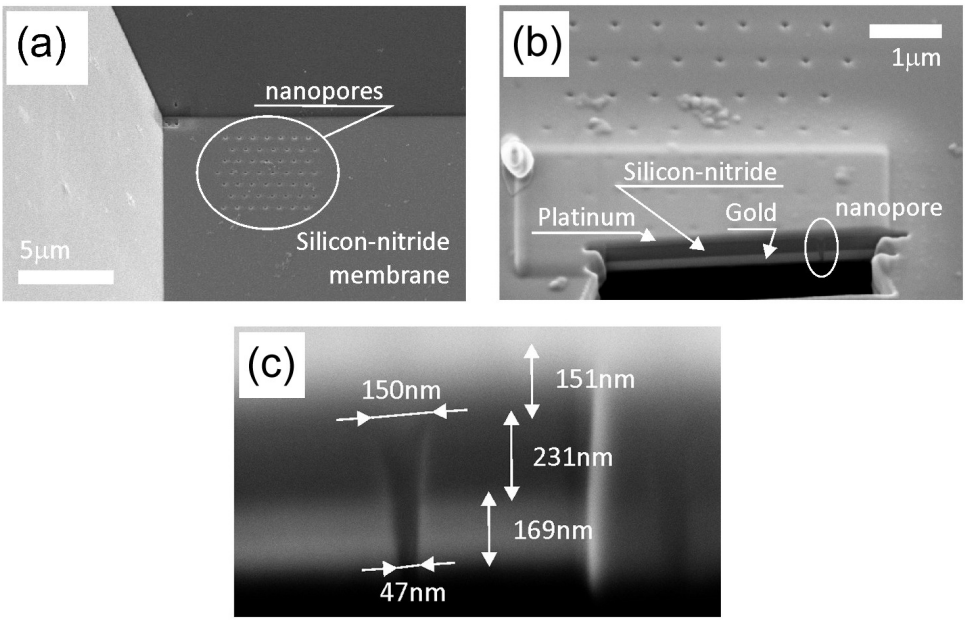

Figure 1. *(a): nanopore array fabricated in MEMS processed Silicon-nitride membrane. (b): the cross section of the membrane represents the layer structure, and (c): the nanopore geometry too.*

The multilayer membrane structures were developed by conventional MEMS technology including Low Pressure Chemical Vapour Deposition (LPCVD) of the supporting non-stoichiometric silicon-nitride (cca. 200nm thick), evaporation of titanium/gold layers (cca. 150nm thick) and anisotropic alkaline etching of silicon. The solid state nanopores were fabricated by Focused Ion Beam milling using accelerated Ga^+ ions applying different milling currents. The resulted nanopore membrane and geometry is demonstrated in the following Fig. 2.

The focused ion beam drilling process was characterized to establish a reliable fabrication technology regarding the accurate engineering of the pore geometry, particularly the pore diameter. The main issue was the tuning of the pore diameter by applying adequate fabrication parameters (milling time and ion current) in case of different material structures. The most interested membrane materials were the bare silicon-nitride and the gold covered Silicon-Nitride. To achieve the lower limit of the pore diameter 5pA and 10pA milling currents were applied. The measured average pore diameters plotted against the milling time in the case of different milling currents and membrane structures are shown in figure. Note, that the nanopore diameters could have significant uncertainty due to the nanoscale fabrication process influenced by the material behaviour and proper focusing of the ion beam. According to the previous experiments 5pA milling current were applied for 3 and 4 second to achieve the proposed pore geometry.

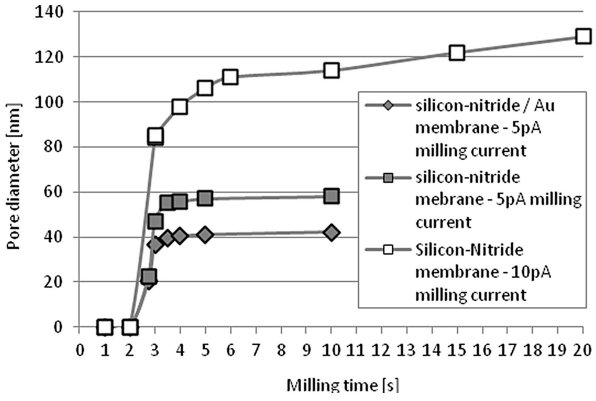

Figure 2. *The average pore diameter resulted by the ion milling of different layer structures as the function of the milling time applying 5 and 10pA ion current.*

Conclusions

The focused ion beam milling of micromachined membranes was characterized to establish reliable nanopore fabrication technology for nanoscale biosensing transducers. Bare and Gold covered Silicon-Nitride membranes were perforated by focused ion beam applying variable milling currents and times. The resulted pore geometries were analyzed to define optimal milling parameters, and statistical limits (as pore diameter accuracy) caused by the uncertainties of nanoscale processes such as beam convergence. The significant influence of the material composition was also clearly presented: the metallization of the dielectric membrane can improve the beam stability due to the reduced electrostatic fluctuations.

Integrated microfluidic environment for solid-state nanopore sensors

(ENIAC JTI CAJAL4EU, OTKA NF69262, János Bolyai Fellowship)

Z. Fekete, G. Huszka, A. Pongrácz, Gy. Jágerszki (BME), R. E. Gyurcsányi (BME), E. Vrouwe (Micronit), and P. Fürjes

The micro- and nanotechnology based biosensing principles open up new possibilities towards the development and realisation of robust, user-friendly and cost-effective in-vitro diagnostic platforms. Furthermore, label-free and multi-analyte detection is envisioned to allow more accuracy and higher throughput in clinical diagnostics. The bioanalytical systems are expected to integrate the nanoscale transducers with interface chemistry, and bio-receptors as well as the microfluidics, control software and hardware. The final goal of this work is to develop nanopore based multi-parametric biosensing platform, applicable for label-free detection of blood marker proteins of cardiovascular symptoms.

Combination of silicon micromachining and subsequent nanostructuring processes were applied to fabricate the transducer device. The fluidic vias, the channel system and the multilayer membrane structure were fabricated by MEMS technology including Low Pressure Chemical Vapour Deposition (LPCVD) of silicon-dioxide (SiO_2), non-stoichiometric silicon-nitride (SiN_x) layers, evaporation of titanium-dioxide and gold layers and multistep Deep Reactive Ion Etching (DRIE) of silicon substrate. The structural materials were extensively characterized by electrochemical impedance spectroscopy and fast chronoamperometry to provide a feedback on the electrical resistance of the mechanical multilayer being of crucial importance considering the electrochemical measurement method.

The realized silicon structure was anodically bonded to the glass microfluidics in wafer level. The final fluidic chips consisting nanopore membranes and vertical vias were mounted onto fluidic connection platform designed and realized by the Micronit Microfluidics (Fig. 1).

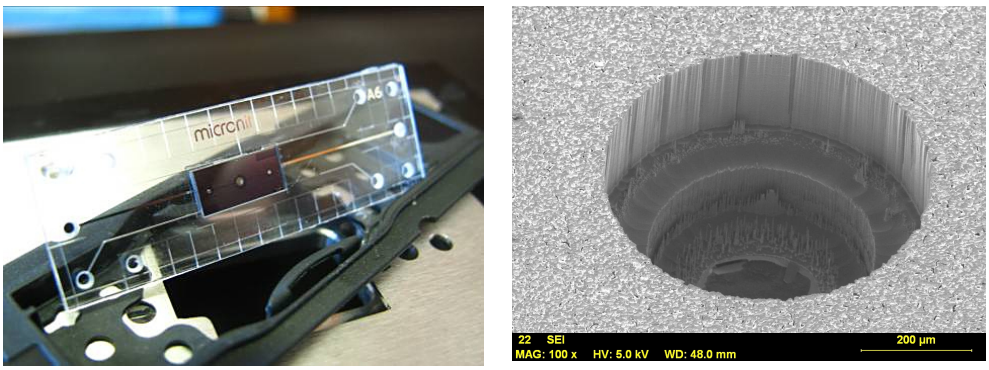

Figure 1. *The mounting realized microfluidic nanopore chips (left) with vertical fluidic vias (right) and the mounting onto the flow cell addressing the nanopores.*

The feasibility of the integrated microfluidics for nanopore sensing is characterized in terms of contingent shunting and proper sealing by impedance spectroscopy. Given the high resistance of the nanopore any leakage or shunting would prohibit the detection of specific changes of pore resistance. DC resistance of microfluidic channels and membrane without nanopores is measured (Fig. 2). The slight change in resistance of the membrane by increasing KCl electrolyte concentration suggests that 3D passivation of the microchip is necessary for improving sensitivity, however, channel resistance is clearly differs due to definite dependence on concentration. According to the preliminary measurements, the above microsystem is a good candidate for the detection of blood proteins in low concentration analytes.

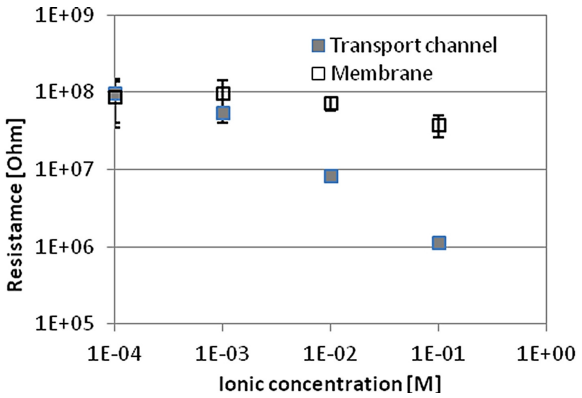

Figure 2. *Concentration vs DC resistance curve measured in the integrated transducer chip through the membrane and the transport microchannel.*

Conclusion

We described functional and design aspects of a silicon based solid-state microsystem consisting of fluidic interface, microfluidic components and nanoscale sensing transducers. The microfluidic system is proposed to cover the sample preparation (e.g. particle separation, mixing etc.) and precise transport, and facilitates the application of whole blood as well. In the further period of the development the main issue will be the proper 3D surface passivation of the whole microfluidic system, to achieve advanced and stabile chemical and electrical resistance of the channel surfaces.

Particle mixing by chaotic advection in polymer based microfluidic systems

(EU FP7 P3SENS, TÁMOP-4.2.1.B-11/2/KMR-2011-0002, TÁMOP-4.2.2/B-10/1-2010-0014 and János Bolyai Fellowship)

P. Fürjes, Z. Fekete, E. G. Holczer, E. Tóth, K. Iván (PPKE), and I. Bársony

The present work is intended to describe the functional aspects and working principles of special microfluidic structures applicable to dilute and transport real biologic sample (as whole blood) to the further functional parts of the sample preparation system or the sensing areas of biosensors. According to the preliminary expectations the fluidic layouts were designed consisting of advanced Herring-Bone type chaotic mixer systems and fabricated in PDMS polymer. The performance of the proposed mixer structures was characterized to optimise the main geometrical parameters of the microfluidic structures to support the design the final sample preparation system. The particle transport in the different mixer structures was visualized and analysed by numerical modelling to support the explanation of the experimental results and functional performance of the fluidic system.

The manipulation of fluids (e.g., biological samples as blood) in bioanalytical systems is a key issue in terms of the final applicability of these devices. According to the customers' requirement the developments aim to apply the simplest analyte at the inlet of the system as whole human blood in case of medical applications. In these novel analytical microsystems the sample manipulation is executed by complex micro-fluidic structures (Lab-on-a-Chip), integrating the main sample preparation tasks as dilution and mixing, blood plasma separation and precise transport also. To improve the performance of the proposed (Zweifach-Fung bifurcation effect based) blood plasma separation system the whole blood has to be diluted for an adequate haematocrite level, so diluting and mixing function has to be optimized also. The mixing possibilities are limited in microscale since turbulent flow cannot be built up due to the dominant viscosity. The chaotic advection could be an optimal mixing method in the case of the microfluidics considering stable and laminar flow in low Reynolds regime also.

Herring-Bone type chaotic mixers

"Herringbone" type chaotic mixer structures with various geometric parameters (Fig. 1) were characterized to reveal the motion trajectories and the mixing behaviour of the biological particles (fungi cells in this case) in the microfluidic systems. For revealing the hydrodynamic performance and behaviour of the different mixing structures the geometries parameters were varied as presented in figure (a: gap between the grooves, b: grove width, c: gap between the blocks, d: grove depth). The experimental microfluidic systems can be fabricated by Rapid Prototyping in PDMS, applying the SU-8 epoxy based negative photoresist as moulding replica developed

by a special multilayer technology. The figure also shows the fabricated SU-8 structure corresponding to the described "herringbone" structure.

The physical phenomena of the particle motions were characterized by mixing/interlocking fungi solution with phosphate buffered salt solution in the chaotic mixer structures. The particle traces were visualized by dark field microscopy (Fig. 2). The recorded light intensity scattered from the corpuscular particles can indicate the local concentration distribution of the fungi cells.

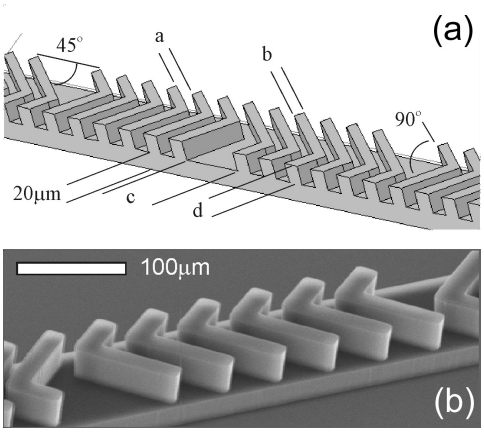

Figure 1. *Schematic structure of the Herring-Bone type microfluidic mixer (a) with the varied geometric parameters, and the multilayer SU-8 molding master (b) for PDMS structuring of the real fluidic channel.*

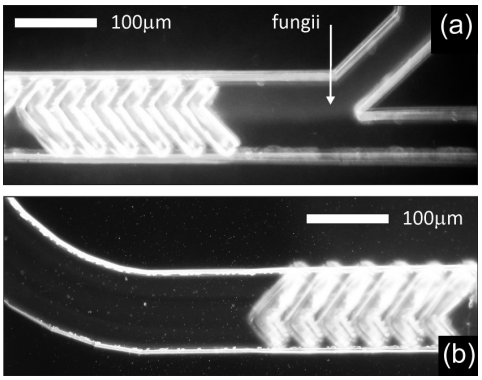

Figure 2. *Particle traces in the Herring-Bone type chaotic mixer structure ((a): inlet, (b): outlet) recorded by dark field microscopy.*

Fig. 3 presents the vertically integrated light intensity in the cross-sections of the "herringbone" type mixer channel at the inlet and the outlet planes referring the particle distribution.

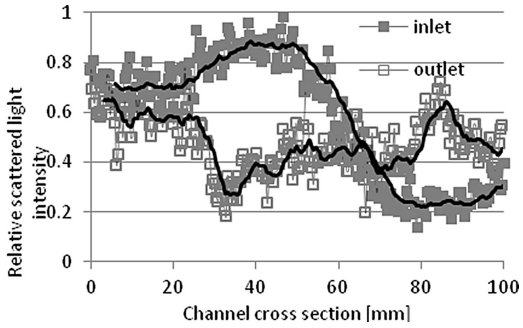

Figure 3. *The relative light intensity scattered from the fungi cells referring the particle distribution in the cross section of the herringbone mixer structure (inlet and outlet planes).*

The mixing process in the different microfluidic structures were analyzed and visualized by particle tracing calculated by Finite Element Modeling using COMSOL Multiphysics. The projection of the particle traces onto the plane perpendicular to the main flow direction is clearly present the mixing states evolving in the fluidic channel. The movement of the representative particles describes the mixing performance while passing through the structure.

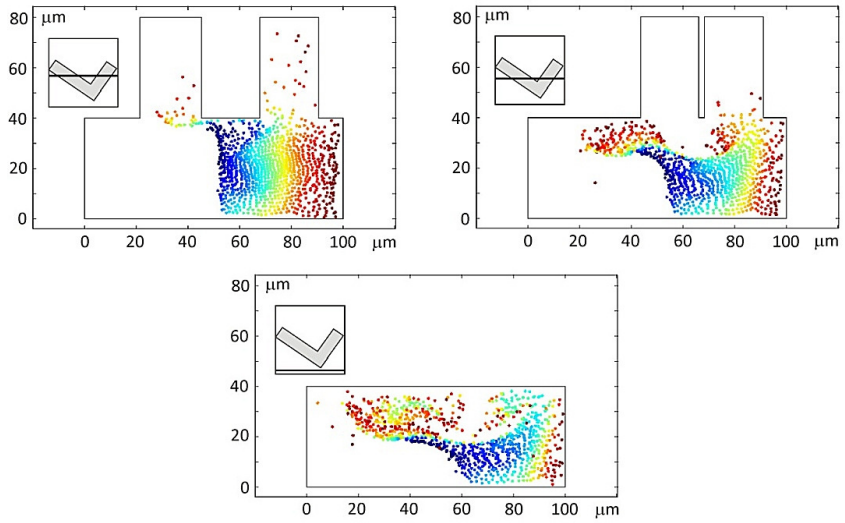

Figure 4. *The Poincare maps represent the particle mixing in the plane perpendicular to the channel direction evolving with the flow front.*

Conclusions

The mixing performance of Herring-Bone type chaotic mixers constructed with various geometric parameters were characterized by FEM modeling. The developing particle distribution in the microfluidic structures was visualized by Poincaré-maps considering the different geometries. The results of the simulations proved that for improving the performance of the mixer we should increase the depth, the number or the width of the grooves of the herringbone structure.

The results of the simulations were verified experimentally by recording the particle trajectories applying dark field microscopy. The experienced behavior of the Herring-Bone type mixer structures were in adequate accordance with the results of the simulations and the modeled trajectories of the individual particles could confirm the experimental results considering the main hydrodynamic effects as pressure gradients and shear forces.

Terahertz spatial light modulator with digital microfluidic array

(OTKA CNK77564 TERASTART)

P. Földesy (SZTAKI), Z. Fekete, T. Pardy, and D. Gergelyi

Generally, the terahertz (THz) spatial waveform modulators are able to control the transmission of an incident terahertz wave. Moreover, beam steering and focusing is also reachable by two-dimensional arrays of beam modulators. The monolithic integrated spatial modulators offer high modulation rate up to several megahertz, while usually limited to a certain resonant frequency or range with a limited switching value significantly less than 100%. Such modulators are the electrically driven terahertz metamaterial spatial modulators and reconfigurable metallic slits. Solid-state THz detector arrays are integrated in individual dies with a limited number of detectors per die due to the relatively long wavelength (0.1–3 mm). The spatially modulated illumination is a possibility to increase this spatial resolution in far field and near field cases (e.g. imaging using compressed sensing or resolution enhancement by structured light). Our proof of concept chip has been chosen from this field.

Droplet based modulation

We propose to utilize the high absorption of water for THz spatial modulation by means of programmable digital microfluidic droplet array. The water in liquid and vaporized form has high absorption coefficient with increasing value from 0.02THz to 30THz with several peaks. The droplet and electromagnetic wave interaction has been utilized in a different context as material analysis or dye laser frequency tuning architecture too. In the investigated sub-THz region this value varies in the range of 50-100 cm-1 with several peaks, which means that a few hundred μm water film constitutes almost total absorption. Our solution takes advantage of this phenomenon by using droplets to create “off” states in a controlled volume, thickness, shape, positioned in a regular rectangular grid. The platform of droplet positioning and movement is the droplet-based digital microfluidics. In digital microfluidics, discrete fluidic droplets are translated, mixed or stored on the surface of an array of electrodes coated with a hydrophobic insulator on within two such layers. The working principle of the droplet manipulation is the electrowetting on dielectric (EWOD). The common solution is to form two layers of hydrophobic substrates, in which the bottom plate is patterned by an array of controllable electrodes and the top plate is coated with grounding electrode. In our scheme, the top electrode must remain “transparent” to the THz radiation, hence a conductive electrode cannot be mounted. Such structure of single electrode plate is called co-planar structure with customized ground electrode system on the bottom plate only. Though the activation is higher than in the two conducting layer structure, the transparency is reached. The concept of modulation is presented in Fig. 1.

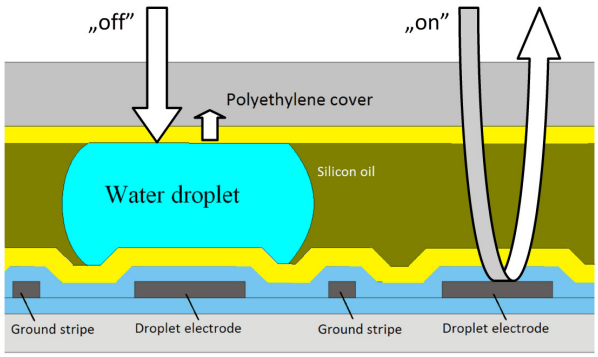

Figure 1. *Illustration of the modulation principle using highly absorptive water droplets and the cross-section of the coplanar microfluidic structure.*

The array was realized by silicon micromachining technology (Fig. 2). The initial substrate was <100> single-crystalline silicon wafer. On the bulk silicon, 1000nm thick thermally grown silicon-dioxide layer was applied. The electrode system was formed by lift-off technology. 300 nm thick aluminum film was deposited by e-beam evaporation and was patterned by conventional photolithography. The dielectric layer of the microfluidic chip is composed of silicon-dioxide and subsequently developed Teflon AF layer. 100 nm thick silicon dioxide was deposited by LPCVD process from silane and oxygen at a temperature of 435°C. Buffered HF removed the oxide from the electric contact pads. Finally, 500nm Teflon AF was spin-coated on the chip and dehydrated at 165°C on hot-plate to form a hydrophobic top layer. The top electrode of polyethylene is also covered with thick Teflon AF. The manufactured chip is shown in Fig. 3. The electrode pitch is 1700µm with 100µm gap, while ground lines in the gap are 20 µm. The droplet height was set in the experiments to 500µm. In spite of the fact, that the ground stripes are also covered by silicon-dioxide and hydrophobic layer (in contrast to co-planar structure, the chip enables very low voltage and stable operation (~60-70V, 10KHz).

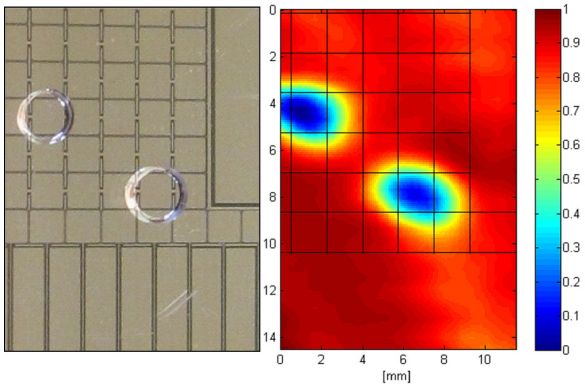

Figure 2. *Visual (left) and raster scan of two droplets in the array at 0.48 THz (λ = 620 µm) by focused irradiation (right) (spot size HWFM was 2.2 mm). The array pitch is 1700 µm, while the droplets had near 2 mm diameter.*

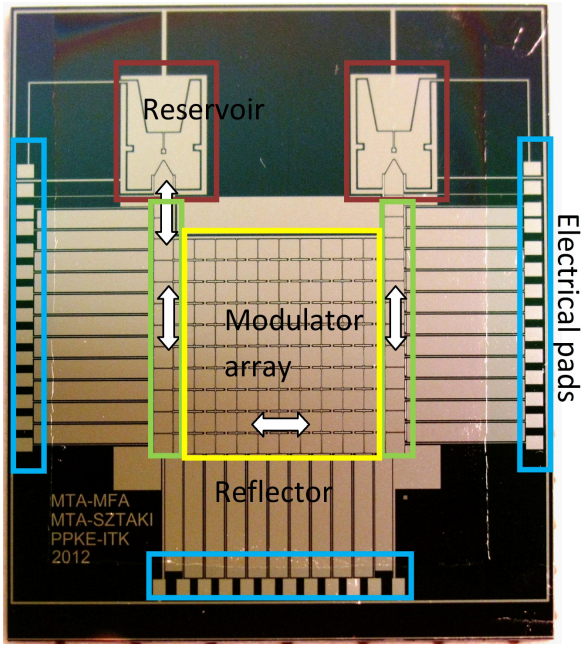

Figure 3. *10×10 pixel modulator digital microfluidic array.*

Results

The droplet translation architecture of the sample chip is designed for compressed sensing imaging applications. This imaging method is based on consequent randomly patterned illumination. First, one of the reservoirs is filled and closed and the vertical chain is driven to form a 1D droplet sequence. Next, the modulator array is used to move the shifted droplets horizontally towards the opposite side. These two steps are repeated, and the array is filled with changing sparse and orthogonal patterns (the fill factor is less than 1/9th in order to avoid droplet collision). The vertical chain of the other side is utilized to collect the droplets and store in the reservoir. Later on the direction of flow is changed to backward direction. A continuous wave VDI sub-THz source provides illumination in a quasi-optical setup. The sensor is a complex integrated CMOS based sensor with embedded amplification, lock-in detection and digital output streaming. For characterization purposes several droplet arrangements have been raster-scanned with focused beam. The droplets above near three free-space wavelength actuates as diffraction-limited near perfect black region, while the rest of the array had near complete reflection.

Neuro-MEMS - Deep-brain silicon multi-electrodes with surface-modified Pt recording sites

A. Pongrácz, G. Márton, Z. Fekete, and G. Juhász (ELTE)

Extreme-long (up to 70 mm) Si neural multi-electrodes and their fabrication technology were developed. Probes with different shaft lengths (15-70 mm) were formed by deep reactive ion etching and equipped with Pt recording sites of various configurations. *In vivo* measurements on rodents indicated good mechanical stability and robust implantation and targeting capability. The probes produced high quality signals from different locations of the cerebrum. The accompanied tissue damage was characterized by histology. Furthermore, by electroplating Pt onto the surface of the electrode sites electrical impedance reduction was achieved, the improved charge transfer capability was characterized by cyclic voltammetry.

Motivation

Micromanufactured Si- or polymer-based neural electrodes are frequently used for in vivo neural recordings close to the brain surface. To apply such silicon probes to access deeper (>1 cm) brain regions is highly unusual due to lack of appropriate devices. In our work we analyze whether much longer Si probes (up to 7 cm) can be manufactured using common MEMS processes. Using such dimensions the issues connected to mechanical and electrical behavior become critical, especially during implantation into the nervous tissue. Signal attenuation and signal-to-noise ratio are also determined by the electrochemical properties of platinum surfaces, which also have to be characterized.

Results

During the development of long Si probes a special fabrication method was worked out, the probes were characterized electrically, Pt electrode surface was modification in order to minimize its impedance and *in vivo* tests of the first extreme-long Si multi-electrodes were performed (Fig. 1).

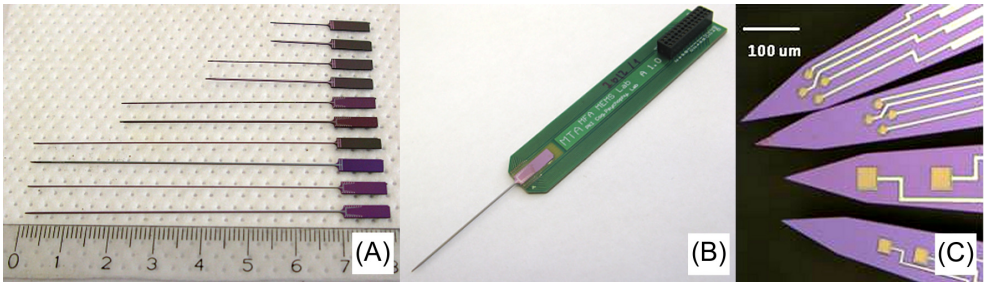

Figure 1. *A) Realized silicon deep-brain probes with 15-70 mm shaft length, B) Wire bonded multielectrode on PCB for acute in vivo testing, C) Different electrode designs.*

Various Si probes with 4-16 Pt recording sites have been created by MEMS technology: 15-70 mm long, 206 and 400 µm wide and 200 µm thick. Schematic step-by-step cross sectional view of the probe during the fabrication process is shown in Fig. 2.
Testing the devices *in vivo*, various, healthy activities could be recorded from rat cortical layers and hippocampus. Afterwards we revealed the injured cells around the implantation site with Gallyas ("dark neuron") staining procedure and found no abnormal cell loss (Fig. 3).

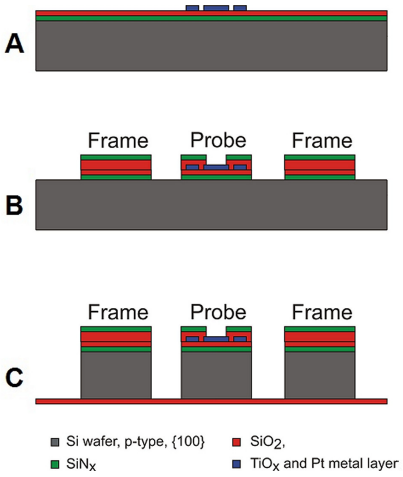

Figure 2. *Fabrication steps. Forming lower insulator and patterned metal layers (A), upper insulator layers, opened at the sites (B), silicon dry etching with Bosch process (C).*

Electrical characterization and surface modification of the Pt recording sites was carried out. Sufficiently low impedance of the electrodes is a key factor in obtaining good quality recordings.

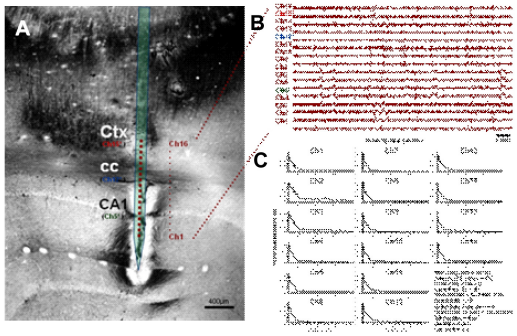

Figure 3. *Histological section, showing multisite silicon probe track and acutely injured "dark" neurons near the track (A). Representative depth profiles of local field potentials patterns (B) and their power spectral densities, which show diverse activities on different channels (C).*

Cyclic voltammetry with a 0.5 M H_2SO_4 solution was used in order to clean and validate the metal electrode surfaces and successfully increased their roughness factor from around 10 to 100s with deposition of Pt from solutions containing $PtCl_4$ and HCl in various concentrations. Our study revealed that even if the length of the multi-electrode is extreme (up to 7 cm) mechanical and electrical properties of the probe are good enough for high quality in vivo signal recording (Fig. 4).

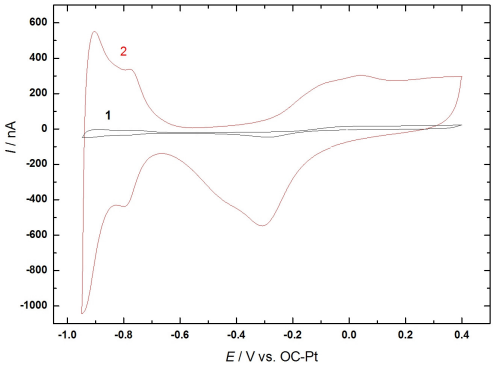

Figure 4. *Cyclic voltammograms of an electrode site before (black curve) and after (red curve) electroplating platinum.*

Deep-brain silicon multi-electrodes for simultaneous neural recording and drug delivery

A. Pongrácz, G. Márton, Z. Fekete, and G. Juhász (ELTE)

Silicon based deep brain multi-electrodes (up to 70 mm) with monolithically integrated microfluidic channels have been realized to perform electrical recording and drug delivery in deep brain regions at the same time. Fabrication process of the drug delivery channels and the Pt recording sites is presented here. Electrical characterization, impedance tuning, and *in vivo* testing of the probes is also presented. The functionality of the microfluidic channel is demonstrated and pressure-flow characteristic of the channels is discussed.

Motivation and results

During the last decade deep brain stimulation (DBS) has become a routine method for the treatment of advanced Parkinson's disease. DBS of selected brain regions can dramatically relieve tremor and rigidity. Multiple groups are attempting to extend this mode of treatment to dystonia, Tourette syndrome, variety of pain, depression, and obsessive-compulsive disorder. Simultaneous chemical and electric interactions with the very same groups of cells of an active brain might induce a huge progress in these studies. Long-term stability of electrophysiologic implants is to be enhanced with the help of continuous dosage of anti-inflammatory drugs. Micromachined neural probes

are widely used in electrophysiology and attempts are made to integrate drug delivery channels to them.
In our work the Si Microtechnology based fabrication method was developed, electrical and fluidic characterization and *in vivo* testing of the first silicon deep brain multi-electrode with monolithically integrated fluidic channel was performed.
Fabrication process and schematic view of the realized probes are shown in Fig. 1. Micromachining of the drug delivery channels take place in the bulk substrate and leave the substrate surface available for further processing. Various Si probes with 4-16 Pt recording sites have been created: 15-70 mm long, 206 and 400 µm wide and 200 µm thick.

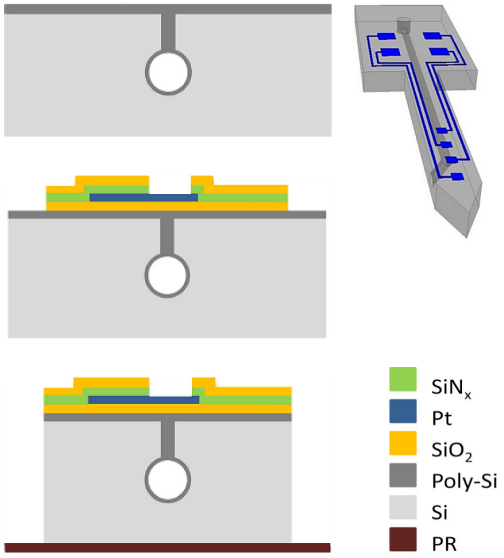

Figure 1. *Schematic view of the realized probes and simplified fabrication process (channel formation, SiO_2 insulating layer is deposited and Pt wiring is formed using conventional Al lift-off technique, LPCVD SiN_x/SiO_2 passivation layer stack is deposited followed by the opening of the recording sites, DRIE is used for the formation of the needle like body).*

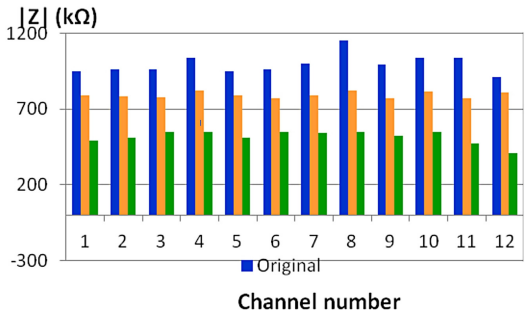

Figure 2. *Impedance values of the electrical channels of a probe. Average of original values: 998 ± 65 kΩ, after activation with 500 mV and 1000 mV amplitude, 0.1 kHz AC signals: 795 ± 19 kΩ and 517 ± 43 kΩ.*

Electrical characterization of the recording sites and impedance reduction was carried out in Ringer's lactate solution. Sufficiently low impedance of the electrodes is a key factor in obtaining good quality recordings. Controlled and monitored activation of Pt

recording sites were carried out, with a two-step process, a 48% reduction was achieved on the average (Fig. 2).
The fluidic microchannels were geometrically characterized by cross sectional SEM imaging; cross section of the channels can easily be tuned in the 5-30 µm range (Fig. 3). A Teflon© tube connection was established between the macro-pump and the microfluidic channel and pressure-flow characteristic of the channel was measured. DI water was pumped through the system with 0.6-1.9 µl/min flow rate, the channel sealing is capable to withstand up to 10 µl/s flow rate (Fig. 4).

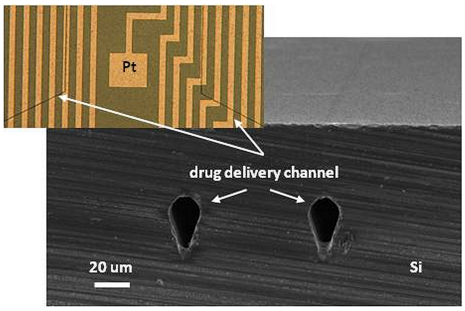

Figure 3. *Optical microscopy image of the Pt wiring and the silhouette of the channel closures and cross sectional SEM image of the monolithically integrated drug delivery channels.*

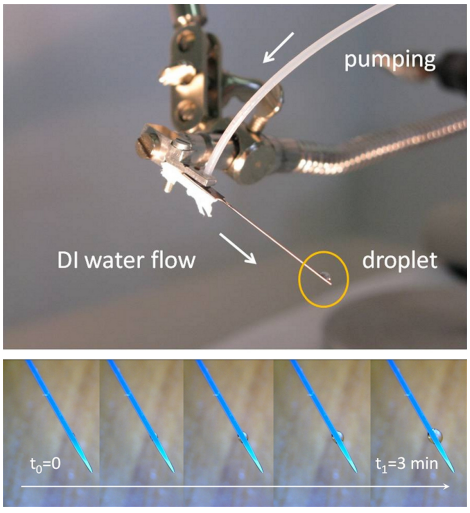

Figure 4. *Pumping DI water through the integrated drug delivery channel (top) Sequential photograph of a delivery of DI water (bottom).*

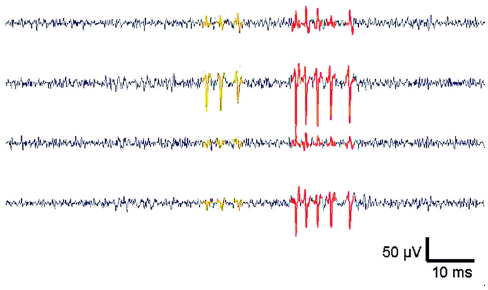

Figure 5. *Recording single unit activities of two different neurons in rat brain using four different channels of the deep brain silicon probe.*

Preliminary in-vivo testing of the novel deep-brain probes was carried out in rat brain (Fig. 5), where it can easily penetrate both the dura and pia mater and exhibit excellent performance in local field potential, multi-unit and single unit activity recordings.

THz Detectors

(OTKA CNK77564 TERASTART)

B. Szentpáli, G. Battistig, Z. Hajnal, and Cs. Dücső

In the frame of OTKA CNK77564 – TERASTART project Si based 3D micromachined small size thermopile device was developed and characterized.
The sensing mechanism of the device was characterized by full wave electromagnetic simulation. To reduce the calculation time the simulated model was simplified to a certain extent, the cross-section with the dimensions are shown in Fig. 1.

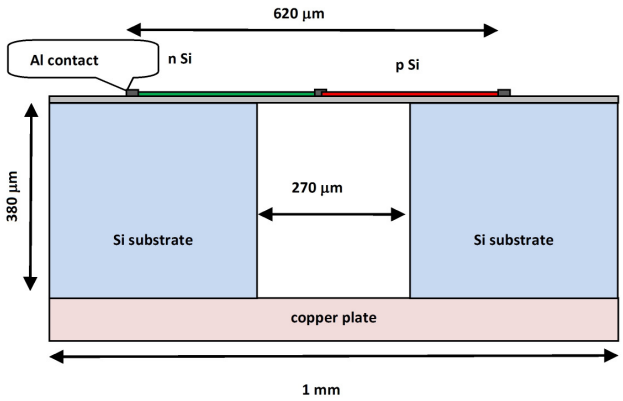

Figure 1. *The dimensions of the simulated structure. The poly Si strips are 10 µm wide and 0.4 µm thick, the spacing between them is 5 µm.*

The THz electric field was always parallel to the thermocouple lines and the value of the induced currents in the mid-point (in the Al contact) of the antenna strips were calculated as the function of the frequency. The value of the contact resistance was 1 Ω, roughly equal to the DC contact resistance. The complete structure contains 48 parallel thermocouple strips, which almost completely cover the slot in the substrate. The result of the simulation is shown in Fig. 2.

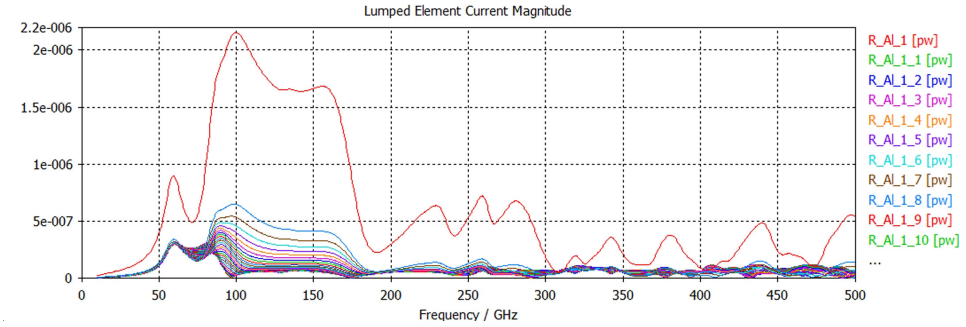

Figure 2. *The induced currents in the mid-points of the strips.*

Each strip line has its own individual current spectrum. The amplitude and the bandwidth of the first order resonance peak are higher at the sides than in the centre. In the centre part, the first order resonance peak is still the greatest but not dominant compared to the further resonant peaks at higher frequencies. It seems that the sensitivity of the central dipoles has an extremely wide bandwidth with a moderate first order resonance peak level while the thermocouples at the side parts have significant higher mode suppression with significant first order peak amplitude. Although it should be noted that even the highest resonant peak is only about ten times higher than the background. Simulation of the structure having a few less strips was performed and the result was very similar, the current in the outermost strip had a resonant peak, and these peaks decrease rapidly in the internal antennas. That is the peak is not due to the vicinity of the silicon substrate. The complete upper layer with the thermocouple strips behaves as conductor sheet.

The versions of the possible mounting were also investigated and compared to each other. Namely simulations were performed for the case when the chip is mounted on a dielectric plate (FR4 printed circuit board) instead of copper. These simulations resulted in higher currents in the central thermocouples, the average increment was 33%, and however in the strips at the edges this difference in mounting had no effect.

The experiments were performed in the broadband THz radiation, which was produced by the excitation of a non-linear crystal (LiN_bO_3) by ps laser pulses. Different equivalent chips (not that which is mentioned above) were mounted on copper plate and also on printed circuit board (FR4). The results are summarized in Table I. It seems that the average responsivities increase with the lengths of the membranes. This effect is similar to the infrared sensitivity. The average responsivities are about twice as high when they are mounted on the printed circuit board than the ones mounted onto the copper plate. This difference is somewhat higher than it was expected from the simulations, where the current was calculated to be about 33% higher in the case of using a dielectric plate instead of the copper in the model. Because the output thermal voltage is proportional to the absorbed power, i.e. the square of the current, an increment of about only 77% would be expected from the simulations.

Table I. *Responsivities to the broad-band THz radiation of four different chips mounted on conducting and dielectric holder. (Each structure contains 49 thermocouples.)*

Structure	**1**	**2**	**3**	**4**
length of the membrane [μm]	270	375	480	1400
Average responsitivity on Cu plate [V/W]	5.6	9.1	13.5	40.1
Average responsitivity on FR4 plate [V/W]	14.9	23.5	30.2	76.5

Electrical characterization of iron silicide nanostructures grown on Si(001) by scanning probe microscopy

Gy. Molnár, and L. Dózsa

Future generation thin film solar cells have to use abundantly available, non-toxic and environmentally friendly chemical elements. One of the possible candidates of that kind of materials is semiconducting β-$FeSi_2$, which has 23% theoretical efficiency in solar cells.

Preparation of artificial low dimensional structures is one of the most challenging research fields in the solid-state physics. Nanoobjects are prepared by physical and chemical or by combined methods and they have attracted huge interest, according to their scientific specificity and technical importance. One of the most commonly used method of nanostructures production is the phenomena of self-assembly, which has been applied in case of compound and group IV semiconductors in a wide range of material and substrate combinations. In case of self-assembly natural laws are used as tools to form nanostructures. The strain induced, self-assembled growth is a basic physical method of the preparation of nanostructures.

Iron silicide nanostructures were grown on p-type, 12-20 Ωcm Si(001) by strain-induced, self-assembly method. 1 nm iron was deposited by electron gun evaporation onto room temperature substrate at an evaporation rate of 0.01-0.03 nm/s and subsequently annealed in-situ in the vacuum chamber at 850°C for different times, between 10-50 minutes. The investigations have shown the development of nanostructure into different shape nanoobjects and reduction of Fe-related deep level defect concentration during annealing. These defects dominate the electrical characteristics of the nanostructures.

The electrical features were measured with conductive atomic force microscopy. Fig. 1(A) shows the morphology of the iron silicide nanostructure annealed for 30 minutes. The image was captured in tapping mode using 20 nm vibration amplitude. The root mean square (RMS) roughness of the samples annealed for different times increased as a function of the annealing time and it is large compared to the reference wafer. This fact indicates that together with the moderate lateral size enhancement a simultaneous emerging of height of the nanostructures occur during annealing as a consequence of the Ostwald ripening.

The current was measured in a contact mode using a 10 nm radius Pt coated silicon tip. The current image recorded at +1V bias in contact mode during the tapping mode scan is shown in Fig. 1(B). The average value of the current on the surface does not strongly vary during annealing, and it is only by 10% above the average current value measured on the silicon reference wafer. It indicates that the average current is dominated by the silicon substrate, i.e. the nanoparticles cover only small part of the surface. However, the RMS values of the current increase with annealing time and it can be about 5 times larger than the value measured in the reference silicon wafer. It shows that the current is strongly increased in a small – below 1 % - area of the surface. The current image statistics show that the current in the neighboring positions does not correlate, i.e. the increased local current is localized to areas below about 10-

20 nm. The current-voltage characteristics of the scanning probe tip-semiconductor junction were measured by sweeping the voltage from -1 V to +1 V, and the current through the tip. The I-V of the Fe-silicide nanostructure in two characteristic positions is shown as red and green plots in Fig. 1(C). It is apparent that in some positions a current is about 100 times larger. The I-V curves are reproducible in these samples.

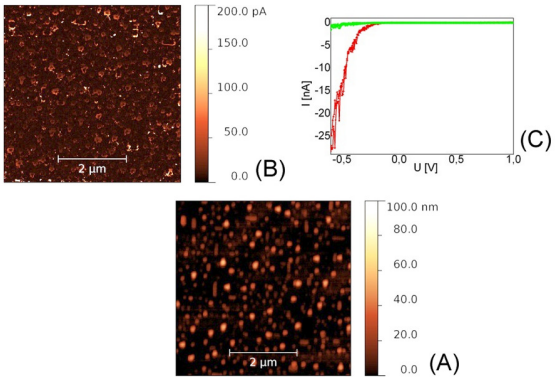

Figure 1. *(A) Tapping mode AFM image of the iron silicide nanostructure annealed for 30 minutes, (B) Current image recorded at +1V bias in contact mode during the tapping mode scan, (C) I-V characteristics of the tip-Fe-silicide nanostructure-semiconductor junction measured in two characteristic positions.*

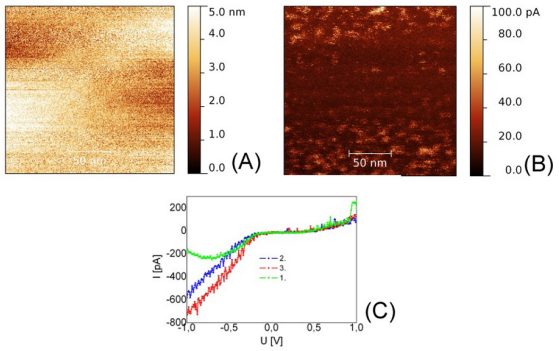

Figure 2. *(A) Tapping mode AFM image of the reference sample, (B) Current image recorded at +0.8 V bias in contact mode during the tapping mode scan, (C) I-V characteristics of the tip-reference semiconductor junction measured three times in the same positions.*

The morphology image of a 200×200 nm area of the reference sample and the current map of the same area, measured in the same scan are shown in Figs. 2(A) and 2(B), respectively. The tapping mode was performed using 20 nm vibration amplitude, and the current through the tip was measured at +0.8 V bias. It is worth mentioning that

the current map is much better structured than the morphology, also in this case, the increased current region sizes are typically around or less than 10 nm diameter, without similar structure in morphology map. We suppose this structure reflects Bohr radius of bound states on or near the surface. In other samples with different deep level defect we have found similar strong localization of the current, and in some cases is prevent collection of the current image in a reasonable time. For this reason we suppose the first step of the current flow – the electron leaving the tip and entering to the semiconductor – is to a localized (bound) state in the semiconductor, and it blocks the emission a second electron from the tip. We suppose the emission time of the captured carrier from this localized state basically determines tip-semiconductor current-voltage characteristics. Further theoretical work is needed to develop a model - usable in experimental work –to characterize this kind of transition.
The current measured in the reference sample (p-type silicon) during sweep of the voltage three times in the same position – marked in the figure by red, blue and green plots- are shown in Fig. 2(C). It is apparent that the I-V is changing during the repeated voltage scans. It is explained by charging of the surface state point defects or to possible chemical reaction of the wafer-air-tip system, which contains some reactive components, for example a monolayer of water, which is usually present on clean silicon in ambient conditions. It is remarkable that stability of the I-V curves is better in processed wafers, we assume due to large defect concentration.

Nucleation and epitaxial growth of atomic layer deposited ZnO

Zs. Baji, Z. Lábadi, and I. Bársony

ZnO has recently attracted considerable attention because of its versatility in a number of applications, such as sensors and photovoltaic devices. It can be doped with aluminum to increase its conductivity, and be used as transparent conductive oxide layer. The atomic layer deposition (ALD) method for ZnO deposition is widely known and has a great variety of applications. Atomic layer deposition of ZnO is commonly used on SiO_x and glass, where the ZnO growth is polycrystalline, and the structure and orientation depend on the deposition parameters. According to our earlier experiments the deposition temperature determines the dominant crystalline orientation of the layers: At lower temperatures (under 200°C) the dominant orientation is the one with the c-axis parallel to the surface, whereas at higher temperatures the c-axis is perpendicular to the surface. An epitaxial growth of ALD ZnO has been shown possible, but the initial growth mechanisms, the exact structure and the nucleation of ALD deposited ZnO films are unknown.
The theory of the ALD method suggests a layer-by-layer growth from the very first deposition cycle, but in reality nucleation issues may appear in this method too. We have examined the nucleation of ALD ZnO on Si, sapphire and GaN surfaces. The growth on GaN is in fact layer-by layer, and a full coverage is achieved already in the first 5 deposition cycles. In the case of Si surfaces an island-like growth occurs in the

initial phase. The initial growth of the layers could be enhanced applying a 100 times longer exposure to the precursors in the first deposition cycles (Fig. 1).

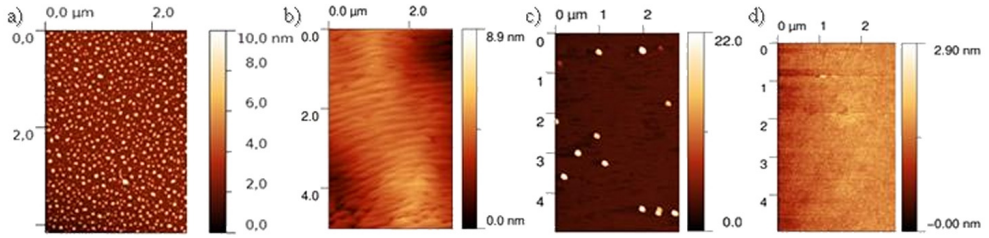

Figure 1. *The nucleation of ALD ZnO. a: island-like growth on Si, b: layer-by layer growth on GaN and a growth depending on the deposition temperature on sapphire: island like growth at 150°C (c) and layer by layer at higher temperatures (d).*

The deposition of epitaxial layers was attempted on GaN substrates at temperatures varying between 150°C and 300°C. The XRD measurements showed that the layers deposited under 270°C are oriented but polycrystalline; above this deposition temperature the layers were epitaxial. Reciprocal space mapping showed that the layers were high quality and without any strain. We also examined double layers with a thin epitaxial buffer layer deposited at 300°C, and a 40 nm top layer deposited at 220°C. This process also resulted in epitaxial layers.

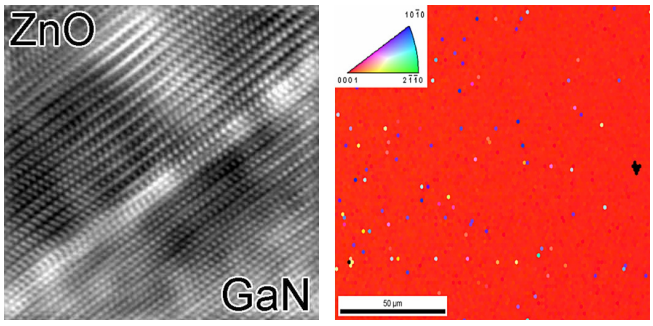

Figure 2. *High resolution TEM image taken on the sample deposited at 300°C (left), and the EBSD map of a doped layer (right).*

Epitaxial growth of aluminum-doped layers with Al contents up to 2 at% was also attempted. These layers are still highly oriented, continuous and uniform but they are not perfectly epitaxial any more. As the electron backscatter diffraction (EBSD) experiments showed, most of the surface of the doped layers is epitaxial to the GaN substrate, only small domains have the c-axis parallel to the surface (Fig. 2).
The resistivity of the epitaxial layers was in the order of magnitude of 10^{-4} Ωcm, with the mobility values between 80 and 200 cm^2/Vs and the carrier concentrations in the order of 10^{20} cm^{-3}. The lowest achieved resistivity was 8×10^{-5} Ωcm. The reason for

these excellent values is the diffusion of the Ga into the ZnO layer. Therefore the Al doping could not further reduce this resistivity.
Using the optimal growth parameters intrinsic n-type ZnO layers were also deposited onto Mg doped (6×10^{18} cm^{-3}) p-type GaN templates. The fabricated mesa structure showed **high quality diode characteristic**. Moreover, according to the **electro-luminescence** measurement the **p-n heterojunction** shows near UV emission at reverse and **near UV/broad VIS emission peaks at forward bias current** (Fig. 3).

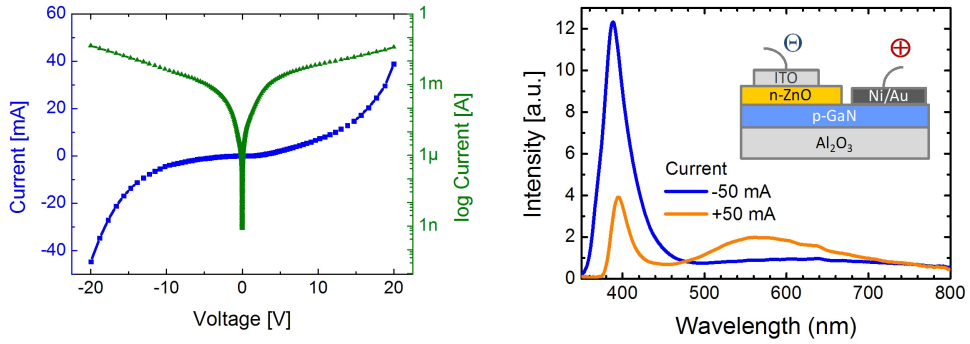

Figure 3. *Linear and logarithmic current-voltage plots of p-GaN/n-ZnO heterojuction (a, left). Light emission spectrum of the mesa structure (b inset) at reverse (blue) and forward (orange) bias current (b, right).*

The role of proximity effects in the nanopatterning of macroscopic surfaces by tunable ion-swelling

Zs. Zolnai, N. Nagy, E. Fülöp, A. Deák, and I. Bársony

Beyond conventional methods like photolithography or electron-beam lithography used to surface micro- and nanopatterning, ion beam proximity lithography as emerging technique can offer apparently a large variety of promising tools, providing both flexibility and precision even with sub-nanometer dimensional control. In this work, the role of proximity effects in the potential use of nanosphere lithography as an easy, fast, wafer-scale nanofabrication method is discussed. Ordered surface nanopatterns with different spatial periods and various characters were prepared on silicon surfaces by masked ion irradiation utilizing the local ion-swelling effect. Langmuir-Blodgett monolayers of hexagonally arranged Stöber silica particles as nanomasks were applied on large area Si substrates during Ar^{+} or Xe^{2+} irradiation exposure. We show that the height and curvature of surface swelling patterns can be tuned by appropriate selection of the particle diameter, ion energy, and ion fluence. We point out that, having knowledge on the diameters and average spacing between the silica particles as extrinsic beam spreading factors, and considering the lateral straggling of the bombarding ions in the mask and in the substrate material as

intrinsic beam spreading factors, a simple model of the radial fluence distribution can be applied to predict the main features of irradiation-induced surface patterns (Fig. 1). In general, the estimation of proximity effects is not only helpful in tailoring of surface morphology nanopatterns, but also in other processes, like magnetic patterning of metallic films with perpendicular anisotropy, or the laterally periodic doping of semiconductor structures (Fig. 2).

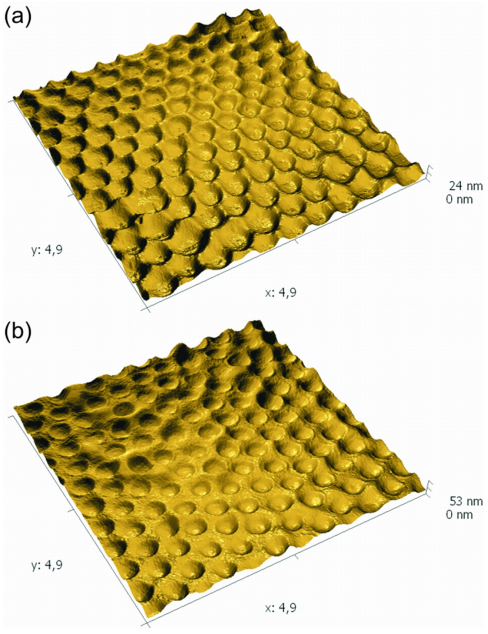

Figure 1. *AFM images of the Si surface after irradiation with 500 keV Xe^{2+} ions carried out at fluences of (a) 6×10^{15} cm^{-2} and (b) 2.4×10^{16} cm^{-2} through a mask of ordered silica particles with diameter of D=450 nm. After removal of the particles the morphology of the Si surface reveals inverse spherical character. The scales of the x and y axes are given in microns.*

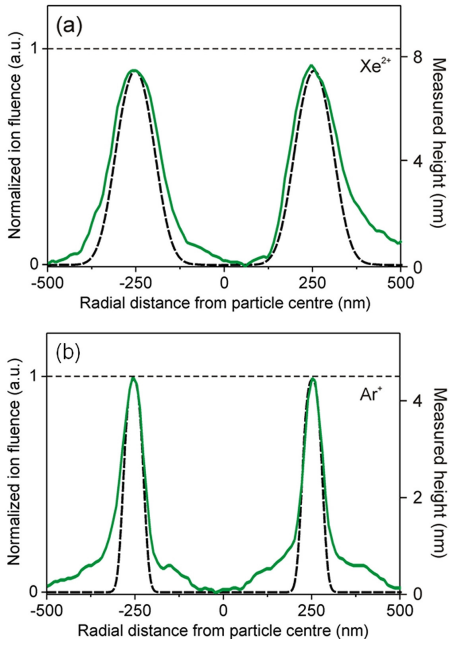

Figure 2. *Calculated (dashed lines) and measured (solid lines) AFM cross-section profiles of surface swelling patterns induced by (a) 500 keV Xe^{2+} and (b) 40 keV Ar^{+} ion irradiation into Si through LB masks of silica particles with diameter of D=450 nm. The role of proximity effects in pattern formation was considered in the calculations.*

Liquid Phase Epitaxy (LPE) of InP, InGaAs and InGaAsP for optoelectronic devices

V. Rakovics, and I. Réti

LPE is a simple but versatile technique which until recently was the mainstay of the fabrication of all optoelectronic devices. One of its advantages is the high growth rate compared with MBE and MOVPE which is important when it comes to the growth of relatively thick layers >1 μm. Thus LPE is eminently suited for the growth of PIN

photodiode and InGaAsP/InP LED structures. LPE layers have high luminescence efficiency due to the low concentration of non-radiative centers and deep levels. The composition of ternary and quaternary layers can be controlled in order to prepare lattice-matched heterostructures. In case of detector structures, one important requirement is that the intrinsic layer doping concentration has to be sufficiently low $< 10^{16}$ cm^{-3} for the layer to be completely depleted under the applied reverse bias. The growth of such high purity layers requires the use of very high purity Indium melts. The most common contaminant is Si, which is present both in the melt, in the polycrystalline sources of GaAs and InAs as well as in the fused silica furnace. Prolonged baking or addition of trace amounts of water vapour in the H_2 stream can reduce silicon contamination. We used computer controlled LPE apparatus with horizontal graphite sliding boat and semitransparent gold plated furnace. Precise control of the temperature and time of the growth, allow us to prepare very thin layers for laser diode fabrication (Figs. 1,2,3).

Here we shortly report the following structures:

- GaInAs/InP hetrustructure on semi-insulating InP wafer for integration with bow-tie terahertz antenna
- 1100 nm high brightness InGaAsP/InP LED structures with circular active region
- InGaAsP/InP pin photodiode with built in short pass optical filter
- DH laser structures for preparation of disk lasers
- Preparation of p-InP/nCdS hetrostructure

Layer structures:

- 0.2 mm undoped InP, 1 mm undoped GaInAs layer on InP:Fe subsrate
- 3 mm Sn doped n-InP, 1.8mm undoped GaInAsP (l_g 1100 nm), 6.5 mm Zn doped p-InP, 0.5 mm GaInAsP (l_g 1020 nm) on InP:S substrate
- 2 mm Sn doped n-GaInAsP, 3 mm Sn doped n-InP, 2 mm undoped GaInAsP, 6.5 mm Zn doped p-InP, 0.5 mm GaInAsP (l_g 1020 nm) on InP:S substrate
- 3 mm Sn doped n-InP, 0.2 mm undoped GaInAsP (l_g 1220 nm), 3.5 mm Zn doped p-InP, 0.5 mm GaInAsP (l_g 1020 nm) on InP:S substrate
- 60 nm CdS, 1500 nm p-InP on p^+ InP:Zn substrate

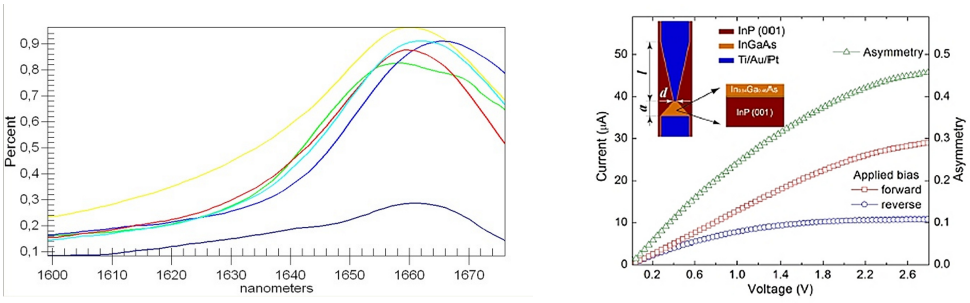

Figure 1. *GaInAs/InP hetrustructure on semi-insulating InP. (a, left): Derivative transmittance of InGaAs/InP wafers, (b, right): Asymmetric bow-tie terahertz antenna.*

GaInAsP/InP LED structures were prepared by dry chemical etching in Ioffe Institute. Device fabrication and characteristics of WGM lasers have not been finished.

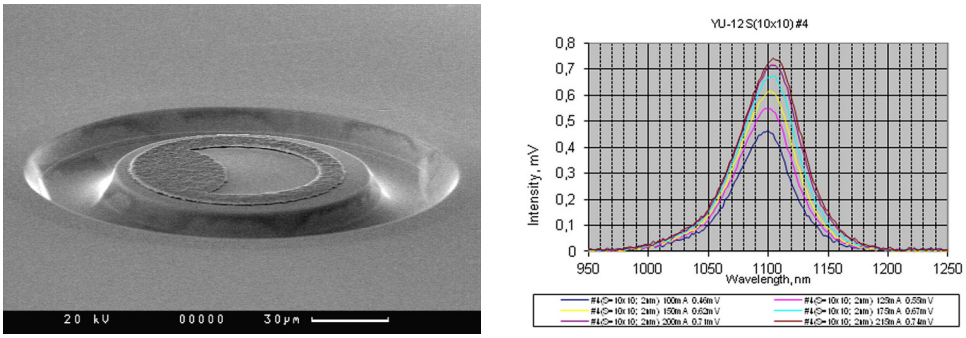

Figure 2. *(a, left): SEM picture of high brightness IR LED, (b, right): Emission spectra as a function of driving current.*

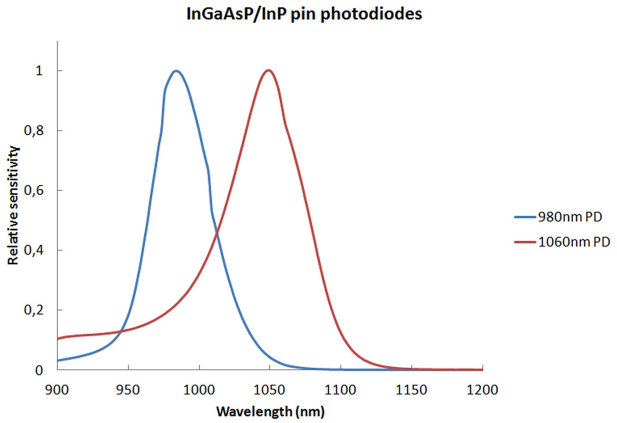

Figure 3. *Sensitivity spectra of two different wavelength pin InGaAsP/InP IR detector.*

Thin Film Physics Department

Head: Dr. János L. LÁBÁR, D.Sc.

Research Staff

- György SÁFRÁN, C.Sc., Deputy Head of Department
- Katalin BALÁZSI, Ph.D.
- Zsolt CZIGÁNY, Ph.D.
- László DOBOS, Ph.D.
- Sándor GURBÁN, M.Sc.
- Miklós MENYHÁRD, D.Sc.
- Fanni MISJÁK, Ph.D.
- Béla PÉCZ, D.Sc., Deputy Director
- György RADNÓCZI, D.Sc.
- György Zoltán RADNÓCZI, Ph.D.
- Attila SULYOK, Ph.D.
- Péter SÜLE, Ph.D.
- Lajos TÓTH, C.Sc.
- Viktória KOVÁCSNÉ-KIS, Ph.D. (on maternity leave from March 2012)
- András KOVÁCS, Ph.D. (on leave: Ernst-Ruska Center, Jülich)
- Olga GESZTI, M.Sc., guest
- Árpád BARNA, D.Sc., emeritus inst.
- Péter B. BARNA, D.Sc., emeritus inst.
- György GERGELY, D.Sc., emeritus inst.

Ph.D. students / Diploma workers

- Zsolt FOGARASSY, Ph.D. student
- Ákos Koppány KISS, Ph.D. student
- László KÓTIS, Ph.D. student
- János SZÍVÓS, Ph.D. student
- Lajos SZÉKELY, Ph.D. student (till March 2012)
- Eszter BOKÁNYI, M.Sc. student
- Tamás KOLONITS, M.Sc. student
- Klára NAGY, B.Sc. student

Technical Staff

- Andrea FENYVESI-JAKAB (replaced by Noémi Szász since 1 October 2012)
- Andor KOVÁCS
- István KOVÁCS
- Valéria OSVÁTH (replaced by Nikolett OLÁH since 1 November 2012)

As a continuation of the successful tradition, both preparation and characterization of 3D and 2D structures have been continued. Separation of phases and formation of texture was proved and explained for TiN/Si_3N_4 and CrN/Si_3N_4 coatings and CuMn systems. The etching rate of SiC nano coating (3-8 nm thick) produced by ion mixing as compared to that of polysilicon was found to be 10^{-3}. Single crystal Ni film was grown and epitaxial graphene layer was successfully deposited on its surface. Buckling of graphene was modeled. New nanostructured wide bandgap structures were synthesized and examined. Research on catalytic nanoparticles continued and new research was initiated in 2012 on FePt nanostructures aiming at denser magnetic recording. Unfortunately, 4 EU projects of the group ended in the previous year (2011). Substantial investment into scientific infrastructure would be needed to keep up with the fast-progressing instrumental development worldwide. (The improved

resolution of the new generation of C_s-corrected TEM has amounted to a change in paradigm.) In an attempt to combine the 50 yearlong experiences in the group with the possibilities of the new generation of instrumentation, young members of the group applied for short time grants and successfully used such experimental facilities to obtain results for home-based projects. For example, *Zsolt Fogarassy* prepared graphene by CVD on homemade Ni substrate and examined it with C_s-corrected TEM during his 2-month visit to Dresden. *Fanni Misják* studied homemade CuMn samples with new C_s-corrected TEMs in Jülich and Nagoya (2-2 weeks). In Linkoping with C_s-corrected TEM *Zsolt Czigány* studied CN_x structures during a 1-month stay, while *György Zoltán Radnóczi* prepared and examined semiconductor structures in a half-year stay. The experimental possibilities of the group were temporarily enhanced, thanks to the help of the NanoMegas company, who loaned us free of charge a precession system for the TEM on the condition that one Ph.D. student (*Ákos Kiss*) further develops a method for grain boundary characterization with the help of this tool. Further investment into both preparation and characterization scientific instrumentation is a must to continue our successful tradition.

As a recognition of his previous results, *J. L. Lábár* was invited to act as co-author of the prestigious monograph "International Tables for Crystallography Vol. H: Powder Diffraction" in the chapter "Electron Diffraction". The manuscript has been refereed and is expected to appear in 2013.

The research group published 25 papers in refereed journals in 2012 with cumulative impact factor of 58.586 and 14 papers in conference publications. The members of the group presented 8 invited lectures, 22 oral talks and 27 posters at international conferences. The group received **1248** independent citations in the examined interval. The members of the group refereed 21 project proposals, 5 dissertations, and 47 scientific papers.

Two members of the group lectured special subjects for full semesters at ELTE and 4 members hold laboratory practices for full semesters (ELTE, BME and Kassa). Additionally 12 weeks of summer practice and special labs were also conducted. In addition to the 4 Ph.D. students, 3 diploma workers were also supervised.

Social activity of the group is landmarked by awards (the prestigious "Fizikai Fődíj" of MTA and "Schmid Rezső Díj" of ELFT) 19 memberships in different committees of the Academy and OTKA and boards of societies, organizing 3 European conferences, editing a journal and an IOP conference volume and giving 2 elected representatives to the General Assembly of the Academy.

Formation and properties of self-organized diffusion barrier layers

(OTKA K18808)

F. Misják, Zs. Czigány, K. Nagy, O. Geszti, J. Lábár, and Gy. Radnóczi

As the continuation of the project further Cu-Mn alloy nanocomposite films were grown by simultaneous UHV DC sputtering of Cu and Mn targets for precise elaboration of the non-equilibrium phase diagram and determination of compositional boundaries of the existing phases. The films were grown in the temperature interval of 20-600 °C either on thin carbon substrates, suitable for direct investigation in TEM or on oxidized Si wafers, which could be investigated in TEM after ion milling. The investigation of the Cu-Mn model system has been also continued for clarifying the processes of structure formation as well as the characteristics of the formed structures. In room temperature films the composition dependence of the observed grain size of the films has been measured. It shows a parabola like function with grains in the nm range for all compositions, and having a minimum of 2-3 nm grain size at 45 at% Mn (Fig. 1).

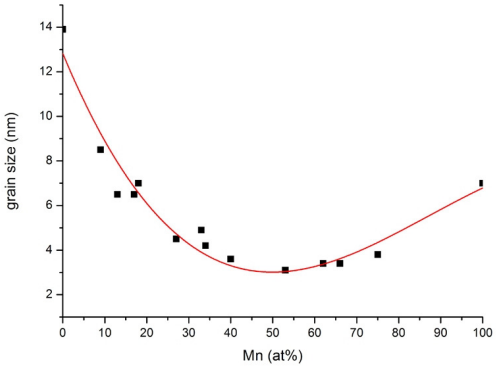

Figure 1. *The size of coherently scattering regions as measured from electron diffraction line broadening as the function of composition.*

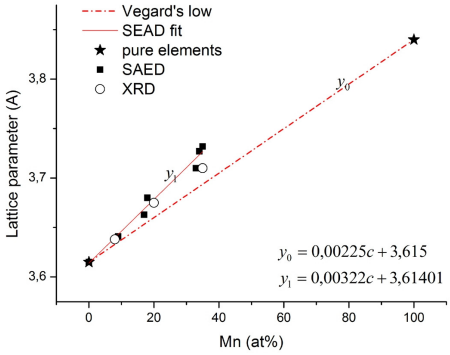

Figure 2. *The variation of the lattice parameter in fcc Cu-Mn solid solution films.*

Similarly, the composition dependence of the lattice parameter was measured in the range of the Cu base fcc solid solutions where Mn<40 at%. The lattice parameter is increasing with increasing Mn content and its growth is faster than expected from the Vegard's rule as shown in Fig. 2 [36]. At Mn concentrations of 45-65 at% the films are practically amorphous. For films containing 65 at% Mn we have shown their short-range order to be characteristic to that of α-Mn [Process Diffraction].

For further characterization of the system 1 μm thick films have been grown. We could show that the excess Mn atoms are located in the grain boundaries of the fcc Cu-Mn solid solution grains. The 40 and 65 at% Mn samples are of typically amorphous nature with some inhomogeneity in the Mn distribution [Measured by Fanni Misják at Ernst-Ruska Microscopy Center, Jülich, and at Nagoya University, Japan]. These examinations needed a lot of efforts and care due to high oxygen affinity of the samples. Due to the difficulties of ion milling the cleaving method of sample preparation for electron microscopy has been also attempted. This proved to be rather laborious and will be continued in a BSC diploma work [Tóth Réka - supervisor F. Misják].
For understanding the diffraction patterns of the 65 at% Mn samples, computer simulations of the scattered intensity distributions have been carried out [by Materials Studio Program]. The best fits and interpretations were obtained for superposition of nm grain α-Mn and textured MnO (Fig. 3). When in the diffraction patterns we observed the presence of MnO, the question of the location of MnO in the films has been arisen. For determination of the distribution of oxygen or MnO in the films ToFSIMS measurements were performed [measured by András Vincze, Bratislava]. The measurements have shown that MnO is present in the form of surface layers, so the internal structure of the films is not affected by oxygen incorporation.

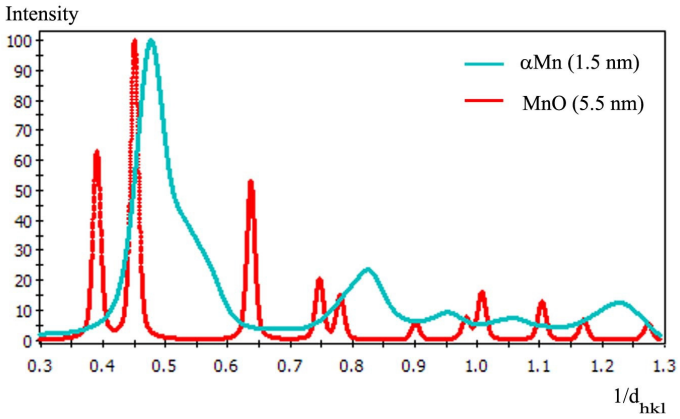

Figure 3. *Simulated diffraction pattern of Cu-Mn alloy (65 at% Mn) film.*

In films grown at elevated temperatures (450 °C) two phases were identified in the whole composition range: the fcc Cu based solid solution and a Mn based solid solution, which could be identified from electron diffraction simulations as a tricklinic phase [Kolonits Tamás, B.Sc. diploma work and 2nd place at the ELTE student competition - supervisor Zs. Czigány].
The authors acknowledge the financial support of the Hungarian National Science Foundation under the grant number of OTKA K81808. F. Misják and Zs. Czigány acknowledge also the support by the János Bolyai Research Scholarship of the Hungarian Academy of Sciences.

Relation between microstructure and hardness of nano-composite CrN/Si_3N_4 coatings obtained using CrSi single target magnetron system

J. L. Lábár, Zs. Fogarassy, J. Morgiel (Krakow), J. Grzonka (Krakow),
R. Mania (Krakow), and S. Zimowski (Krakow)

A search for new coatings, which would show substantially improved mechanical properties over columnar TiN that dominates the cutting tool market at present, drew attention to mixed amorphous-crystalline TiN/Si_3N_4 type structures. Veprek, who reported the highest hardness for coatings from that group, claims that in addition to the composition, the second most important condition necessary to obtain a super-hard class material is that contamination with oxygen must be avoided [S. Veprek at al.: Surface and Coatings Technology 200, 2006 3876-85]. It was also stressed, that extreme hardness can only be expected for nano-composites in which the TiN crystallites are covered with just a one-mono-layer, i.e. extremely small amounts of amorphous Si_3N_4 [S Veprek at al.: Surface and Coatings Technology 133-134, 2000 152-9].

The application of simple single target magnetron systems for deposition of nano-composite coatings is hindered by the difficulties of preparation of proper targets. Usage of compacts sintered from elemental powders allows a more precise control over coatings compositions as a sputtering practically replicates the target Cr:Si ratio of the target in the layer. Using such targets one has to accept their high oxygen contamination. Experiments showed that for deposition performed on substrates at 600 °C the change from crystalline to amorphous microstructure takes place between 30 and 40 at. % Si [E. Martinez et al.: Thin Solid Films 447-448, 2004 332-6]. This means, that in single target systems the transition takes place at much higher silicon contents than in coatings deposited using double magnetron sputtering or hybrid arc ion plating and sputtering systems, showing such change in microstructure at ~3 and ~10 at. % Si, respectively. Only deposition performed at ambient temperatures produce nano-composite microstructure starting from 20 at. % Si and fully amorphous one at 40 at. %. Here we show that it is also possible to obtain a nano-composite microstructure with chemically segregated components, when CrSi targets with high silicon content are sputtered on substrates kept at high temperatures. Second, we verified that hardness is improving when a nano-crystalline microstructure is substituted with a nano-composite in which crystallites are separated by thin layers of an amorphous material.

We deposited coatings through magnetron reactive sputtering of $CrSi_x$ compound targets having 10, 20, 30, 35 and 40 at. % of silicon in nitrogen-argon gas mixture with base pressure $<5*10^{-3}$Pa on substrate at 600 °C. Both cross sectional and lateral samples were prepared for TEM and energy filtered TEM (EFTEM). HRTEM and electron diffraction (SAED) showed that by increasing the Si content to 30% and above an amorphous phase appeared and its fraction increased with increasing Si content. Fig.1 shows that the sample with 35% Si is a nanocomposite with

nanocrystals enriched in Cr and an amorphous tissue phase enriched in Si. The structure of samples with the lowest Si content is crystalline, while the 40% Si sample is amorphous. Correlation of the structure with hardness measurement confirms that the hardest samples are those with nanocomposite of nanocrystals surrounded with a thin amorphous phase. (The amorphous phase in the 30% Si samples was too thin to record elemental maps with EFTEM.)

The microstructure of coatings deposited from $CrSi_{35}$ targets on substrates kept at 600 °C was the closest to the model nano-composite, i.e. equiaxed crystallites separated by small amount of amorphous material. Additionally, it was shown for the first time, that also in these coatings (deposited at high temperature) the segregation of chromium and silicon indeed takes place to crystalline and amorphous phase, respectively.

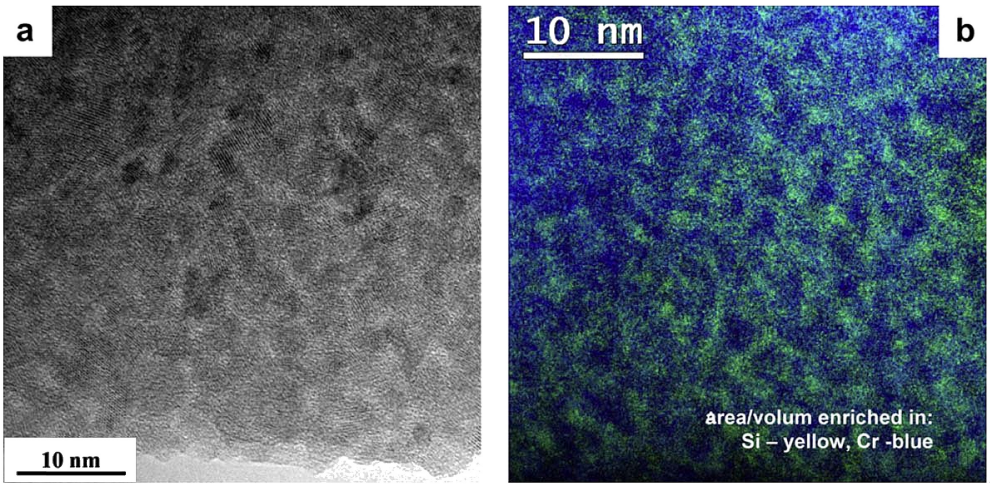

Figure 1. *HR TEM image of microstructure (a) with corresponding composite map with distribution of Cr and Si (b) in coating obtained from $CrSi_{35}$ target deposited at 600 °C.*

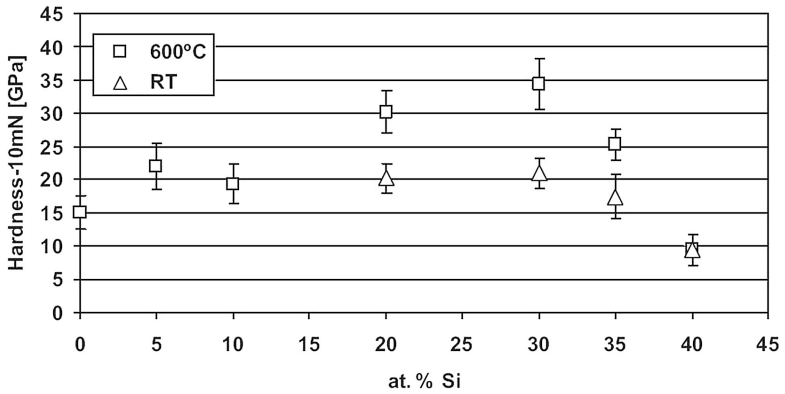

Figure 2. *Hardness of coatings deposited on silicon substrates at RT and 600°C as a function of composition of targets from which they were deposited.*

The DFT and molecular dynamics multiscale study of the corrugation of graphene on Ru(0001): the unexpected stability of the Moiré-buckled structure

P. Süle

It has been accepted in the last years that graphene exhibits various curved or buckled nanostructures and the perfectly flat form of graphene occurs in nature rarely. The magnitude of the out-of-plane distortion is under serious debate [M. Batzill: Surface Science Reports, 67, 83, 2012]. The potential applications of the non-flat graphene are unclear yet. One research direction is emerged in which the tailored opening of the band gap in graphene-nanostructures should be obtained (gap engineering) in order to construct graphene-nanotransistors. The corrugation leads to band gap opening, but still not in a controlled manner [A. O'Hare, et al.: Nano Lett., 12, 1045, 2012].

The buckling of graphene can be analyzed by various microscopy methods (STM, HRTEM, AFM). However, the detailed analysis of the results is challenging and theoretical explanations are needed. It has been well established in the last decade that the best way for understanding nature is to use the unified approach of the *experimental-simulation-theoretical* way of research. Theory can be rigorously understood as phenomenology (e.g. the theory of membranes or continuum mechanics can be applied for graphene). My research work covers mostly computer simulations, which can also be taken as computer experiments. Numerical computer simulations have become standard approaches for nowadays since large-scale program codes have been developed (e.g. LAMMPS, CP2K). Using these codes various properties of graphene can be reproduced or predicted (e.g. elastic, thermal conductivity or structural properties, real time simulations, time development, DFT: band structure, charge distribution, adhesion, etc.) (Fig. 1).

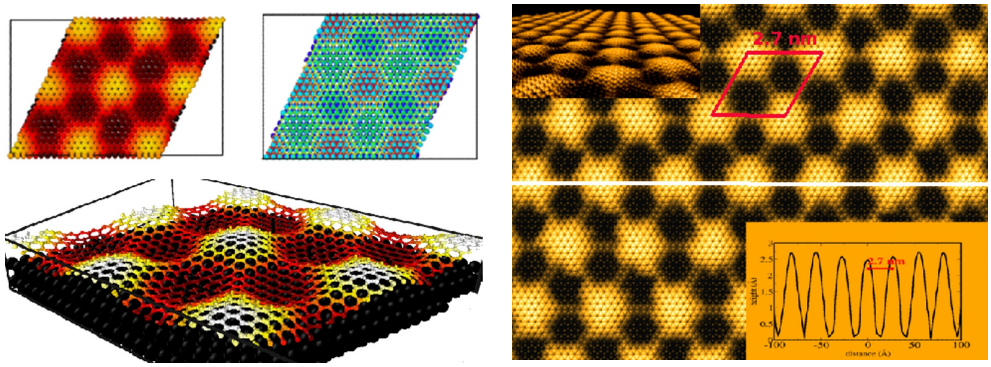

Figure 1. *Graphene superstructures on Ru(0001): (a) (left) a rhomboid supercell, (b) (right) an extended system as obtained by CMD simulations. The moire-humps are well recognizable.*

The accurate simulation of nanoscale corrugation is still challenging, however. Adequate empirical force fields for graphene-support interfaces are not available, unfortunately, especially, which are able to describe properly Moiré-superstructures. My last year work focused on the development of an adequate interfacial force field for the prototypical graphene on /Ru(0001) system. The obtained new parameters enable us to model the recently discovered pseudo-magnetic nanobubbles [N. Levy, et al.: Science, 329, 544, 2010]. Nanobubbles occur under compressive stress or by the enrichment of defects [J. Lu, et al.: Nature Commun., 3, 823, 2012] and the controlled production of them offers great promise for the development of graphene-nanotransistors.

Results from first principles density functional theory (DFT) calculations and classical molecular dynamics (CMD) simulations are presented on Moiré-corrugation of graphene. We find that the Moiré-corrugated graphene could be surprisingly stable against the perfectly flat graphene-sheet as pointed out by CMD simulations and DFT calculations. We also show that using the cost-effective CMD approach one can simulate graphene on e.g. Ru(0001) with a correct binding registry and reasonable corrugation and adhesion energy. A new force field has been parameterized for the interface using an angular-dependent Tersoff potential. The newly parameterized Tersoff interface potential provides correct Moire superstructures in accordance with scanning tunneling microscopy images and with DFT results. Based on *ab initio* DFT calculations, we also find that the CMD Moiré superstructure can be used as a preoptimized structure for DFT calculations and for further geometry optimization. The nearly flat graphene (the corrugation $\xi \approx 0.02$ nm) on Ru(0001) is slightly energetically unfavorable vs. the Moiré-corrugated graphene-system ($\xi \approx 0.2$ nm) as revealed by Van der Waals DFT structural relaxation.

Investigation of grain boundaries by HRTEM

Á. K. Kiss, and J. L. Lábár

Many properties of polycrystalline materials are influenced by the geometry of the interfaces between the grains. This is why it is important to characterize the geometry of grain boundaries (GB) by using high resolution TEM (HRTEM).
We try to tilt the sample to an orientation when both neighboring crystals can be seen with lattice resolution simultaneously. A computer program has been written that gives advice if such orientation exists at all and if so, it specifies the goniometer tilts needed to reach that orientation. For optimum scenario, the GB-plane should also be parallel to the electron beam. For a less favorable case, both grains are imaged with lattice resolution, but the GB-plane is tilted to the beam, resulting in Moiré-patterns in the projection of the plane. Starting from a random orientation of the sample, the crystallographic orientations of the grains can be determined from two different ways: convergent beam electron diffraction (CBED) can be taken on the neighboring crystals for calculating the orientation one by one, or a scanning tool installed on the TEM can be used to get an orientation map from the area of interest. Two examples are given here for the application of the program: a cubic (Ag) and a non-cubic (Al2O3) polycrystalline sample. Without any tilt, the grains were far off-zone. We used a double tilt sample holder that allowed ±20° tilt at the maximum. Fig. 1 shows the BF images and the CBED patterns of the grains before and after the tilt and confirms that correct zone-axis orientations were reached.

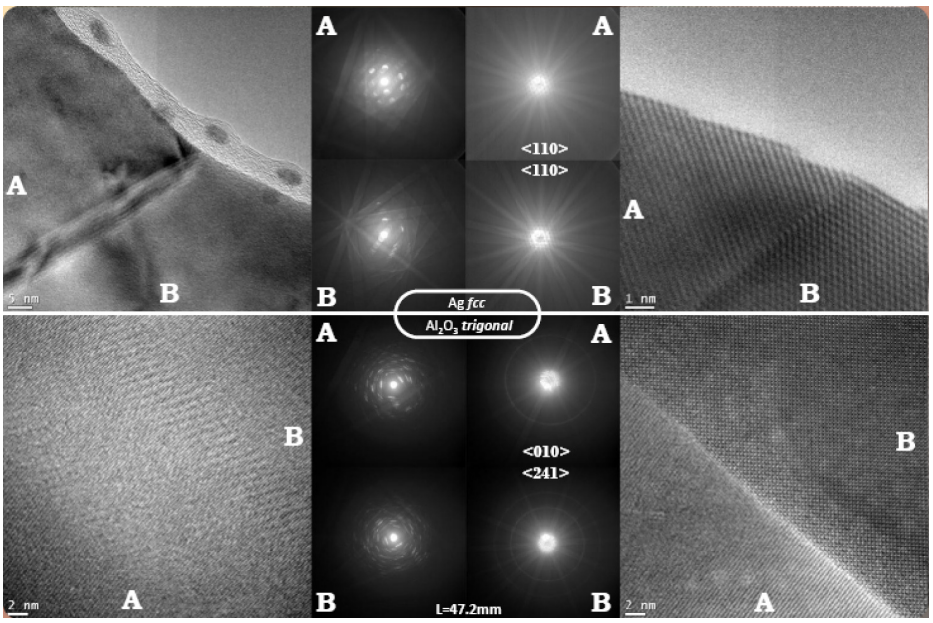

Figure 1. *Ag (top) and Al_2O_3 (bottom) samples are shown before (left side) and after (right side) the tilt. In both cases a grain boundary is present; the neighbouring grains and the corresponding CBED images are labelled by "A" and "B".*

Microscopy of ZnO layers deposited by ALD

(OTKA K75735)

B. Pécz, Zs. Baji, Z. Lábadi, and A. Kovács (Jülich)

ZnO layers were deposited onto sapphire and GaN substrates, by ALD (Atomic Layer Deposition) at 300 °C without any buffer layer. The layers were characterized by transmission electron microscopy. The ZnO layer on sapphire was found polycrystalline, what is explained by the large misfit and by the low deposition temperature. The ZnO deposited on GaN was single crystalline due to the low misfit.
The layer deposition took place in a Picosun-Sunale R-100 type ALD reactor. Diethyl Zinc (DEZ) and water were used as precursors for growth of ZnO. The deposition was carried out at 300 °C and the nominal thickness of the layers was 40 nm.
An overview of a typical layer grown on sapphire is shown in Fig. 1. The domains seen in Fig. 2 are about 80-100 nm long (twice of the layer thickness). The contrast of the neighbouring grains is quite similar. When this layer was investigated in detail in high resolution a perfect epitaxy between hexagonal ZnO layer and the GaN substrate was observed. The misfit in this configuration is about 1.8%, far smaller than was in the case of sapphire substrate. It can be clearly seen, that ALD can provide crystalline and even single crystalline thin layers of ZnO on different substrates

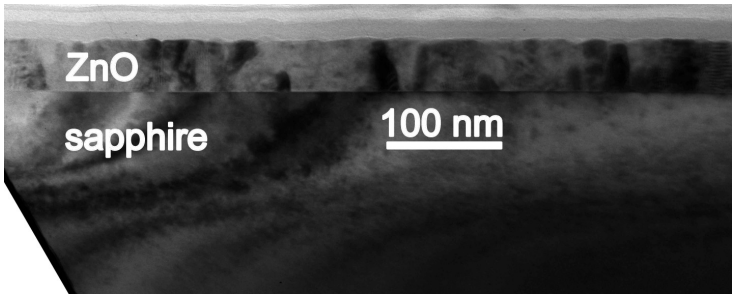

Figure 1. *XTEM micrograph of ZnO layer grown on sapphire at 300 °C showing a contrast that suggest a polycrystalline nature of the laterally homogenous layer.*

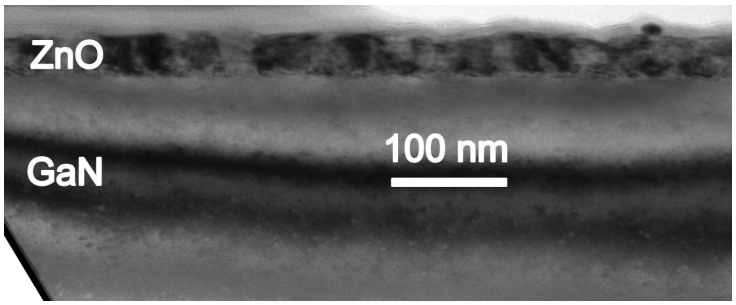

Figure 2. *XTEM micrograph of ZnO layer grown on GaN at 300 °C. Large domains can be seen, which propagate through the whole thickness of the layer.*

GaN films grown on (111) diamond with AlN buffer

(OTKA K75735)

B. Pécz, L. Tóth, Á. Barna, G. Tsiakatouras (FORTH), A. O. Ajagunna† (FORTH),
A. Kovács (Jülich), and A. Georgakilas (FORTH)

Hexagonal GaN films with the [0001] direction parallel to the surface normal were grown on (111) oriented single crystalline diamond substrates by plasma-assisted molecular beam epitaxy. Pre-treatments of the diamond surface with the nitrogen plasma beam, prior the nucleation of a thin AlN layer, eliminated the inversion domains and reduced the density of threading dislocations in the GaN epilayers. The films have an in-plane epitaxial relationship $[10\underline{1}0]_{GaN}[110]_{diamond}$. Thus GaN (0001) thin films of single epitaxial relationship and of single polarity were realized on diamond with AlN buffer.
Fig. 1. shows nitride layers grown onto diamond without nitridation.

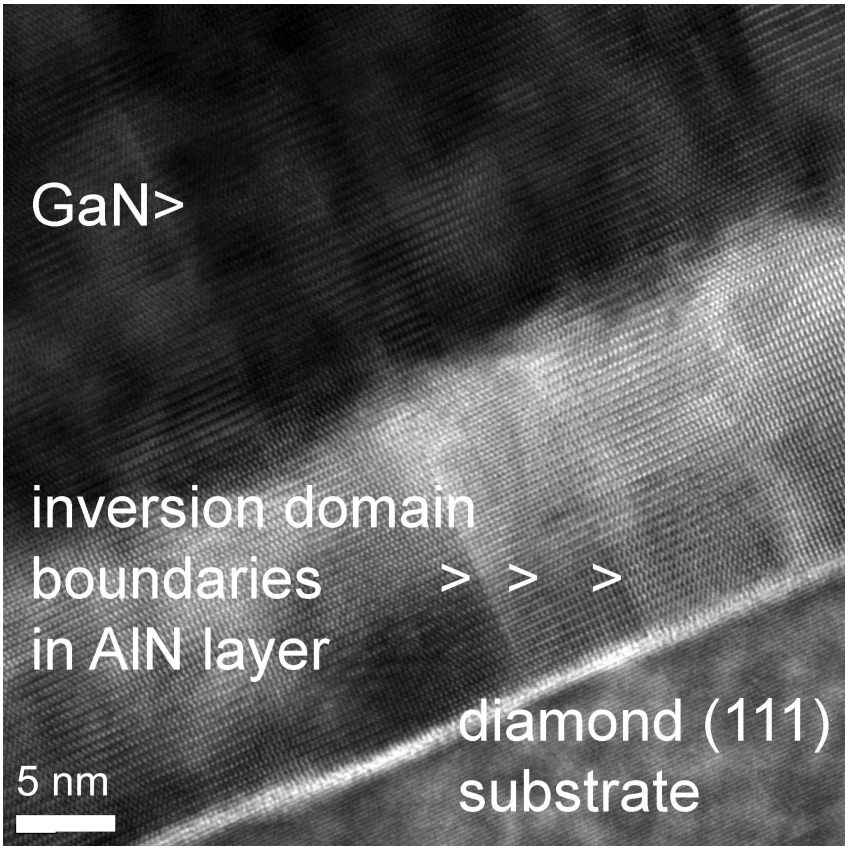

Figure 1. *High-resolution XTEM image of the GaN/AlN/diamond interfacial region showing a high-density of IDs in the GaN/AlN layers.*

A high-density of Inversion Domain Boundaries (IDBs) propagates from the AlN nucleation layer to the overgrown GaN film, these IDBs originate directly from the surface of the diamond substrate. Also, high density of threading dislocations was observed in the thick GaN layer.
In the next set of experiments the surface preparation of diamond was modified by nitridation prior the deposition of the nitride layers.

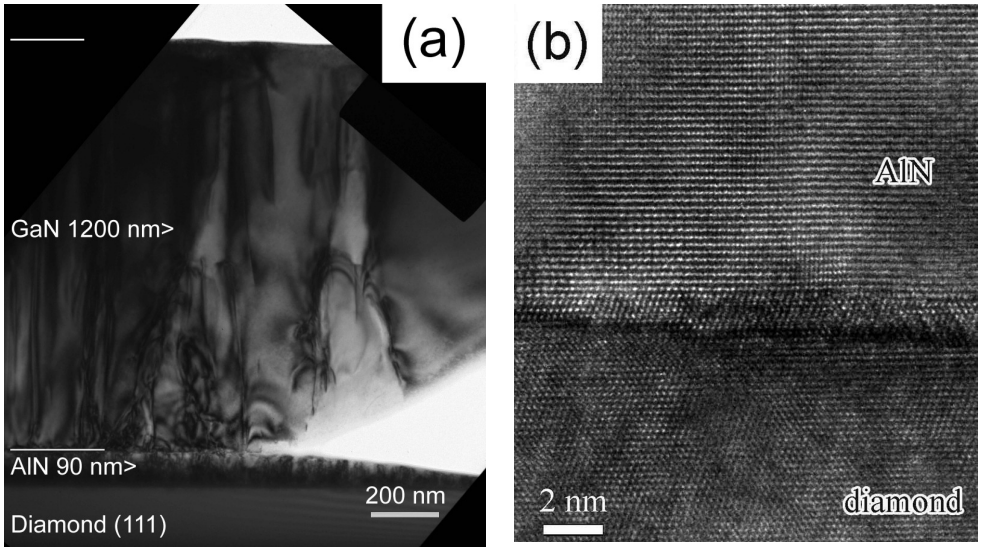

Figure 2. *(a) BF TEM image of GaN/AlN layers grown on nitrided diamond (111) surface. (b) aberration-corrected high-resolution XTEM image of the AlN /diamond interface.*

The following epitaxial relationships were observed: (0002)GaN//(111) diamond and (1$\underline{1}$00)GaN//(220) diamond. The nitrogen treatment removes the oxygen and carbon contamination from the surface and also modifies the surface roughness of the treated substrate. GaN thin films of high structural quality were grown on (111) single crystal diamond substrates by MBE using an AlN nucleation layer. The optimized growth samples exhibited a single epitaxial relationship of GaN (0001) on diamond (111) with single polarity.

Development of carbon – titanium nanocomposite thin films

(OTKA PD101453, János Bolyai Research Scholarship)

K. Balázsi

Carbon-based nanocomposite thin films have large application potential because they possess unique mechanical properties. Combination of pure carbon-based thin films with metallic nanoparticles can enhance physical properties of nanocomposites. Modern methods of vacuum deposition provide great flexibility for manipulating material chemistry and structure, leading to films and coatings with special properties. The new line of this research is a development of biocompatible carbon–metal nanocomposites. Nanocomposite coatings are found to be promising solution for protective applications. Ti and C are suitable elements to optimize surface chemistry and promote fast osteointegration. The combination process of Ti and C is relatively easy and cheap, and in the same time TiC possess good mechanical properties. It can be expected that the formation of TiC based surface coating has a passivation effect on titanium implant. This passivation effect means that TiC layers act as a barrier and Ti ions are kept in the bulk implant introduced in the living organism.

The ultimate goal of research is the development of sputtered C-Ti thin films as potential barrier coating for interfering with Ti ions from pure Ti or Ti alloy implants.

The films have been deposited on silicon (001) substrates with 300 nm thick oxidized silicon sublayer, at 25 and 200 °C deposition temperatures. The thickness was approximately 300 nm. The structural properties of the films were investigated by TEM. Columnar TiC crystallites with 15–20 nm width have been embedded in 5 nm thin amorphous carbon matrix. MG63 osteoblast cells have been used for in vitro study of nanocomposites. The initial adhesion, subsequent growth and viability of human osteoblast-like MG63 cells in cultures on different substrates have been studied. The 7 day lasting tests showed a higher value of cells on TiC/a:C nanocomposite surface than the cells on control samples. Structural and biological aspects showed that the sputtered TiC nanocomposite thin film is biocompatible and it will be a good candidate as potential barrier coating for Ti implants (Fig 1.).

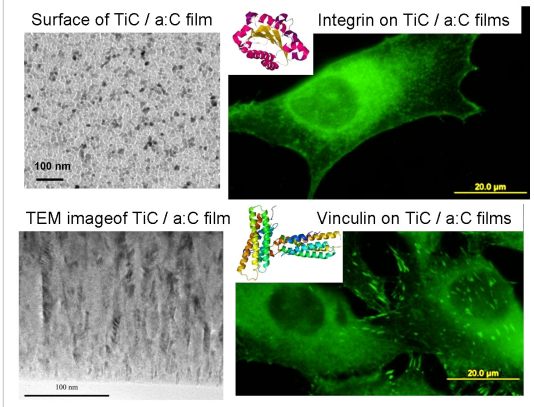

Figure1. *TEM image of TiC/a:C nanocomposite film and microscopic image of vinculin and intergrin on TiC/a:C films.*

A TEM study of Ni and AuNi catalysts for dry reforming

(OTKA NN107170, K101854 and K101897)

G. Sáfrán, A. Horváth (EK FKL), O. Geszti, A. Beck (EK FKL), L. Guczi (EK FKL), and N. Nagy (EK FKL)

TEM and associated analytical techniques are very efficient in studying and solving catalyst problems. We determine the structure, morphology, composition, grain size and elemental distribution of the catalyst before and after the reaction process and trace the alterations of both support and nanocrystals. The mixing and the alloying of the chemical components, and also the appearance of the by-products were studied using HRTEM imaging, EDS and EELS elemental mapping. The results are fed back to the preparation. The revealed nanostructure changes are expected to provide information on the degradation scenario, and enable us to improve the activity, selectivity and lifetime of the catalyst system.

In this project we investigated the structural changes of $MgAl_2O_4$-supported Ni and AuNi catalysts prepared by different methods and applied in dry reforming reactions. In methane dry reforming ($CH_4 + CO_2 \leftrightarrow 2CO + 2H_2$) the formation of carbonaceous deposits is almost inevitable on Ni catalysts, that might lead to structural degradation, deactivation and reactor plug-in in long term runs.

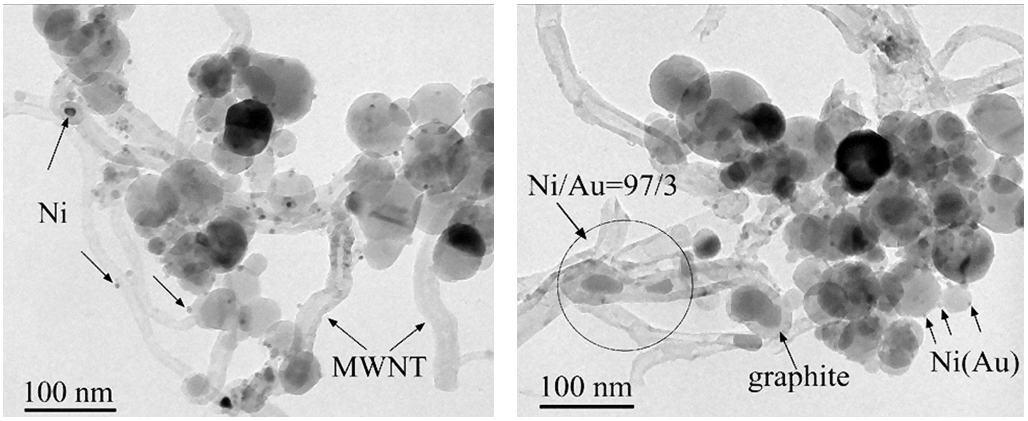

Figure 1. *TEM micrographs of Ni (a, left) and NiAu0.45_sol (b, right) after the second DRM reaction. Ni/Au ratio was determined by EDS.*

According to the literature on steam reforming research ($CH_4 + H_2O \leftrightarrow CO + 3H_2$), the immiscible Au and Ni bulk phases at very low Au content form surface alloy that is very sensitive to the temperature but able to reduce surface carbon formation. Such effect of Au in dry reforming has not been investigated before. The aim from catalytic point of view has been to develop novel Au-containing Ni catalysts supported on commercial $MgAl_2O_4$ spinel. Two main preparation methods were tested: a unique sol-method based on the sequential reduction of Ni(II) and Au(III) ions in water in the presence of stabilizers ("sol" samples) and the impregnation of the support with

Ni(II) ions and the subsequent deposition precipitation of Au species in water on the surface of the calcinated Ni sample ("imp" samples).
The TEM image in Fig. 1a shows the formation of multi-wall carbon nanotubes (MWNT) beside graphite shell around the Ni nanoparticles that may poison the catalyst. Fragment of only 0.45% Au caused very similar phenomena as shown in Fig. 1b. Here, we see also bamboo-like carbon MWNTs and agglomeration of graphite around the Ni/Au 97/3 composite particles, due to repeated dry reforming.

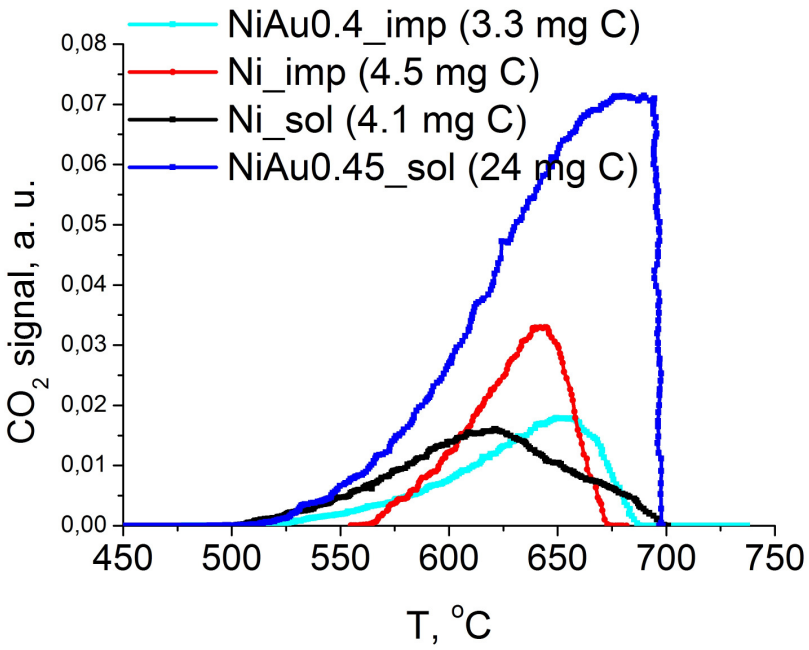

Figure 2. *Temperature programmed oxidation of surface carbon deposits after 24 hours dry reforming reaction showing higher amount of deposited carbon on Au-containing sol samples compared to the corresponding impregnated one. The shift of peak maxima for Au containing samples shows the negative effect of gold on the carbon removal as well.*

HRTEM and TEM+EDS investigations revealed the intimate contact of Au and Ni phases (AuNi alloy) after catalytic runs. The addition of Au has a negative effect in terms of catalyst stability and the easiness of carbon removal (Fig.2.), although no straightforward relation between Au content and the amount of surface carbon can be given at the moment. In summary, carbon formation was not eliminated by 0.45% Au addition to Ni catalyst for methane dry reforming. The search for optimum conditions and understanding of the mechanisms for the development of an improved Ni-Au bimetallic DRM catalyst need further investigations.

Nanoscale masks from AlO_x fabricated by UV excimer laser

(TÁMOP-4.2.2/B-10/1-2010-0025)

G. Sáfrán, J. Szívós, M. Serényi, and E. Fülöp

Next generation of magnetic recording will apply bit-patterned media (BPM). Our aim was to develop nanoscale masks applicable for BPM. Samples covered with Langmuir-Blodgett (LB) films were treated with UV excimer laser (248 nm) pulses. Self-assembled silica nanospheres of diameter ~300 nm of the LB film acts as individual lenses that focus the laser light to the surface under. This creates an ordered array of patches (120 nm dia) on the surface. Fig. 1a is a calculated energy distribution of the laser light that passed the LB film. Experiments showed regular hole or hillock patterns (Figs. 1b, c, d*)* depending on the intensity of laser pulses, which can be applied for direct patterning or preparing masks from amorphous AlO_x layers.

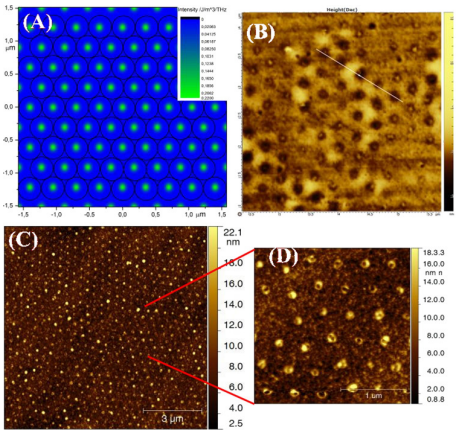

Figure 1. *(a): Simulated energy distribution of UV laser light behind an LB film; intensity scales up from blue to green. (b): A hole pattern in AlO_x. (c): Hillock pattern obtained by AFM. (d): Magnified area from (c).*

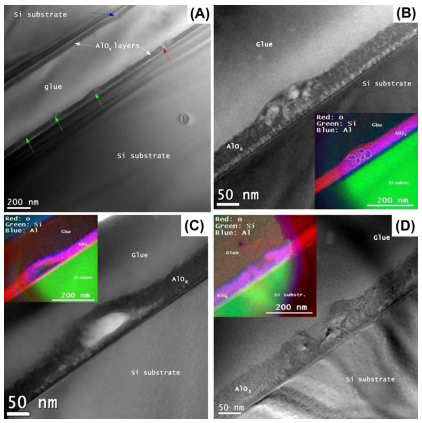

Figure 2. *(a): Cross-section TEM overview of a patterned AlO_x layer. (b): Hillock on the AlO_x. (c): Large single bubble. (d): Blown out bubble (a crater). Colour insets are EELS elemental maps of O, Si and Al.*

Fig. 2a shows the TEM side view of an obtained pattern in an AlO_x layer. Figs. 2b, c and d represent the details of individual patterns formed under gradually increased pulse energies. In Fig. 2b a hillock was formed that contains crystallized grains and small discrete bubbles. Fig. 2c shows a large single bubble formed at higher laser energy. In Fig. 2d a blown out bubble is seen, due to the applied highest energy.
HRTEM revealed that at moderate laser energies our model layer undergoes a local crystallization and appearance of small bubbles that forms hillocks. An increase of the energy is suggested to provoke intense local plasma and gas release that blows up large single bubbles (Fig. 2c*)*. Further increase of the energy causes the blowing out of the bubbles leaving craters behind (Fig. 2d), which refers to the holes in Fig. 1b.
According to our results, using LB films and carefully controlled laser pulses, suitable masks can be fabricated for nanopatterning - various thin films including BPM.

Production of nano-layers by ion mixing

A. Barna, S. Gurbán, L. Kótis, J. L. Lábár, A. Sulyok, M. Menyhárd, A. L. Tóth, L. Illés, A. Pongácz, and É. Vázsonyi

C/Ta/C... and C/Si/C… layered systems of various thicknesses were irradiated by Ga^+ ions in the energy range of 2–30 keV. In the case of C/Ta system the irradiation resulted in a strongly asymmetric ion mixing. Because of the asymmetrical transport the C/Ta interface remained sharp independently from the applied fluence. The carbon transported to the Ta layer formed TaC_x.

The mixing process in the case of the C/Si system was considerably different resulting in an only slightly asymmetric intermixing of the top C and Si layers (consequently sharp interface did not form), which could be modeled by TRIDYN code. During ion mixing, part of the intermixed C and Si atoms reacted, forming amorphous SiC the amount of which scales with the square root of the Ga+ fluence. Thus, using FIB of appropriate energy and fluence an amorphous, SiC-rich, thin film in the range of several nm-s could be produced.

To study the chemical resistance of the produced SiC rich layer four areas (100x100 μm^2) of different irradiations with increasing fluences (10-80x10^{15} Ga^+ ions/cm^2) were applied for the same sample. This irradiation resulted in C cover layers of decreasing thickness (18-10nm) on the top of SiC rich layers of increasing thickness (3-9 nm). First the covering C was removed by oxidation. Then the sample was subjected to an etchant used for polysilicon. Fig. 1 shows the result. The irradiated areas resisted to the etching and thus columns, covered by the SiC rich layer remained on the surface. The etching rate of the 3 nm SiC layer, with respect to that of the polysilicon, r_{SiC}/r_{polySi} was estimated to be < 10^{-3}. Thus, such an extremely thin layer can effectively protect the sample from the etchants.

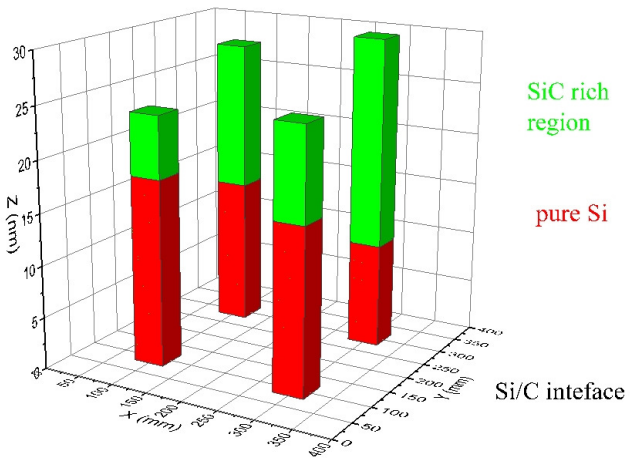

Figure 1. *The SiC rich regions protect the underlying regions against the etching, which readily removes the Si layer.*

XPS analysis of technical solders

(Contract Research, Budapest University of Tech. # 40391)

S. Gurbán, A. Sulyok, and M. Menyhárd

XPS in-depth chemical analysis of the newly applied industrial solders after various treatments was carried out to check the oxide layer thicknesses formed. The studied samples contained metallic tin and various types and amounts of tin oxides. The types of oxides could be classified based on the binding energy measurements. The various chemical states along the depth of Sn have been identified by the binding states of the Sn 3d5/2 and O 1s peaks, which were determined by deconvolution.

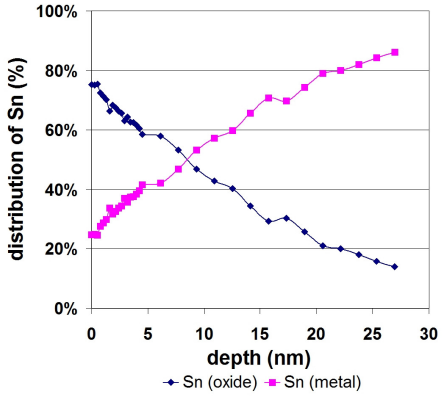

Figure 1. *The in-depth distribution of metallic and oxidized Sn ; an untreated 'SO_4' sample.*

groups of samples		shift of oxide binding energy	the surface oxide (>50%)
untreated	'Cl'	0 - 0.3 eV	0 – 3 nm
	'SO_4'	~ 0.6 eV	8 – 10 nm
treated	'Cl'	0 - 1.5 eV	20 - 50 nm
	'SO_4'	~ 1 eV	10 – 15 nm

Table 1. *The summarized results of the studied groups of samples.*

The oxidized Sn showed different depth distribution from sample to sample. The non-treated samples always contained some thin native oxides. The thickness of native oxides also varied from sample to sample. The treatments have changed the oxide thicknesses significantly; thick oxide layers were grown up due to the treatments (see Table 1). The thickness of the formed oxide layer also depended on the type of treatments. The 'Cl' type of treatments resulted in thicker oxide layer than that of the 'SO4' type of treatments. Table 1 also shows the changes in binding energies of oxide peaks that indicate changes in the characteristics of the oxidation degree. Based on these data we could show that the distributions of various oxides along the depth were also different. Tin-oxides did not form well-defined layers. The oxidation fronts were rather inhomogeneous. These inhomogeneities did not hide, however, that the various treatments resulted in strongly different oxide thicknesses.

NTPCRASH

(NKTH TECH-08 NTPCRASH)

M. Menyhárd, S. Gurbán, A. Sulyok, Z. Kabács (Panac), G. Kőfalvi (IbB), Cs. Balázsi, V. Varga, and F. Wéber

In the framework of the NTPCRASH project, bio-composite based protection material against under run for trucks has been developed. The main purpose of the project was to decrease the weight of the protection while maintaining the safety. Two different types were studied: bio-fiber and carbon fiber reinforced polyester composites. In the last year chemical treatment of cellulose fibers was studied in the framework of the project.

The treatments included

- Addition of Teflon suspension to suppress the hydrophilic feature of cellulose and to increase the lifetime with lowering the interaction with water.
- NaOH treatment to improve the mechanical capability of the composite with the improved adhesion between the fiber and the epoxy resin.
- NaOH+KMnO4 treatment to achieve better mechanical stress for a longer lifetime with less water sensitivity.

The applied investigation techniques were: low energy SEM images of broken surface, stress-strain diagrams with composite sheet bending, XPS measurements for revealing chemical changes, tribological tests.

Results

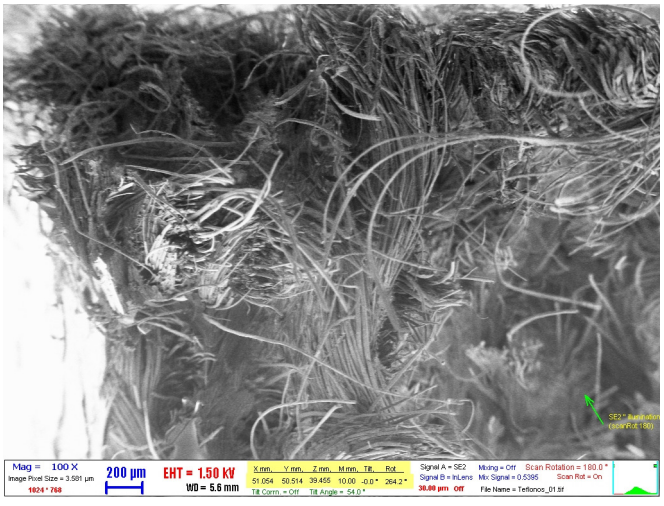

Figure 1. *SEM image on the fractured surface of composite -with teflon treated fibers.*

Teflon treatment of fibers significantly reduced the mechanical capability of the composite. The mechanical tolerance, measured by the maximal mechanical stress was decreased by 30% after Teflon treatment. The lower adhesion between the fibers and the resin resulted in a particular image (Fig. 1) of the broken surface: a huge number of long free fibers without bonding resin.

Because of the greatly reduced stress tolerance, the application of Teflon treatment is not recommended.

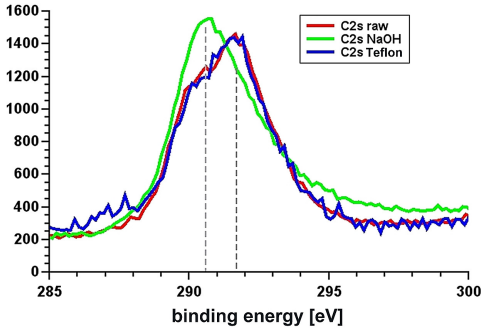

Figure 2. *Carbon 2s line in the XPS spectra of different treated fibers.*

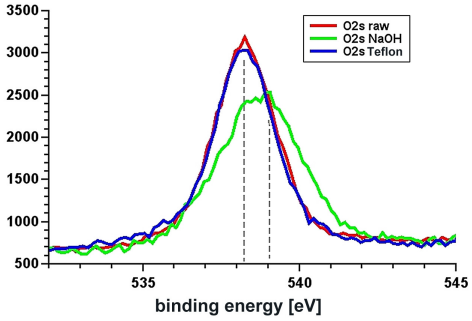

Figure 3. *Oxygen 2s line in the XPS spectra of different treated fibers*

Significant chemical changes on the fiber surface due to NaOH treatment were observed by XPS. Beside the Na bound to fiber surface in 3 % quantity, both the carbon and the oxygen lines have changed (Figs. 2 and 3, respectively) in comparison to the raw state. Both carbon (Fig 4.) and oxygen peaks (not shown) were decomposed for sub-peaks belonging to different chemical states and the quantitative change of peak shape was followed by the change of the ratio of subpeaks. Ion bombardment of the raw fiber surface resulted in so alteration of peak shapes as that seen after NaOH treatment. The carbon /oxygen ratio was also calculated from all of the spectra. It was stable in NaOH treated fiber, while depth dependent in the other two fiber types measured. The peaks' shape and the composition changed, because the NaOH treatment removed the original surface region and it became similar to the of the bulk cellulose.

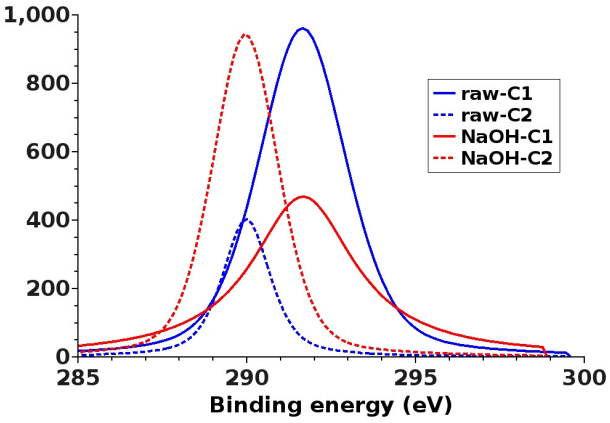

Figure 4. *Decomposition of carbon 2s lines for raw fiber and for NaOH treated fiber in the XPS spectra.*

The maximum tolerated mechanical stress of the composite was improved by 6% after the NaOH treatment, and further 7% after the NaOH+$KMnO_4$ treatments.
Their application may be recommended.

$Ge_{84}Mn_{16}$ layer formed on Ge(100) by ion implantation and annealing

G. Pető, B. Pécz, L. Dobos, and A. Kolitsch (FZR Dresden)

Spintronics is a very hot subject of microelectronics, but still in the basic research phase. A possible material for spintronics application is the GaMnAs compound, whose Curie temperature is not high enough. GeMn, or SiMn could also be promising alloys, mainly because they could utilize the well-developed Si technology. Earlier experiments on the GeMn system faced the problem of the regrowth into GeMn compound of the Ge wafer heavily damaged by Mn implantation. For the recrystallization of the Mn implanted Ge at high concentration of Mn doping elevated temperature was necessary.

Having similar experience in our work, we have assumed that the Mn atoms are too light to amorphize successfully the Ge(100) wafer. Therefore, we have developed a special method to improve the quality of the regrown GeMn, even at high concentrations Mn implantation doping. This is based on two steps of the ion implantation, namely, first the Ge(100) was amorphized by Ge ions and then this Ge overlayer was doped by Mn to very high concentration ($8x10^{16}/cm^2$).

Both kinds of GeMn samples were in situ annealed in UHV at (500 °C for 30 min) following in situ Angular resolved photoemission at normal electron emission. After the annealing the samples were examined by transmission electron microscopy (TEM). The sample implanted by Mn and annealed is shown in Fig. 1.

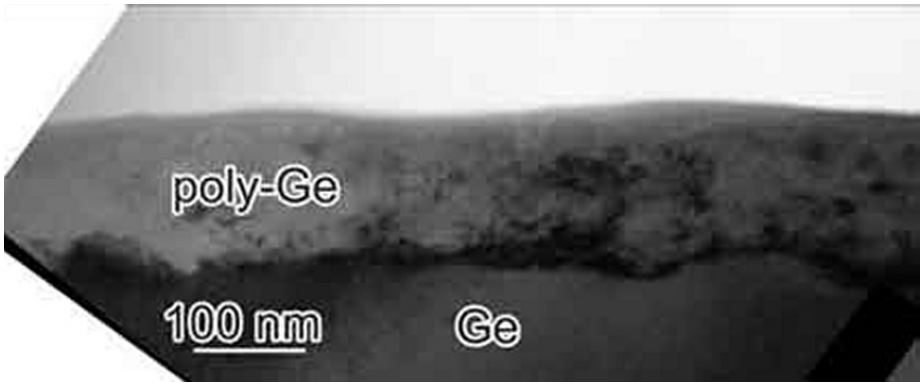

Figure 1. *Cross section of Mn implanted and annealed sample showing a polycrystalline layer on the top.*

The surface of the Mn implanted and annealed sample seems to be quite flat showing some regrowth on the surface. The rest of the implantation-damaged layer is polycrystalline. The interface of the damaged and undamaged part seems to be rather rough. It is surprising that this interface is not the only source of the regrowth in contrast to the earlier observed regrowth process.

The sample, which was pre-amorphized by Ge ions, implanted by Mn and annealed is shown in Fig. 2. The amorphized region is completely recrystallized. The top region

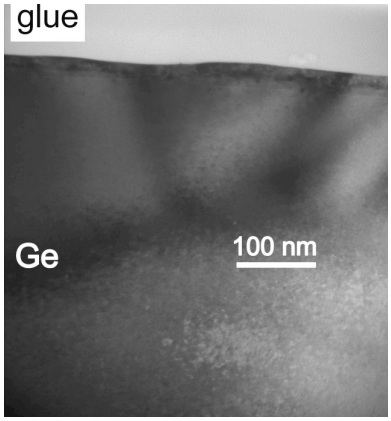

Figure 2. *Cross section of a sample, which was pre-amorphized by Ge ions before the Mn implantation.*

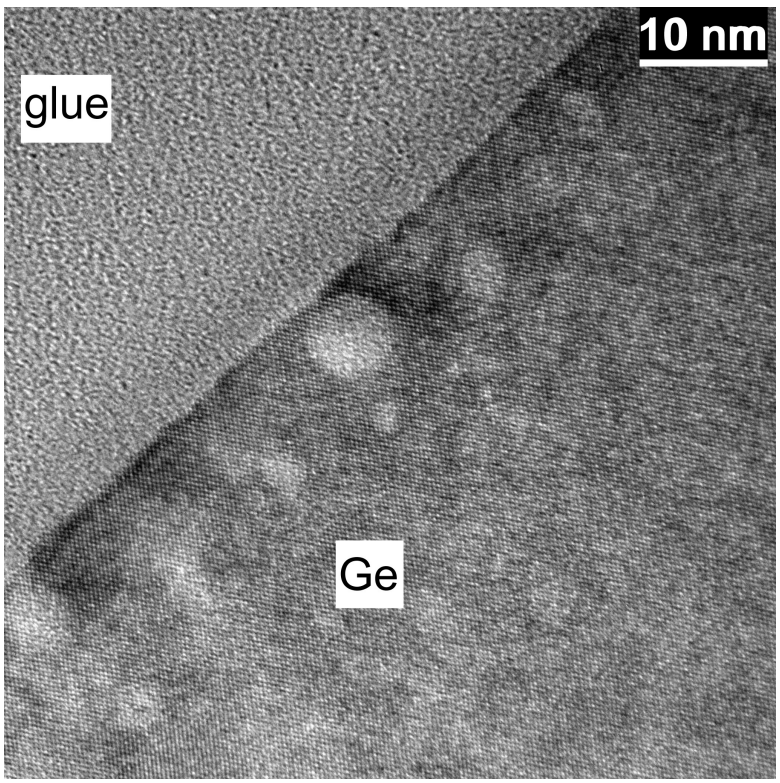

Figure 3. *High resolution TEM image of the sample shown in bright field in the former figure.*

is single crystalline (Fig. 3), the interface of the former amorphous/crystalline part is almost invisible. No sign of compound formation was observed. Manganese is present in Ge as a solid solution with the nominal content of 16 at% in the top 200 nm thick, single crystalline region.

Ceramics and Nanocomposites Department

Head: Csaba BALÁZSI, Ph.D.

Research Staff

- János VOLK, Ph.D., Deputy Head of Department
- Csaba Sándor DARÓCZI, dr. Univ.
- András DEÁK, Ph.D.
- Gréta GERGELY, Ph.D.
- Ngyuyen Quoc KHANH, Ph.D.
- István Endre LUKÁCS, Ph.D.
- Allazadeh Mohammad Reza, PhD.
- Attila Lajos TÓTH, Ph.D.

Technical Staff

- Levente ILLÉS, engineer
- Attila PETRIK, engineer
- Viktor VARGA, technician
- Ferenc Viktor Wéber, engineer

Ph.D. students / Diploma workers

- Róbert ERDÉLYI, Ph.D. student
- Eszter FÜLÖP, Ph.D. student
- Gergő FÜLÖP, diploma worker
- Ádám GYARMATI, diploma worker
- Péter KONCZ, diploma worker
- Viktória KONRÁD, diploma worker
- Imre KULCSÁR, diploma worker
- Péter KUN, diploma worker
- András LÁSZLÓFFY, dipl. worker
- Blanka MOHÁCSI, diploma worker
- Zsuzsanna MOLNÁR, dipl. worker
- Áron NAGY, diploma worker
- Szilárd POTHORSKY, dipl. worker
- Etelka Rovács, diploma worker
- Zoltán SZABÓ, Ph.D. student
- Orsolya TAPASZTÓ, Ph.D. student
- Mihály TÓTH, diploma worker

The main task of the laboratory is to study the relationships between processing parameters, micro- and nanostructures as well as properties of ceramics and their nanocomposites. Some recent activities are as follows:

- Investigation of structural, mechanical, electrical, biological properties.
- Development of CNT/nano-graphite silicon nitride nanocomposites.
- Study of 1D, 2D and 3D semiconductor (ZnO, WO_3) oxides for sensor devices.
- Application of advanced methods for the preparation of nano-hydroxyapatite biocomposites for medical and environmental uses, outcome of advanced preparing methods.
- Development of nanostructured stainless steels by powder metallurgy.
- Pilot scale production of silicon nitride tools and parts exists as well.

The Department has intensive co-operation with universities and industries. Joint laboratories with BME (Chemical nanostructures and Electron-beam Lithography) have been established. The experienced research staff is actively participating in training and supervising of undergraduate and graduate students (Summer School, TDK, M.Sc., Ph.D.); we are active as chairpersons and scientific committee members in international conferences.

Controlled ZnO nanostructures for novel excitonic solar cells

(LIOS OMAA and JSPS-MTA mobility grants)

Z. Szabó, Á. Nagy, E. Fülöp, A. Deák, and J. Volk

ZnO, as a wide band gap transparent semiconductor with high electron mobility is very promising both for polymer/inorganic type electron donor and dye sensitized (DSSC) type excitonic solar cells. However, for these photovoltaic applications only nanostructured ZnO with well-controlled geometry can results in a competitive device performance. In this collaborative work with LIOS (Austria) and NIMS (Japan) we optimized two alternative techniques to fabricate uniformly ordered ZnO nanorod structures onto transparent conductive back contacts.

In the first approach the polymer layer masking for the growth was patterned using nanoimprint lithography. The vertically ordered uniform ZnO nanorods were subsequently infiltrated by standard poly(3-hexylthiophene) (P3HT) electron donor polymer. By comparing the fabricated device with a control hybrid PV cell with random ZnO nanostructure it turned out that the regularity of the nanostructure promotes the infiltration of P3HT which increases the donor-acceptor interface and therefore the short circuit current density (J_{SC}). Moreover, it was also found that the open circuit voltage (V_{OC}) can be increased from V_{OC}=0.30 to 0.71 V by near atmospheric nitrogen plasma treatment after the hydrothermal growth. It can be explained by the formation of a carrier compensating shell layer on ZnO nanorods, which reduces the carrier recombination at ZnO/P3HT interface.

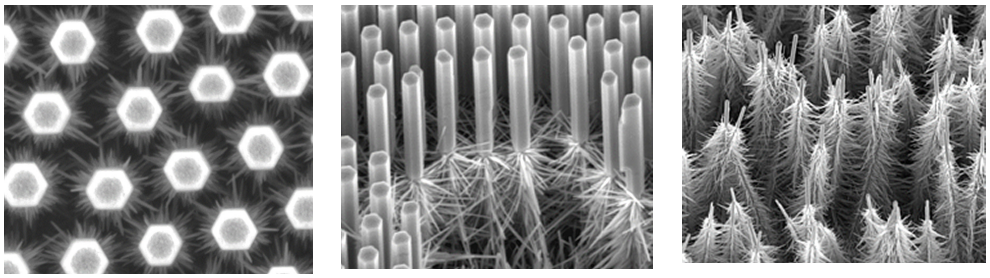

Figure 1. *Hierarchical nanostructures with high roughness factor grown by multiple hydrothermal method.*

In the second approach, the ZnO nanostructures were optimized for solid-state electrolyte type DSSC. Here, the ordered ZnO pillars (diameter ~200-300 nm) were obtained on large surface by nanosphere photolithography. To increase the specific surface and therefore the dye uptake fine secondary side branches (diameter ~20-30 nm) were wet chemically grown by wet chemical process on the primary pillars. Some typical examples on hierarchical nanostructures obtained by multiple hydrothermal growths are shown in Fig. 1.

Nanomechanical characterization of InAs nanowires

(OTKA PD77578)

E. Róbert, L. Illés, I. E. Lukács, and J. Volk

High aspect ratio vertical InAs nanowires were mechanically characterized using SEM, equipped with two micromanipulators. One, equipped with a calibrated atomic force microscope probe, was used for in-situ static bending of single nanowires along the <11–20> crystallographic direction (Figs. 1a,b). The other one was equipped with a tungsten tip for dynamic resonance excitation of the same nanowires (Figs. 1c,d). The crystal structure was analyzed using TEM, and for InAs nanowires with a hexagonal wurtzite crystal structure, the mean bending modulus value was found to be BM=43.5 GPa. This value is significantly lower than previously reported for both cubic zinc blende InAs bulk crystals and InAs nanowires. Up to our knowledge this is the first time that the two techniques are applied on the same individual nanostructures to cross-confirm the results. Although as it turned out the two in-situ methods lead to the very similar result (Fig. 1e) both of them have advantages and disadvantages. While with the resonant excitation only high aspect ratio nanowires can be characterized the static bending technique can be applied even for low aspect ratio (<20) and rigid nanowires and nanorods. Furthermore the latter method does not depend on the electrical properties of the nanowires to be measured. Moreover, with the bending technique it is also possible to investigate the change of the Young modulus along the axis of the nanowire by taking a series of bending experiments at different vertical load positions.

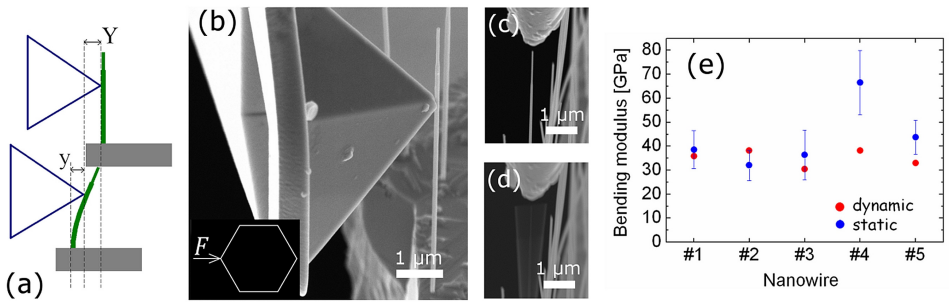

Figure 1. *Schematic of the static bending test on a single InAs nanowire: (a) snapshots were taken in relaxed and stressed states to determine both cantilever and nanowire deflections (Y and y) and the vertical position of the applied load. (b) The corresponding SEM micrograph of the measurement. Resonance excitation of a nanowire using alternating electric field: two typical SEM images recorded (c) far from the natural resonance frequency of the nanowire and (d) at the resonance frequency. (e) Bending modulus values of InAs nanowires provided by the in-situ bending experiment (blue circles with error bar) and the resonance excitation method (red circles).*

On the other hand for homogenous, high aspect ratio nanowires the resonant method can be easier since there is no need to carefully calibrate and prepare the probe. The resonance excitation technique can provide the quality factor of the oscillating nanowire system. Due to their high resonance quality factor (Q>1200), the wurtzite InAs nanowires are shown to be a promising candidate for sub-femtogram mass detectors.

SEM-EDS analysis of nanoparticles

(TÁMOP-4.2.2/08/1/2008-0016)

A. L. Tóth , L. Illés, and T. Szörényi (DUF)

Ultrashort laser pulses ablate nanoparticles from the target into vacuum, gas or liquid environment. In our study Al target was irradiated under water (Fig. 1), resulting in a colloid solution of spherical and tetrahedral particles and their agglomerates (Fig. 2). The aim of the study is to determine the shape, substructure (Fig. 3), size and composition of these particles using TEM and SEM imaging with EDS microanalysis.

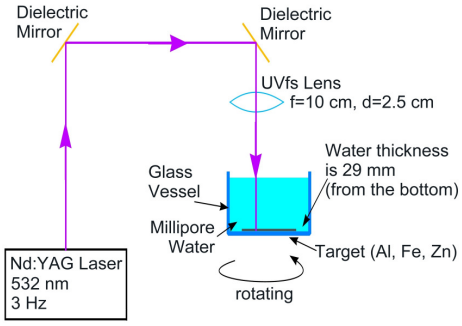

Figure 1. *Laser ablation of Al nanoparticles into water.*

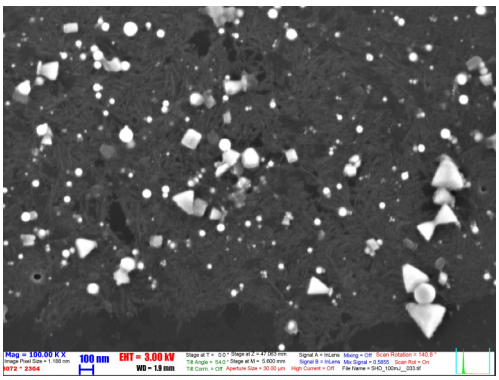

Figure 2. *Nanoparticles of different sizes and shapes prepared onto C foil.*

As the O/Al intensity ratios measured in TEM and SEM differ, Monte Carlo (MC) simulations were performed in order to clear the dependence of the O/Al ratio on the size and shape of the particles as well as on the excitation parameters (200 keV electrons are exciting the whole particle in the TEM, while focused 5 keV beam excites in the SEM).

Backward calculations have been made, on Al_2O_3 particles of different sizes (10 nm – 10 mm), shape (spherical, hemispherical, cubic and layer) under SEM excitation.

For nanospheres TEM results were also calculated (Fig. 4). Comparing this curve with the SEM excited one (Fig. 5 blue line) it can be seen, that the measured relative

intensity depends strongly on particle size, but this dependence is radically different for the two methods.
The shape dependence was modeled for SEM excitation (Fig. 6). The curves have the same form, but the values are wildly different just in the interesting particle size region. Summarizing the facts, in order to guess the composition of the particles, their size, shape and X-ray intensity values have to be taken into account.

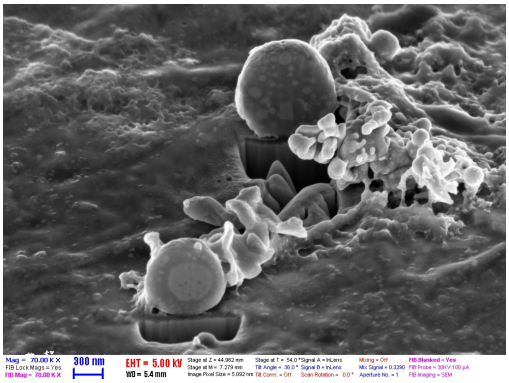

Figure 3. *Substructure of nanospheres revealed by FIB cross-sectioning.*

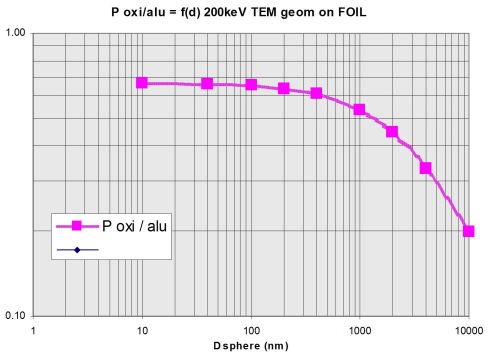

Figure 4. *TEM excited O/Al intensity ratio as a function of nanospere diameter.*

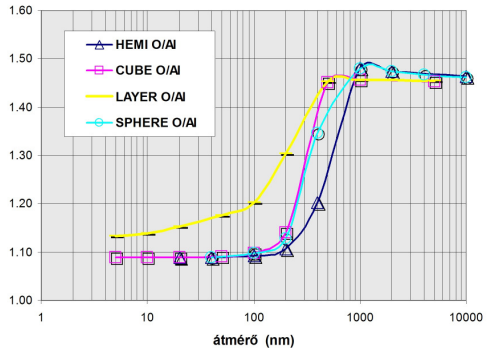

Figure 5. *SEM excited O/Al Al intensity ratio as a function of size of different shaped particles.*

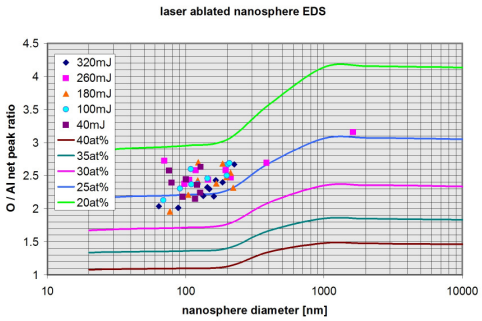

Figure 6. *Plot of measured size-O/Al ratio points from nanospheres over simulated curves with different Al-O composition.*

A set of intensity ratio vs. diameter curves have been calculated for nanospheres of different Al content (20-40 at%). If we plot the measured (intensity ratio – diameter) points over these curves, it can be seen, that their Al content is between 22 and 26 at% (supposing that the spheres contain no elements undetectable for EDS, e.g. hydrogen) .The measurements and calculations clearly demonstrate, that even the semiquantitative X-ray microanalysis can become quite complicated task in the nanorange, where the beam diameter, the excitation volume and the particle size all are in the same order of magnitude: 10-1000 nm.

Nanosized hydroxyapatite based bio-compatible composites

(OTKA BIOCER, TéT KR-10/2009)

Cs. Balázsi, G. Gergely, M. Tóth (BME), I. Kulcsár (BME), A. L. Tóth, and I. E. Lukács

Nanomaterials have wide-ranging implications in a variety of areas, including chemistry, physics or biomedical sciences.

Hydroxyapatite (HAp) has been widely used as an artificial bone substitute because of their high biocompatibility and good bioaffinity, as well as osteoconductability. HAp is not only a main component of hard tissues, such as bones and teeth, but also a material applied for bioceramics and adsorbents because it has an excellent affinity to biomaterials such as proteins. Chemical analysis has shown that these products, which otherwise considered as bio-waste, are rich sources of calcium in the form of carbonates and oxide.

In this work, the HAp powder was prepared from a non-expensive and environmental friendly material – eggshell. The mechano-chemical activation was used for HAp preparation. The bone regeneration of HAp successfully applied as material for tissue-engineering applications were studied by in vivo experiments.

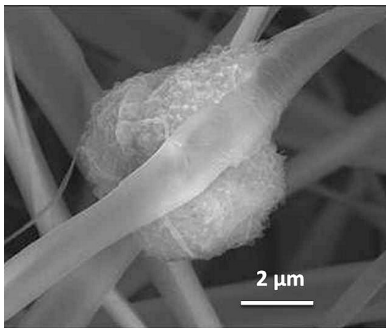

Figure 1. *Osteoblast cells grown on CA fibers only.*

Figure 2. *mCT images of nano-HAp grafted group at 8 weeks.*

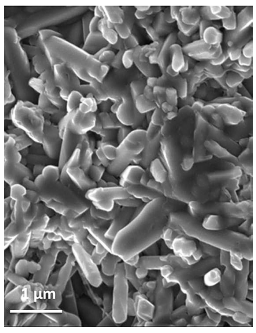

Figure 3. *SEM image of SPS sinterd HAp with ZrO_2 addition.*

Artificial bone tissue scaffolds based on natural hybrids of cellulose acetate (CA) and nano-hydroxyapatite (nHA) in a bio-mimicking 3D matrix architecture using a single step nanomanufacturing technique have been developed in co-operation with Department of Materials Science and Engineering, State University of New York at Stony Brook (USA), Molecular Foundry at Lawrence Berkeley National Laboratory (Fig. 1). Bone regeneration of nano-hydroxyapatite (nHA) produced from eggshell with or without silk fibroin scaffold and compared to the unfilled control in the animal and human clinical model has been studied in co-operation with Hallym University and Gangneung-Wonju National University, Korea (Fig. 2).

In co-operation with Department of Human Physiology and Clinical Experimental Research, Semmelweis University (Hungary) we tested the biological properties of

nano-hydroxyapatite-zirconia (nHA)-(ZrO_2) composites produced by spark plasma sintering (SPS) (Fig. 3). The biological compatibility of the products was tested by seeding human bone marrow, derived mesenchmyal stem cells onto autoclave-sterilized composites and kept under standard cell culture conditions. Cell survival and proliferation was monitored for 18 days with confocal microscopy. All of the observed products provided suitable surface for cell culture.

In co-operation with BME, we studied the bone (femur) resistance to applied mechanical loads. We divided the bone to epiphysis region and corticalis region, and adopted to them the material models of cortical bone, and spongy bone. The elastic modulus of the ABS-M30 material is much lower (2 GPa) than the average cortical bone (17 GPa).

As a result, the bone regeneration process should allow applying loads to the bones to assure building up a strong bone tissue. In the beginning of the regeneration process the implant should take a larger load from the missing bone tissue, but by time it would be better if the new bone is getting more and more load to prevent osteoporosis. The ideal material of the implant is similar to the bone tissue, helps the bone tissue to regenerate and after regeneration it disintegrates.

Silicon nitride /multilayer graphene composites

O. Tapasztó, P. Kun (BME), F. Wéber, A. Petrik, V. Varga, Zs. Czigány, Cs. Balázsi

Graphene multilayers have been prepared by mechanical method based on milling graphite in high efficient attritor mill. We demonstrated that the highly efficient milling is a successful tool for producing graphene multilayers. The results showed that intensive milling in ethanol is a better way to separate the graphite layers, rather than in water or in air.

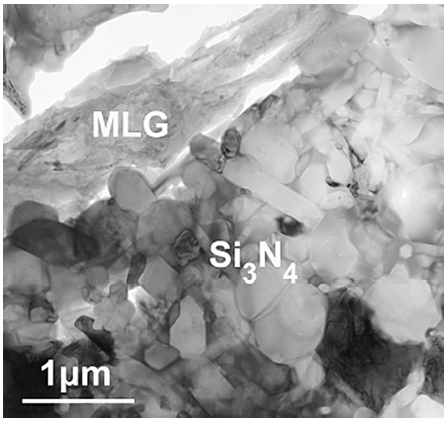

Figure 1. *TEM image of Si_3N_4 nanocomposite reinforced by 1 wt% Angstron graphene.*

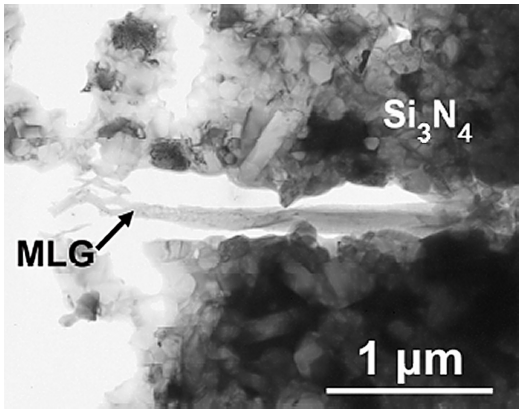

Figure 2. *TEM image of Si_3N_4 nanocomposite reinforced with multilayer graphene made by mechanical milling.*

The largest distance (which can exceed 1 μm) between separated adhering multilayers that is the highest degree of exfoliation has been obtained by 10h milling. The average thickness of graphene multilayers was LC = 13.76 nm. This result implicates that the graphene multilayers were composed of approximately 40 graphene layers on average.

Silicon nitride based nanocomposites have been prepared with different amount (1, 3 and 5 wt%) of multilayer graphene (MLG) in comparison with nano graphene platelets (Angstrom, Fig. 1) and exfoliated graphite nanoplatelets (Fig. 2).

The results showed that some individual MLG layers are embedded well into silicon nitride matrix. However it seems that some MLG layers formed bundles during the preparation process with length of 1-6 mm and thickness of approximately 100-800 nm. The measurements also proved that porosity is generated mostly at the MLG/Si_3N_4 grain boundary.

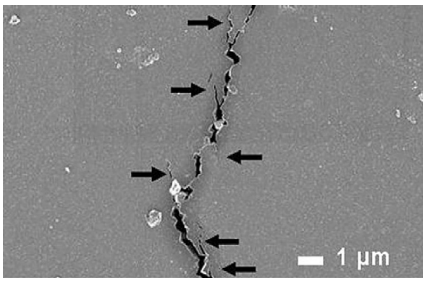

Figure 3. *Crack branching during crack propagation in the nano-graphene platelet - reinforced composite (SEM).*

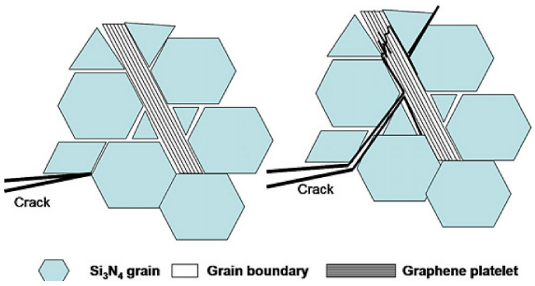

Figure 4. *Schematic illustration of the toughening mechanisms in the ceramic – GPL composite.*

The GPLs are relatively well distributed in the Si_3N_4 matrix of all systems. These single or multiplatelets are located at the Si_3N_4/Si_3N_4 grain boundaries and are often connected with the presence of pores.

The micro hardness (Leco Instruments) and hardness were measured using the Vickers indentation method at loads from 9.81 to 150 N with co-operation of Institute of Materials Research, Kosice, Slovakia. The indentation fracture toughness of the composites is significantly higher compared to the monolithic silicon nitride, with the highest value of 9.92 MPa m0.5 in the case of a composite reinforced by multilayer graphene nanosheets. We frequently observed in our systems similar pullout of the graphene sheets that are tucked and semi-wrapped around the matrix grains. We expect that the energy required to pull out a sheet is greater than that of a SWNT, MWNT or nanofiber due to “sheet wrapping” around the matrix grain boundaries and the increased contact area with the matrix (Figs. 3 and 4). Therefore the contribution of this mechanism to the toughness improvement is high.

Applying this approach, together with the carbon based nano-filler strengthening approach, there may result a synergy effect in improving the fracture toughness and electrical conductivity of silicon nitride based ceramics similarly to that demonstrated in the Si_3N_4 + CNTs composites.

Nanotechnology for oxide dispersion-strengthened steels

P. Koncz (PE), F. Wéber, A. Petrik, V. Varga, and Cs. Balázsi

The development of oxide dispersion strengthened (ODS) steel has been aimed at the field of application for fast reactor fuel cladding and fusion reactor materials. ODS steels show high strength at high-temperatures. We have developed oxide dispersed (ODS) steels produced by intensive milling together with spark plasma sintering. The structure of powders is considerably changed after intensive combined (wet and dry) milling.

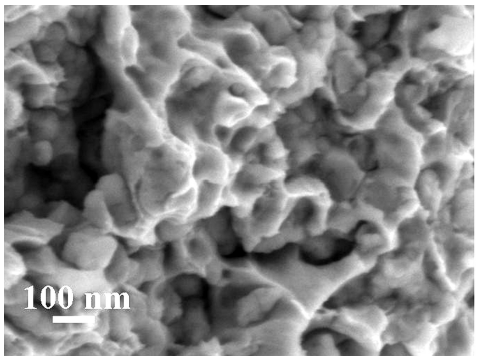

Figure 1. *SEM images of fracture surface of sintered austenitic ODS with 1 wt% Y_2O_3 addition.*

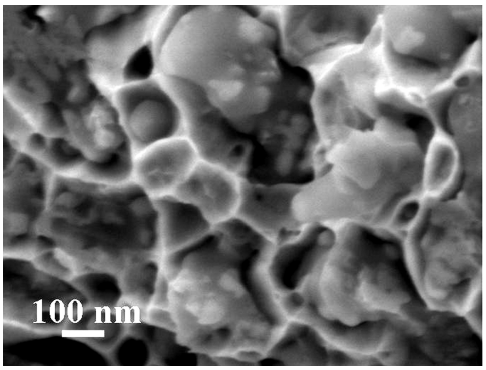

Figure 2. *SEM images of fracture surface of sintered martensitic ODS with 1 wt% Y_2O_3 addition.*

Using SEM we have observed grains of steel with 100 nm mean size in austenitic ODS steel (Figs. 1 and 2). In comparison, the martensitic ODS steel microstructure consisted of grains with 100-300 nm size. Combined milling resulted high hardness and strength.

Application of the reinforced Al-MC in brake pads and disks

(TÉT_10-1-2011-0288)

M. R. Allazadeh, and Cs. Balázsi

Automotive industries have a trend to manufacture lighter vehicle, therefore, the aim of the research in this arena is to reduce the weight of the parts by changing the design or reducing the density of the constituent material of components used in the parts of the vehicle. A large body of literature review has been discussing the application of aluminum metal matrix composites (Al-MMC) instead of the conventional and commercial brake pads and disk drums in the vehicles to improve their performance considering the material behavior in the braking mechanism.

Understanding the mechanism of braking helps to perceive the advantages of fabricating brake pads from aluminum metal matrix.

This study compares the mechanical properties of Al-MMC brake friction material with those made of steel alloy material. The current investigations elaborate advantages and disadvantages of Al-MMC as friction material to optimize the brake pad properties based on the essential standards and parameters in vehicle industries and on the properties of Al-MMC. The hard ceramic reinforcements and soft lubricants are incorporated into aluminum alloy to increase the wear resistance property of Al-MMC. The reinforcing contaminant of the Al-MMC were fabricated from a variety of shape and size and material by combining particles, fibers or whiskers of SiC, Al_2O_3, B_4C, TiB_2 and $ZrSiO_4$ and Silicon Carbide Particulate (SiCp).

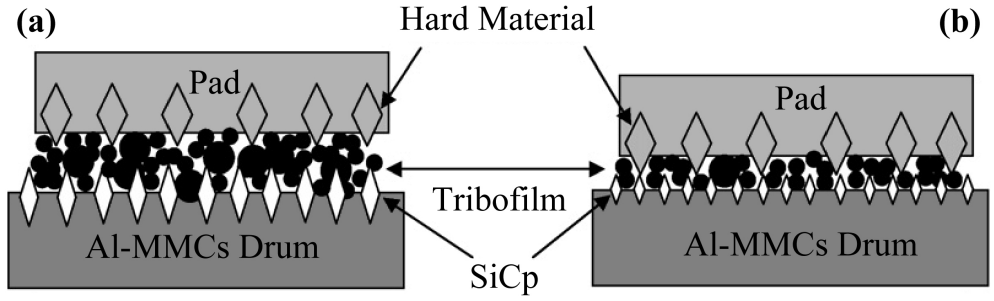

Figure 1. *Mechanism of tribofilms behavior in response to increasing on applied load.*

Fig. 1 illustrates the accumulation of the tribofilm evolving in the wearing process between the pad and the drum. The additional pressure compresses the tribofilms in more compact volume. In an increasing load abrasion wear test the pressure shatters some of small plateaus formed by the hard ceramic particles and fills with the tribofilms a portion of the grooves.. Analyzing the results obtained by researchers suggests that the reinforced Al-MMC could be a good candidate as alternative material for the brake pad and the disk drum. Although, Al-MMC-SiC_p shows supreme properties over the commercial friction material made of cast iron or steel, the research results approve a numbers of failing points for the currently developed Al-MMC material to be used in the brake system of the vehicles. Therefore, this is still an open investigation topic and search for appropriate Al-MMC need further studies and laboratory experiments to overcome the weaknesses of the current friction materials.

Porous tungsten oxide nanofibers for gas sensors

(TÉT_10-1-2011-0305)

I. E. Lukács, Á. Nagy, and Cs. Balázsi

We report on a technique for fabrication of porous tungsten oxide nanofibers with a diameter under 200 nm and a macroscopic length. The decisive method of the production is electrospinning. A technique has been developed to monodisperse tungsten oxide nanoparticles in polymer solution for electrospinning. The ideal mass ratios of solvents, polymer and the maximum amount of tungsten oxides have been determined by a series of experiments. A solution of polymer (polyvinyl alcohol) and dopant is put in a syringe, which is controlled by a stepper motor. The solution leaves the needle, and flies to the target (metal plate) driven by the high voltage switched between the target and the needle. A microchip specially developed for gas sensing is fixed on the target. At this state the hexagonal tungsten oxide nanoparticles are coated with polymer. We developed methods to eliminate the polymer whilst the nanofibers remain and the tungsten oxide nanoparticles form porous nanofibers on the surface of gas sensor chip.

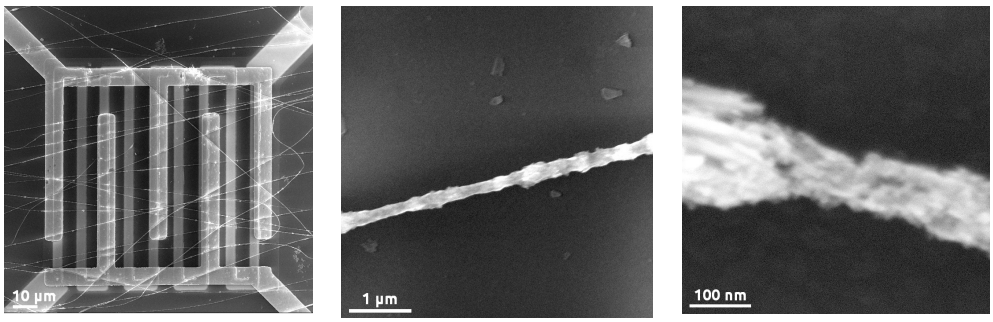

Figure 1. *Porous tungsten oxide nanofibers as a special chip designed for gas sensor.*

Our aim was to maximize the concentration of $WO_3 \bullet 1/3H_2O$ content in the produced polymer fibers. After electrospinning the polymer was burned by heat treatment at 400 °C 4 hours in tube furnace or oxygen stripping at 300 W RF power 1 hour in vacuum, and UV tube generated ozone 24 hours. Finally, the samples were heat-treated in air at 330 °C, 3 hours to obtain porous hexagonal tungsten oxide nanofibers. $WO_3 \bullet 1/3H_2O$ doped polymer composite nanofibers were fabricated by electrospinning. Then the polymer content was eliminated by several methods (Fig. 1). The porous tungsten oxide nanofibers can be produced on a special chip designed for gas sensor.

Nanoparticle films

E. Fülöp, and A. Deák

We focus on the preparation and characterization of nanoparticle thin films and mainly use dielectric (e.g. silica) and metal/dielectric core/shell nanoparticles (e.g. gold/silica nanorods) for the preparation of the thin films.
The formation of two-dimensional films of the particles is studied at the water/air interface with the aid of a Wilhelmy film balance. The film of the nanoparticles can be deposited on different substrates (glass, silicon, etc.) by the Langmuir-Blodgett method. The solid supported structure can open up several ways for applications, e.g. large area patterning by nanosphere lithography, substrates with special optical properties for optoelectronics, and diagnosis etc.
When using plasmonic gold nanorods as the basic building block of the films, the optical properties of the film can be tuned with the size and aspect ratio of the gold nanorods (Fig. 1). The elastic nature of the shell allows the core/shell nanorod to core/shell nanosphere transition upon heat treatment, while the mesoporosity of the shell enables chemical reactions to be performed directly at the core. When reducing e.g. gold ions inside this mesoporous, elastic nano-containers, the spherical particles are transformed back into core/shell nanorods (Fig. 2).

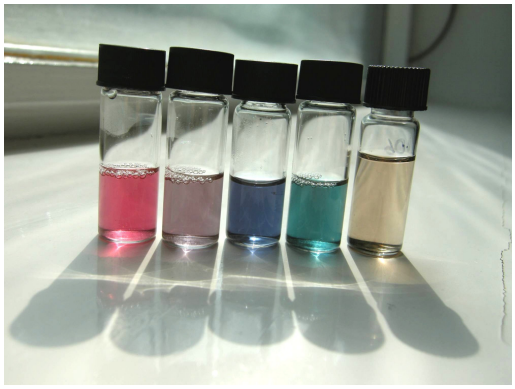

Figure 1. *Gold nanorods with different sizes and aspect ratios in aqueous medium.*

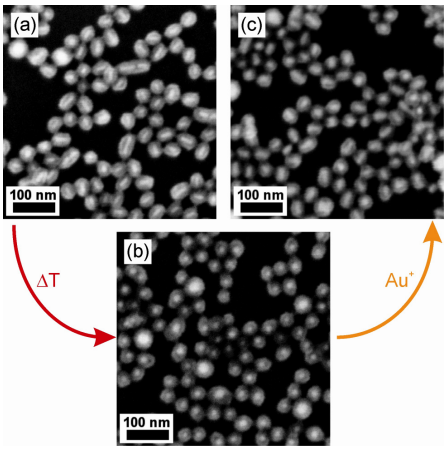

Figure 2. *Reversible shape transition upon heat treatment and reaction with gold ions.*

The monolayers of larger silica or polystyrene particles can be used as a template to prepare different structures (nanorings or inverse spheres). Example is given below where small spherical gold (ca. 16 nm) and silica (ca. 40 nm) nanoparticles are arranged into ring-like and inverse sphere structures via directed self-assembly (capillary lithography, Figs. 3 and 4).

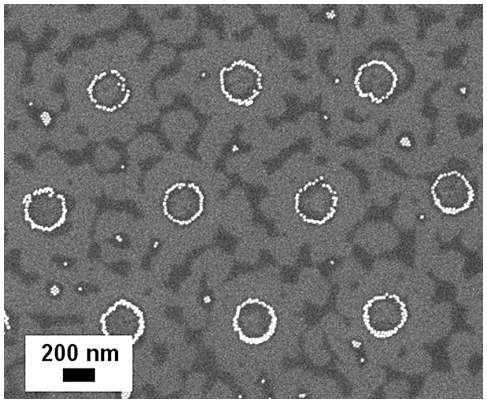

Figure 3. *SEM image of nanorings composed of gold nanospheres prepared by capillary lithography.*

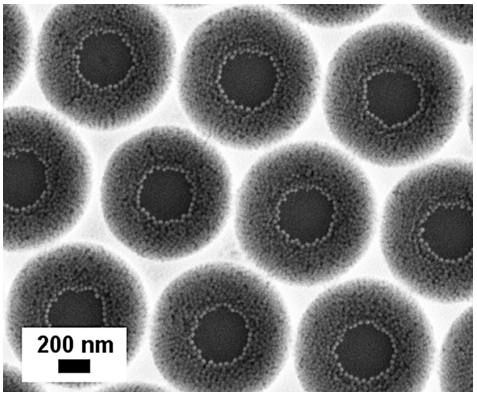

Figure 4. *SEM image of an inverse sphere structure prepared from silica nanospheres by capillary lithography.*

Conductive Modulation of Horizontal ZnO Nanowires Grown by Hydrothermal Technique

(OTKA K76287)

N. Q. Khanh, I. Lukács, Z. Szabó, R. Erdélyi, K. Kubina, and J. Volk

ZnO as a biocompatible, wide band gap semiconductor is a very promising candidate material for sensor application. For this purpose, we have successfully grown the horizontal multiple ZnO nanowires from a preformed electrode array (Fig. 1, inset) by hydrothermal technique, thereby demonstrate the ability of this method for realization of integrated nanoscale devices on a planar substrate.

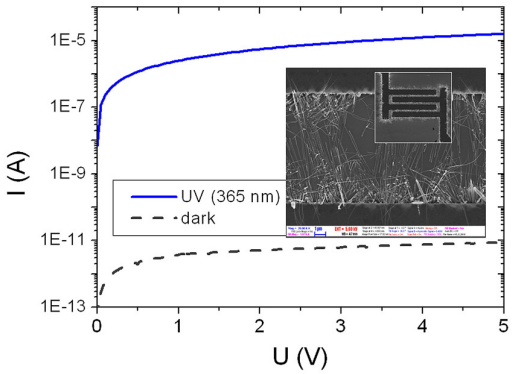

Figure 1. *I-V characteristics of UV illuminated multiple nanowire device (inset).*

Grown closely on oxide layer, the lateral multiple nanowires also enable the back gating via the substrate, which is very essential in sensor application (refreshing, enhancing sensitivity).
About six-orders-of-magnitude modulation upon UV light (360 nm) illumination was observed (Fig. 2). This is not only caused by the photocurrent, but also by the eliminating of the depletion layer due to desorption of surface oxygen.

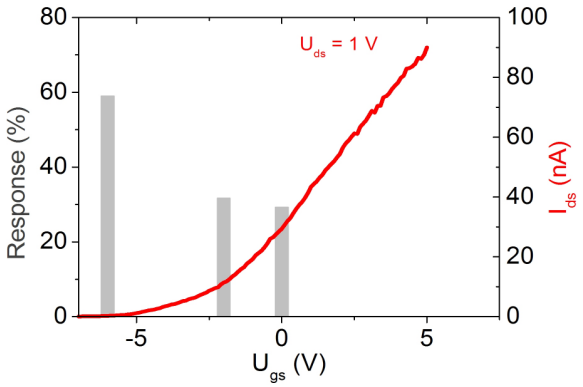

Figure 2. *100 ppm H response vs prebias gate voltage (grey bars). Ids-Ugs curve is also shown (red line).*

The I-V characteristics depicted in Figs. 1 (I_{ds} – U_{ds}) and 2 (I_{ds} –U_{gs}, red line) show the conductive modulation of the nanowires by the substrate (gate) potential. They exhibited n-channel depletion-mode behavior, as the ZnO nanowires are naturally n-type semiconductor. The benefit of back gating is revealed in Fig. 3 for 100 ppm hydrogen sensing. The highest relative current modulation (best sensitivity) for hydrogen was obtained with the pre-bias of substrate into the subthreshold region (-6V), where the current depends exponentially on the gate potential.

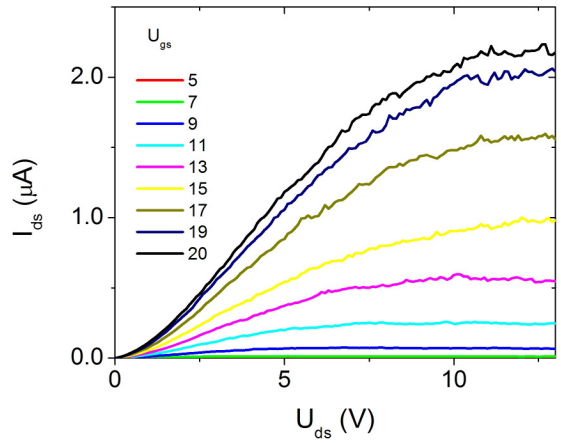

Figure 3. *I_{ds}-U_{ds} characteristics of multiple nanowire FET at different gate bias(U_{gs}).*

Complex Systems Department

Head: György SZABÓ, D.Sc.

Research Staff

- István BORSOS, engineer
- Imre EÖRDÖGH, dr. Univ. engineer
- Zoltán JUHÁSZ, Ph.D. researcher
- Géza ÓDOR, D.Sc., scientific advisor
- Károly SZÁSZ, engineer
- Attila SZOLNOKI, D.Sc., scientific advisor
- Erika TUNYOGHI, engineer
- Jeromos VUKOV, Ph.D. researcher

Ph.D. students / Diploma workers

- Lilla CZAKÓ, M.Sc. student
- Ábel HALASI, M.Sc. student
- József NYITRAI, B.Sc. student
- Zoltán DOMOKOS, B.Sc. student

The main scientific activity of this group is focused on the application of tools and concepts of non-equilibrium statistical physics for the quantitative investigation of various mathematical models. The most successful topics belong to the field of evolutionary game theory, the spreading of infection on inhomogeneous graphs, and exploration of relatedness between genetic features and different cultures in folk songs as detailed below. As a large portion of their efforts is based on numerical simulations therefore new algorithms are studied to enhance the efficiency of the computational capacities. Recent investigations are focused on spatial evolutionary potential games and on simple spatial games with zero-determinant strategies.

Two engineers, Imre Eördögh and Károly Szász, improved the efficiency of image processing algorithms developed by them previously for the quantification of morphological features used in the control of several technological processes

The scientific results achieved by the members of this group in 2012 are published in 24 articles that appeared in ranked international journals, and their previous papers were cited about 900 times during the last year. Some of their articles are available in the list of TOP 10 most cited papers for several journals. The researchers of this group write about a hundred referee reports a year on manuscripts submitted for publication in different scientific journals.

Modelling evolutionary games

(OTKA K101490 and
FQEB Grants from the Templeton Foundation under No RFP-12-22)

Gy. Szabó, A. Szolnoki, J. Vukov, and I. Borsos

The evolutionary game theory provides a general mathematical background for the quantitative analysis of large living systems composed of small objects that can represent microbes, plants, animals, human individuals or even their groups (firms, countries, etc). The mathematical concept of payoff matrix is used to describe the interactions between the players who can change their own strategy (decision, types, etc.) by following an evolutionary rule determined by payoff differences dependent on the neighboring strategies.

Now we show only one model based on the ultimatum game between neighboring players located on the sites of a lattice. This type of game describes two-person real life situations when the first player (proposer) proposes a share [p and (1-p)] of a unit sum that the second player (acceptor) can accept or refuse. If the second player accepts the proposal then they share this sum as suggested, otherwise the players receive nothing. The players play this game with using both roles against all their neighbors while their strategy is characterized by q and the acceptance level p. During the evolutionary process a randomly chosen player can adopt the more successful neighbor's strategy with a probability dependent on their payoff difference. The resultant evolutionary process is illustrated in Fig. 1 where the length of vertical lines denotes the frequency of the given strategy after different time steps.

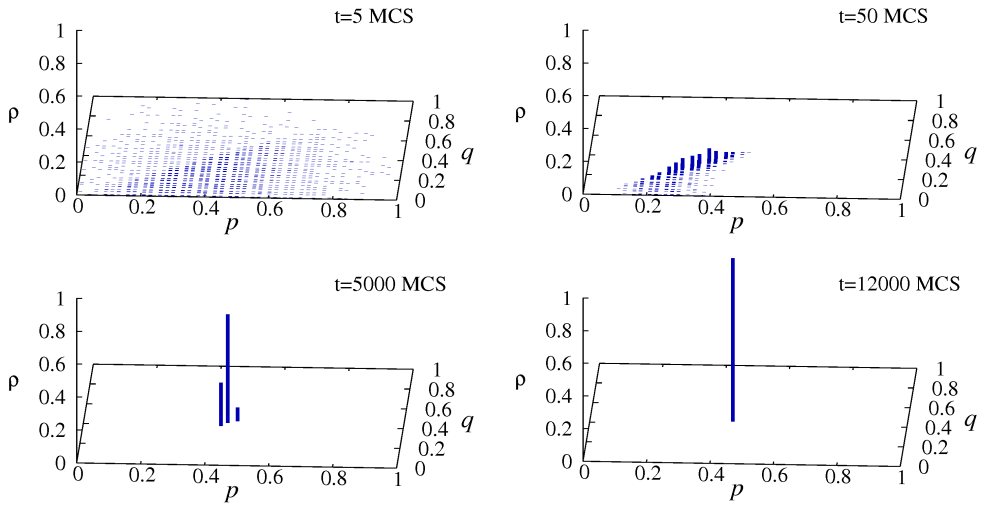

Figure 1. *Frequency of discretized (p,q) strategies after times t indicated for each plot.*

Simulations are performed when the discretized p and q values are positioned in the center of boxes obtained by dividing the whole regions into N_xN identical portions. The above plots illustrates that the system evolves into a homogeneous state where all the players use the same strategy (p_i,q_i) dependent on N characteristic to the accuracy of strategy adoption.

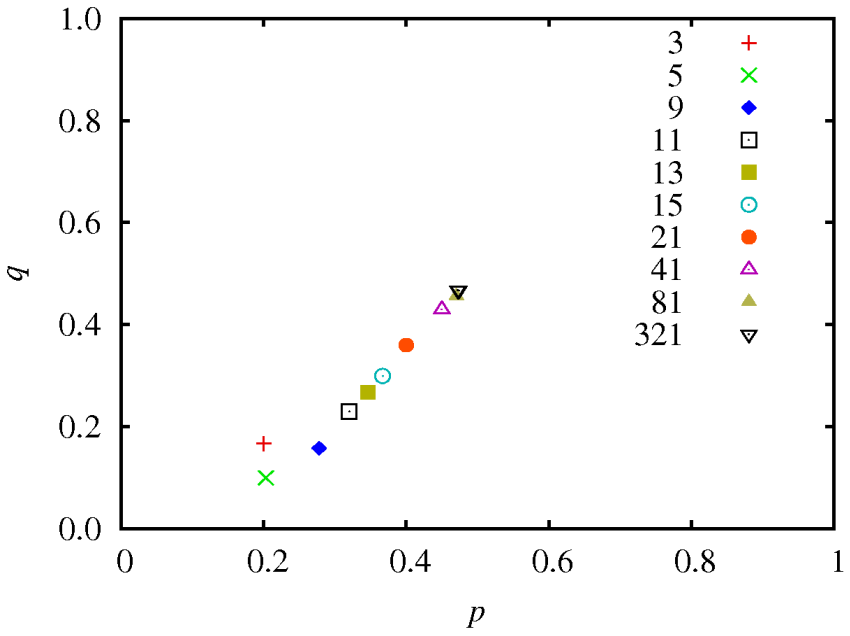

Figure 2. *Surviving strategies in a spatial ultimatum game when using different N values for both pi and qi as denoted inside the plot.*

Results in Fig. 2 clearly indicate that the strategy of each player tends towards the "fair" behavior (p_i=q_i) and both parameters go to 1/2 (referring to fraternal feature) if the accuracy of imitation is increased. In the opposite case, two strategies can coexist as denoted by two symbols for the value of p=0.2.

Besides the above model evolutionary games based on ultimatum games and other social dilemmas are also studied for different connectivity structures to quantify the effect of punishments and rewards as well as the effect of the connectivity structure on the maintenance of cooperative behavior. The latter analyses are based on evolutionary rules resembling imitation processes. In addition, the effects of other types of evolutionary rules are also investigated. For example, assuming more intelligent players, who are capable of choosing a better strategy for the given neighborhood, coexistence of different types of fraternal and egoist players is found using Monte Carlo simulations. More precisely, the chessboard like arrangements of strategies and personalities could help the maintenance of cooperative behavior until the "sucker's payoff" remains above a threshold value dependent on the advantage of exploitation.

Spreading of infection on weighted graphs

(OTKA K77629)

G. Ódor

The analysis of the spreading of infection has a long tradition in statistical physics by studying the contact process among agents distributed on lattices. In the simplest model the agents can be healthy or infected, and two elementary steps govern the evolutionary process: i) the infected agents recur and ii) the healthy agents are infected by one of their neighbors. The ratio between the two elementary processes is characterized by a parameter λ. The analysis of these models is extended to systems where the agents are distributed on inhomogeneous networks representing real social connectivity structure. In contrary to the spatial systems the latter model exhibit basically different behaviors as illustrated in Fig. 1.

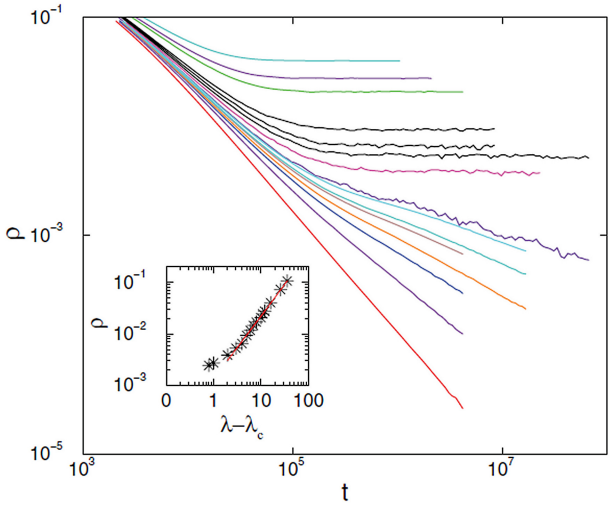

Figure 1. *Time dependence of the ratio of the infected agents on a Barabási-Albert scale-free network for several values of λ. .*

The numerical simulations show three different scenarios in the evolution of infection:

- the ratio of the infected agents tends to a fix value, dependent on λ;
- the infection becomes extinct by following a power law behavior (Griffiths phase) within a wide range of time interval, and
- the ratio of infected agent goes to zero exponentially.

The slowly vanishing infection plays relevant role in many other systems. For example, such processes are also expected in the above-mentioned evolutionary games if imitations control the evolution of strategy distribution for quenched connectivity structures.

Simultaneous study of folk music and genetics using AI

(OTKA K81954)

Z. Juhász

In recent years, we have elaborated on a software system, which characterizes the overall similarity of different folk song databases using a scalar measure. The basic idea of this system is that musical information propagates and evolves by endless variation of melodies, since variation is an essential feature of most oral cultures.
This led us to the question whether these connections are merely accidental or can they possibly relate to the migration of populations in any way? Does the complex structure of musical connections display a clear picture and can we interpret this connection system on a genetic basis as well?
We found that close musical relations of populations indicate close genetic distances (\0.05) with a probability of 82%. It was observed that there is a significant correlation between population genetics and folk music; maternal lineages have a more important role in folk music traditions than paternal lineages (Fig. 1).

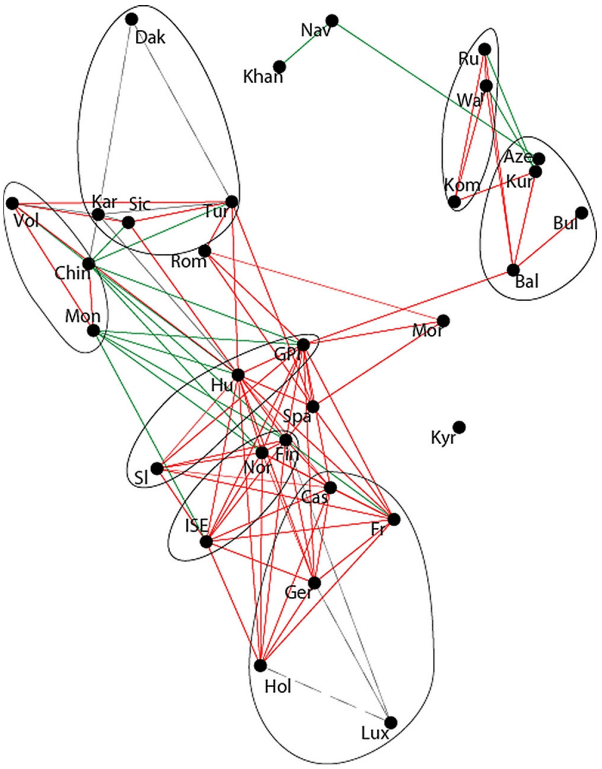

Figure 1. *Map of musical language groups of 31 folk music cultures.*

Red edges: simultaneous musical and genetic contacts.

Green edges: musical contacts without genetic support.

Grey edges: musical contacts indicated, no genetic data were found.

ACTIVITIES

MFA Seminar Talks

2012.01.11

Péter HARMAT
(MTA TTK MFA, Budapest, Hungary): "*Cyclic morphological changes of nano-silicate gels as a result of ultrasonic excitation*"

2012.01.18

András KOVÁCS
(MTA TTK MFA, Budapest, Hungary - Jülich): "*Transmission electron microscopy without lens distortions: examples and opportunities*"

2012.01.25

András DEÁK
(MTA TTK MFA, Budapest, Hungary): "*Plasmonic nano-particles and organic semiconductors*"

2012.02.08

György RADNÓCZI
(MTA TTK MFA, Budapest, Hungary): "*Spinodal decomposition, as mechanism for layer formation in Ag-Cu and TiN-AlN films*"

2012.02.15

Antal KOÓS
(MTA TTK MFA, Budapest, Hungary): "*Preparation by CVD method of carbon nano-structures from doped carbon nanotubes to graphene*"

2012.02.16

Frank GÜELL
(University of Barcelona, Spain): "*Synthesis, structural characterization and optical spectroscopy of ZnO nanowires*"

2012.02.22

László KÓTIS
(MTA TTK MFA, Budapest, Hungary): "*Study of the effects of ion bombardment by Auger electron spectroscopic in-depth mapping*"

2012.03.21

Zoltán JUHÁSZ
(MTA TTK MFA, Budapest, Hungary): "*The self-organizing cloud and the language families of folk-music*"

2012.03.22

Yahachi SAITO
(Nagoya University, Japan): "*Carbon nanotube field emitters: fundamental properties and applications*"

2012.03.22 **Chuhei OSHIMA**
(Waseda University, Japan): "*Honeycomb monolayer of B, C and N on solid surfaces*"

2012.04.17 **Leonid CHERNYAK**
(University of Central Florida, USA): "*Studies of electron trapping in ZnO semiconductor*"

2012.04.18 **Krisztián KOHÁRY**
(University of Exeter, UK): "*Memflector – An optical analogue of Memristor using phase-change materials*"

2012.04.25 **Orsolya TAPASZTÓ**
(MTA TTK MFA, Budapest, Hungary): "*SiN nano-composites doped by carbon nano-structures*"

2012.05.16 **Attila GRANDPIERRE**
(MTA Csillagászati Intézet, Budapest, Hungary): "*The relation between the Bauer principle and the quantum physics*"

2012.05.23 **Szabolcs CSONKA**
(BME, Budapest, Hungary): "*Quantum circuits in InAs nano-rods*"

2012.08.30 **Zoltán FEKETE**
(MTA TTK MFA, Budapest, Hungary): "*Development and characterization of silicon microfluidic components and systems*"

2012.09.18 **Keiichi NAMBA**
(Osaka University, Japan): "*High resolution high throughput cryo EM helical image analysis of macromolecular assemblies*"

2012.11.14 **Zoltán OSVÁTH**
(MTA TTK MFA, Budapest, Hungary): "*Low temperature STM and transport measurements on metal-graphene junctions*"

Research and Development Partners, Foreign Visitors

ALEXEY, Klochkov *(Institute of Ultra High Frequency Semiconductor Electronics, Russian Academy of Sciences, Moscow, Russia)*
AP, Zsolt *(Babes-Bolyai Science University, Kolozsvár, Romania)*
BÍRÓ, Csaba (Sapientia Erdélyi Magyar Tudományegyetem, Romania)
BÍRÓ, Domokos *(Sapientia Erdélyi Magyar Tudományegyetem Tg-Mures, Romania)*
BURAK, Boguslaw *(COMEF, Poland)*
CACCIOLA, Matteo *(Universita degli Studi Mediterranea di Reggio Calabria, Department of Civil, Energy, Enviromental and Material s Engineering, Italy)*
CAYREL, Frederic Cayrel *(LMP, Tours University, France)*
CEBULSKI, Józef *(COMEF, Poland)*
CHAN-YONG, Hwang *(Korea Research Institute for Standards and Science, Daejeon, Korea)*
CHERNYAK, Leonid *(University of Central Florida, USA)*
CHUHEI, Oshima *(Waseda University, Japan)*
DARNIL, Guillame *(FRANCELAB, Hungary)*
DHAR, Ajay *(National Physical Laboratory, India)*
DMITRY, Ponomarev *(Institute of Ultra High Frequency Semiconductor Electronics, Russian Academy of Sciences, Moscow, Russia)*
FLEISCHER, Maximilian *(Siemens Corporate Technology, München, Germany)*
FRIEDMANN, *Juergen (University of Alaska, USA)*
FRIGERI, Cesare *(CNRS, Parma, Italy)*
GAJEWSKA, Magda *(Institute of Metallurgy Krakow, Poland)*
GALTIER, Gaal *(LMP, Tours University, France)*
GANEM, Jean-Jacques *(INSP University, France)*
GEORGII, Lashkarov *(Institute for Materials Science, National Academy of Science of Ukraine, Kiev)*
GÜELL VILÁ, Frank *(University of Barcelona, Spain)*
HARRIS, Adam *(FRANCELAB, Hungary)*
HEGEDÜSOVÁ, Noémi *(Comenius University of Bratislava, Slovak Republic)*
IEVTUSENKO, Arsenii *(Institute for Materials Science, National Academy of Science of Ukraine, Kiev)*
INDYKA, Paulina *(Institute of Metallurgy, Krakow, Poland)*
IN-HO, Lee *(Korea Research Institute for Standards and Science, Daejeon, Korea)*
JUN-SIK, Hong *(National Research Foundation of Korea)*
KEIICHI, Namba *(Osaka University, Japan)*
LAMBIN, Philippe *(Facultes Universitaires Notre-Dame de la Paix, Namur, Belgium)*
LANYI, Stefan *(Physics Intitute of Slovak Academy of Sciences, Slovak Republic)*
LOBOTKA, Peter *(ELU SAV Bratislava, Slovak Republic)*
LOMBARDO, Ersilia *(Universita degli Studi Mediterranea di Reggio Calabria, Department of Civil, Energy, Enviromental and Material s Engineering, Italy)*

MARBACH, Hubertus *(Friedrich-Alexander-Univ., Erlangen-Nürnberg, Germany)*
MATVEEVA, Anna *(Univ. Minho, Guimaraes, Portugal)*
MIZUGUCHI, Masae *(Tatayema Kagaku, Toyama, Japan)*
MIZUGUCHI, Shoichiro *(Tatayema Kagaku, Toyama, Japan)*
MOON-YEARN, Hwang *(Vice Minister, President Council of Future and Vision, Korea)*
MRAVEC, Boris *(Comenius University of Bratislava, Slovak Republic)*
MUKHOPADHYAY, Subhas Chandra *(School of Engineering and Advanced Technology, Massey University Manawatu, Palmerston North, New Zealand)*
NONGLATON, Guillaume *(DTBS, SBSC/LCMI, France)*
PARK-YOUNG, Hoon *(Korea Research Institute of Bioscience and Biotechnology - KRIBB, Korea)*
PECHEVA, Emilia *(Institute of Solid State Physics Bulgarian Academy of Scienes, Bulgaria)*
PLOCH, Dariusz *(COMEF, Poland)*
RAMSDEN, Jeremy *(Collegium Basilea, Switzerland)*
ROMANOVSKY, Vladimir *(University of Alaska, USA)*
RYSSEL, Heiner *(Fraunhofer IISB, Erlangen, Germany)*
SOPCAK, Tibor *(IMR, SAS, Slovak Republic)*
SRIVASTAVA, Avanish Kumar *(National Physical Laboratory, India)*
STAN, Katarzina *(Institute of Metallurgy Krakow, Poland)*
STOEMENOS, J. *(University of Thessaloniki, Greece)*
STRECKOVA, Magdalena *(IMR, SAS, Slovak Republic)*
SZEREGIJ, Eugeniusz *(COMEF, Poland)*
SZLEZYNGER, Macej *(Institute of Metallurgy Krakow, Poland)*
TAKAHIRO, Nagata *(NIMS, Tsukuba, Japan)*
TOIVOLA, Minna *(Picosun Oy, Finnland)*
TOMÁS, Ivan *(CSTA Physical Institute, Praha, Czech Republic)*
TSUNEO, Morita *(Tateyama Ltd. Japan)*
VÁVRA, Ivo *(ELU SAV, Bratislava, Slovak Republic)*
VÖRÖS, János *(Institute for Biomedical Engineering, Zürich, Swirzerland)*
WATANUKI, Masaru *(Tatayema Kagaku, Toyama, Japan)*
WITTMANN, Marion *(Biogen Idec Ltd., Boston, USA)*
WON-DOM, Kim *(Korea Research Institute for Standards and Science, Korea)*
YAHACHI, Saito *(Nagoya University, Japan)*
YAKOVLEV, Yuri *(LIRO at Ioffe Physico-Technical Institute, Russia)*
YONG-SUK, Kim *(KOTRA, Korea)*
YONG-SUNG, Kim *(Korea Research Institute for Standards and Science, Korea)*

Hungarian Academy of Sciences
Research Centre for Natural Sciences
Institute of Technical Physics and Materials Science

SERVICES OF THE ACCREDITED ELLIPSOMETRY LABORATORY

http://www.ellipsometry.hu/

The Institute of Technical Physics and Materials Science (MFA) of the Hungarian Academy of Sciences has an experience of many decades in the analysis and assessment of materials. Ellipsometry is an optical method based on the change of light polarization during reflection on the sample. The method is suitable for the measurement of sub-nanometer to several microns thin layers with a typical sensitivity of Angstroms. The refractive index and all the layer properties influencing the optical response (e.g. crystallinity, homogeneity, surface roughness, density, optical absorption) can be mesured with high sensitivity in a quick and non-destructive way that allows monitoring during layer preparation or processing.

The National Accreditation Board according to the ISO 17025 standard has accredited the Ellipsometry Laboratory of MFA. The laboratory is a member of the ANNA consortium that offers a wide range of analytical techniques for nanotechnologies (http://www.i3-anna.org/).

AKKREDITÁLÁSI OKIRAT
ACCREDITATION CERTIFICATE

A NEMZETI AKKREDITÁLÓ TESTÜLET
a 2005. LXXVIII. törvény felhatalmazása alapján elismeri, hogy a
Authorized by the law LXXVIII of 2005 the Hungarian Accreditation Board recognizes that

Magyar Tudományos Akadémia
Műszaki Fizikai és Anyagtudományi Kutató Intézet
Fotonika Osztály Ellipszometria Laboratórium
1121 Budapest, Konkoly Thege Miklós út 29-33.

megfelel az MSZ EN ISO/IEC 17025:2005 szabvány követelményeinek és a
complies with the criteria of MSZ EN ISO/IEC 17025:2005 standard as

VIZSGÁLÓLABORATÓRIUM
TESTING LABORATORY

kategóriába az alábbi számon bejegyzi
and has been assigned registration number

NAT-1-1617/2010

Az akkreditálás területét az akkreditálási határozat tartalmazza.
The scope of accreditation is specified in the accreditation decision.

Az akkreditálási okirat érvényes
The accreditation certificate is valid until

2014. január 26.

Az akkreditálási okirat kiadva
The accreditation certificate is issued

Budapest, 2010. január 27.

a Nemzeti Akkreditáló Testület képviseletében
Director of the Hungarian Accreditation Board

Applications:

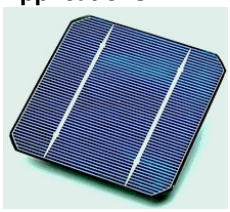

Photovoltaics

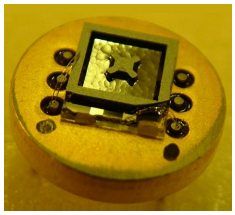

Sensorics

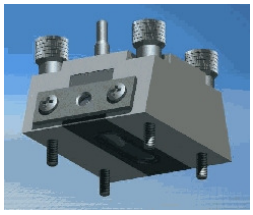

Biosensorics

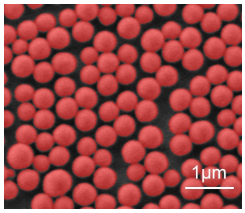

Surface nanostructure

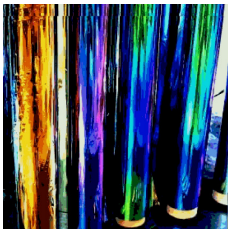

Coatings

Surface quality

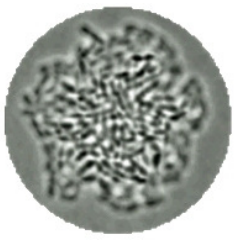

Biological films

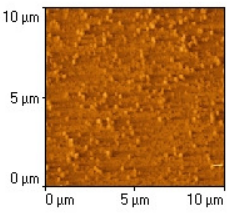

Nanoroughness

Visitors: Konkoly-Thege M. út 29-33, BUDAPEST, 1121 HUNGARY, **Mail:** P.O. Box 49., H-1525, **Web:** http://www.mfa.kfki.hu/
Phone, Director: +36-1-3922224, **Phone, Administration:** +36-1-3922227, **Fax:** +36-1-3922226

Hungarian Academy of Sciences
Research Centre for Natural Sciences
Institute of Technical Physics and Materials Science

Some key sample properties that are measurable with high precision

- Layer thickness (0.1-1000 nm)
- Refractive index (precision: ~0.001)
- Homogeneity
- Assessment of interface quality
- Porosity (e.g. the volume fraction of voids in porous layers)
- Surface nanoroughness
- Composition (e.g. volume fraction of nanocrystals in a dielectric matrix)
- Crystallinity (order and disorder in crystalline materials)

Specifications of the spectroscopic ellipsometer

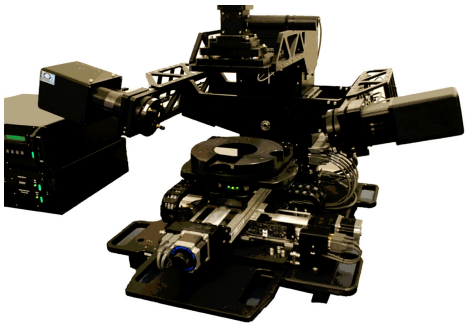

- Manufacturer and type: Woollam M-2000DI
- Wavelength range: 193-1690 nm
- Precision: 0.1-5.0 nm (depends on the sample)
- Maximum sample size: 200 mm x 200 mm
- Minimum sample size: 5 mm x 3 mm
- Mapping area: 150 mm x 150 mm
- Measurable sample: **optical quality layer in the thickness range from several angstroms to several microns** (the root mean square roughness of the interfaces must not be greater than several times 10 nm; samples that have a matt, non-shiny surface are usually not measurable)

Protocol

The measurement is documented in a protocol in compliance with the ISO 17025 standard.
The protocol consists of the description of
(1) Sample preparation,
(2) Measurement,
(3) Measured spectra,
(4) Development of optical models,
(5) Details of parameter fit,
(6) Determined sample properties.

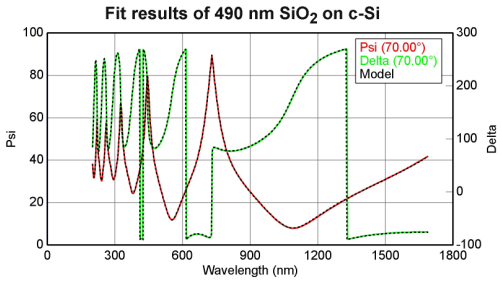

Contact

Dr. Péter PETRIK, Head of Laboratory
petrik.peter@ttk.mta.hu
+36 1 392 2502

Visitors: Konkoly-Thege M. út 29-33, BUDAPEST, 1121 HUNGARY, **Mail:** P.O. Box 49., H-1525, **Web:** http://www.mfa.kfki.hu/
Phone, Director: +36-1-3922224, **Phone, Administration:** +36-1-3922227, **Fax:** +36-1-3922226

MFA Publications in 2011

1. **Abo S**, Azuma T, Lohner T, Wakaya F, Takai M: „Study on spatial resolution of three-dimensional analysis by full count TOF-RBS with beryllium nanoprobe", *Nucl Instrum Meth B 273: 266-269 (2012), IF:1.211*
2. **Abo S**, Horiuchi H, Wakaya F, Battistig G, Lohner T, Takai M: „Time of flight elastic recoil detection analysis with toroidal electrostatic analyzer for ultra shallow dopant profiling", *Surf Interface Anal 44: (6)732-735 (2012), IF:1.180*
3. **Abo S**, Masuda N, Wakaya F, Lohner T, Onoda S, Makino T, Hirao T, Ohshima T, Iwamatsu T, Oda H, Takai M: „Difference of soft error rates in SOI SRAM induced by various high energy ion species", *Nucl Instrum Meth B 273: 262-265 (2012), IF:1.211*
4. **Agócs E**, Petrik P, Fried M, Nassiopoulou AG: „Optical characterization using ellipsometry of Si nanocrystal thin layers embedded in silicon oxide", In: *B Yan, S Higashi, C C Tsai, Q Wang, H Gleskova (Eds.) MRS Spring Meeting and Exhibit., Cambridge: Materials Research Society, 2012. pp.367-372. (2012)*
5. **Allazadeh MR**: „Cooling rate optimization of as-cast consciously cast steel", *IJEM 9: (3)1-16 (2012)*
6. **Árkai P**, Abad I, Nieto F, Németh T, Horváth P, Kis VK, Judik K, Jiménez-, Millán J: „Retrograde alterations of phyllosilicates in low-grade metapelite: a case study from the Szendro{combining double acute accent} Paleozoic, NE-Hungary", *Swiss J Geosci 105: (2)263-282 (2012), IF:0.879*
7. **Attolini G**, Bosi M, Watts BE, Battistig G, Dobos L, Pécz B: „The influence of C_3H_8 and CBr_4 on structural and morphological properties of 3C-SiC layer", *Mater Sci Forum 711: 22-26 (2012)*
8. **Baji Zs**, Lábadi Z, Horváth ZE, Bársony I: „Structure and morphology of aluminium doped Zinc oxide layers prepared by atomic layer deposition", *Thin Solid Films 520: (14)4703-4706 (2012), IF:1.890*
9. **Baji Zs**, Lábadi Z, Horváth ZE, Molnár Gy, Volk J, Bársony I, Barna P: „Nucleation and Growth Modes of ALD ZnO", *Cryst Growth Des 12: (11)5615-5620 (2012), IF:4.720*
10. **Baji Zs**, Szanyó A, Gy Molnár, Tóth AL, Pető G, Frey K, Kótai E, Kaptay G: „Formation of nanoparticles by ion beam irradiation of thin films", *J Nanosci Nanotechno 12: (6)5009-5015 (2012), IF:1.563*
11. **Balázsi Cs**, Gergely G, Sahin FC, Göller G: „Spark Plasma Sintered Hydroxyapatite–Zirconia Composites: Structural and Mechanical Properties", In: *18th International Conference on Composite Materials 2012. pp.1-3*
12. **Balázsi Cs**, *Gergely G, Xue R, Goldbeck C, Perrotta PL, Balázsi K, Gouma PI: „Biogenic nanosized hydroxyapatite / cellulose acetate composites for tissue engineering", Cell Mater 24: (sul.1)35 (2012)*
13. **Balázsi Cs**: „Silicon Nitride Composites with Different Nanocarbon Additives", *J Korean Ceramic Soc 49: (4)352-362 (2012)*

14. **Balázsi K**, Gergely G, Chae CH, Sim HY, Choi JY, Kim SG, Balázsi Cs: „Biogenic hydroxyapatite from eggshell as bone formation material", *Cell Mater 24: (supl.1)18 (2012)*
15. **Balázsi K**, Horváth Á, Horváth M, Koncz P, Göller G, Cina- Sahin F, Yücel O, Balázsi Cs: „Nanostructured Oxide Dispersed Strengthened Steels: Preparation and Investigation", *Powder Metall Progr - J Sci Tech Part Mater 12: (1)27-33 (2012)*
16. **Balázsi K**, Vandrovcová M, Bacáková L, Bertóti I, Balázsi Cs: „Development of biocompatible TiC/a:C nanocomposite barrier coating for dental implants", *Cell Mater 24: (Supl.1)36 (2012)*
17. **Bálint Z**, Kertész K, Piszter G, Vértesy Z, Biró LP: „The well-tuned blues: the role of structural colours as optical signals in the species recognition of a local butterfly fauna (Lepidoptera: Lycaenidae: Polyommatinae)", *J R Soc Interface 9: (73)1745-1756 (2012), IF:4.402*
18. **Bányász I**, Berneschi S, Bettinelli M, Brenci M, Fried M, Khanh NQ, Lohner T, Conti GN, Pelli S, Petrik P, Righini GC, Speghini A, Watterich A, Zolnai Zs: „MeV Energy N^+-Implanted Planar Optical Waveguides in Er-Doped Tungsten-Tellurite Glass Operating at 1.55 μm", *IEEE Photonics J 4: (3)721-727 (2012), IF:2.320*
19. **Bányász I**, Berneschi S, Khanh NQ, Lohner T, Lengyel K, Fried M, Péter A, Petrik P, Zolnai Zs, Watterich A, Nunzi-Conti G, Pelli S, Righini GC: „Formation of slab waveguides in eulytine type BGO and CaF_2 crystals by implantation of MeV nitrogen ions", *Nucl Instrum Meth B 286: (1)80-84 (2012), IF:2.11*
20. **Bányász I**, Zolnai Zs, Pelli S, Berneschi S, Nunzi-Conti G, Fried M, Lohner T, Petrik P, Brenci M, Righini GC: „Fabrication of barrier-type slab waveguides in Er^{3+} - doped tellurite glass by single- and double energy MeV N+ ion implantation", *Proceedings of Spie 8264: (2012)*
21. **Barna Á**, Gurbán S, Kótis L, Lábár J, Sulyok A, Tóth AL, Menyhárd M, Kovac J, Panjan P: „Growth of amorphous SiC film on Si by means of ion beam induced mixing", *Appl Surf Sci 263: 367-372 (2012), IF:2.103*
22. **Barna Á**, Kótis L, Pécz B, Sulyok A, Sáfrán G, Tóth AL, Menyhárd M, Kovács A, Savenko A: „Thin TaC layer produced by ion mixing", *Surf Coat Tech 206: (19-20)3917-3922 (2012), IF:1.867*
23. **Battistig G**, Grand L, Karmos Gy, Payer K, Pongrácz A, Ulbert I, Vázsonyi É: „Eljárás CMOS technológiába integrálható, egykristályos Si alapú, nedves kémiai marással készített, párhuzamos oldalfalakkal és lekerekített élekkel határolt extracelluláris elektródok előállítására", *Registration Num.: P0900774/2, 2009/2012*
24. **Battistig G**: „Orientation dependent growth of SiC nanocrystals at the SiO_2/Si interface", *Thin Solid Films 520: 1973-1977 (2012), IF:1.890*
25. **Biró LP**, Hevesi L, Lambin P: „The Narrowest Possible Graphene Nanoribbon was Synthesized Fifty Years Ago", *Nanopages 7: (1)25-27 (2012)*
26. **Biró LP**, Nemes-Incze P, Lambin P: „Graphene: nanoscale processing and recent applications", *Nanoscale 4: (6)1824-1839 (2012), IF:5.914*
27. **Blahó M**, Egri Á, Hegedüs R, Jósvai J, Tóth M, Kertész K, Biró LP, Kriska Gy, Horváth G: „No evidence for behavioral responses to circularly polarized light in four scarab beetle

species with circularly polarizing exocuticle", *Physiol Behav 105: 1067-1075 (2012), IF:2.869*

28. **Blahó M**, Egri Á, Horváth G, Hegedüs R, Kriska Gy, Jósvai J, Tóth M, Kertész K, Biró LP: „A cirkulárisan fénypolarizáló szkarabeuszok nem reagálnak a cirkuláris polarizációra – I. Rész", *Fizikai Szemle 62: 217-221 (2012)*
29. **Blahó M**, Egri Á, Horváth G, Hegedüs R, Kriska Gy, Jósvai J, Tóth M, Kertész K, Biró LP: „A cirkulárisan fénypolarizáló szkarabeuszok nem reagálnak a cirkuláris polarizációra – II. Rész", *Fizikai Szemle 62: (9)294-298 (2012)*
30. **Broitman E**, Furlan A, Geuorguiev GK, Czigány Zs, Högberg H, Hultman L: „Structural and mechanical properties of CN_x and CPs thin solid films", *Key Eng Mater 488-489: 581-584 (2012)*
31. **Chen X**, Szolnoki A, Perc M, Wang L: „Impact of generalized benefit functions on the evolution of cooperation in spatial public goods games with continuous strategies", *Phys Rev E Stat Nonlin 85: (6) (2012) 066133, IF:2.255*
32. **Chen X**, Szolnoki A, Perc M: „Averting group failures in collective-risk social dilemmas", *Europhys Lett 99: (6) (2012) 068003, IF:2.171*
33. **Chen X**, Szolnoki A, Perc M: „Risk-driven migration and the collective-risk social dilemma", *Phys Rev E Stat Nonlin 86: (3) (2012) 036101, IF:2.255*
34. **Csákberényi-Malasics D**, Rodriguez-Blanco J, Kovács-Kis V, Recnik A, Benning LG, Pósfai M: „Structural properties and transformations of precipitated FeS", *Chem Geol 294-295: 249-258 (2012), IF:3.518*
35. **Csató A**, Szabó A, Fonseca A, Vuono D, Kónya Z, Volodin A, Van Haesendonck C, Biró LP, Giordano G, Nagy JB: „Synthesis and characterisation of coiled carbon nanotubes", *Catal Today 181: (1)33-39 (2012), IF:3.407*
36. **Czigány Zs**, Misják F, Geszti O, Radnóczi Gy: „Structure and phase formation in Cu–Mn alloy thin films deposited at room temperature", *Acta Mater 60: (20)7226-7231 (2012), IF:3.755*
37. **Czigány Zs**, Misják F, Radnóczi Gy: „Development of phases and morphology in DC sputtered Cu-Mn alloy thin films at temperatures below 600 °C", *In: Proceedings of the 15th European Microscopy CongressManchester: 2012. pp.*
38. **Dangelo M**, Deokar G, Steydli S, Pongrácz A, Pécz B, Silly MG, Sirotti F, Deville-Cavellin C: „In-situ formation of SiC nanocrystals by high temperature annealing of SiO_2/Si under CO: A photoemission study", *Surf Sci 606: 697 (2012), IF:1.994*
39. **Daróczi CsS**: "MFA Open Day", and "MFA Summer School" in *Menyhárd M and Daróczi CsS (Eds.), MTA MFA Yearbook 2011, pp.23-24, MTA MFA, Budapest, Hungary (2012)*
40. **Detrich A**, Hild E, Nagy N, Volentiru E, Hórvölgyi Z: „Combined Langmuir-Blodgett and sol-gel coatings", *Thin Solid Films 520: 2537-2544 (2012), IF:1.890*
41. **Dimopoulos T**, Radnóczi GyZ, Horváth ZE, Bruckl H: „Increased thermal stability of Al-doped ZnO-based transparent conducting electrodes employing ultra-thin Au and Cu layers", *Thin Solid Films 520: (16)5222-5226 (2012), IF:1.890*
42. **Dobos L**, Tóth L, Pécz B, Horváth ZE, Tóth AL, Beaumont B, Bougrioua Z: „The microstructure of Ti/Au contacts on n-type GaN annealed in nitrogen", *Microelectron Eng 90: 118-120 (2012), IF:1.557*

43. **Dobos L**, Tóth L, Pécz B, Horváth ZsJ, Horváth ZE, Tóth AL, Beaumont B, Bougrioua Z: „Bilayer Cr/Au contacts on n-GaN", *Vacuum 86: 769-772 (2012), IF:1.317*
44. **Dobrik G**, Nemes-Incze P, Tapasztó L, Lambin P, Biró LP: „Nanoscale lithography of graphene with crystallographic orientation control", *Physica E 44: (6)971-975 (2012), IF:1.532*
45. **Dobrik G**, Tapasztó L, Biró LP: „Nanometer wide Ribbons and Triangles by STM Lithography of Graphene", *Nanopages 7: 1-7 (2012)*
46. **Domenico G**, Dortu F, Bernier D, Johnson NP, Sharp GJ, Hou L, Khokhar AZ, Fürjes P, Kurunczi S, Petrik P, Horváth R, Aalto T, Kolari K, Ylinen S, Haatainen T, Egger H: „NIL fabrication of a polymer-based photonic sensor device in P3SENS project", *Proceedings of Spie 8435: 843529 (2012)*
47. **Dózsa L**, Lányi S: „Local capacitance analysis using a modified deep level spectrometer", *Cent Eur J Phys 10: (5)1178-1182 (2012), IF:0.909*
48. **Dózsa L**, Molnár Gy, Zolnai Zs, Dobos L, Pécz B, Galkin NG, Dotsenko SA, Bezbabny DA, Fomin DV: „Formation and characterization of semiconductor Ca_2Si layers prepared on p-type silicon covered by an amorphous silicon cap", *J Mater Sci 2012.oct: DOI: 10.1007/s10853-012-6945-6 (2012), IF:2.015*
49. **Dusza J**, Morgiel J, Duszová A, Kvetková L, Nosko M, Kun P, Balázsi Cs: „Microstructure and fracture toughness of Si_3N_4 + graphene platelet composites", *J Eur Ceram Soc 32: (12)3389-3397 (2012), IF:2.353*
50. **Erdélyi R**, Halász V, Szabó Z, Lukács IE, Volk J: „Mechanical characterization of epitaxially grown zinc oxide nanorods", *Physica E 44: 1050-1053 (2012), IF:1.532*
51. **Erdélyi R**, Madsen HM, Sáfrán G, Hajnal Z, Lukács IE, Fülöp G, Csonka Sz, Nygard J, Volk J: „In-situ mechanical characterization of wurtzite InAs nanowires", *Solid State Commun 152: 1829-1833 (2012), IF:1.649*
52. **Fabian M**, Sváb E, Pamukchieva V, Szekeres A, Petrik P, Vogel S, Ruett U: „Study of As-Se-Te glasses by neutron-, X-ray diffraction and optical spectroscopic methods", *J Non-Cryst Solids 358: 860-868 (2012), IF:1.537*
53. **Fekete Z**, Huszka G, Pongrácz A, Jágerszki Gy, Gyurcsányi RE, Vrouwe E, Fürjes P: „Integrated microfluidic environment for solid-state nanopore sensors", *Procedia Engineering 47: 13-16 (2012)*
54. **Fekete Z**, Nagy P, Huszka G, Tolner F, Pongrácz A, Fürjes P: „Performance characterization of micromachined particle separation system based on Zweifach–Fung effect", *Sensor Actuat B Chem 162: 89 (2012), IF:3.898*
55. **Fekete Z**, Pongrácz A, Fürjes P, Battistig G: „Improved process flow for buried channel fabrication in silicon", *Microsyst Technol 18: 353 (2012), IF:0.931*
56. **Frey K**, Iablokov V, Sáfrán G, Osán J, Sajó I, Szukiewicz R, Chenakin S, Kruse N: „Nanostructured MnO_x as highly active catalyst for CO oxidation", *J Catal 287: 30-36 (2012), IF:6.002*
57. **Fried M**, Juhász Gy, Major Cs, Németh A, Petrik P, Polgár O, Salupo C, Dahal LR, Collins RW: „Application of a Dual-spectral-range, Divergent-beam Spectroscopic Ellipsometer for High-Speed Mapping of Large-area, Laterally-inhomogeneous, Photovoltaic Multilayers", In: *Ji H, Ren B, Mannivanan V, Tsakalakos L (Eds.), MRS Spring Meeting and Exhibit., Cambridge: Materials Research Society, 2012. pp.157-162.*

58. **Frigeri C**, Serényi M, Csik A, Szekrényes Zs, Kamarás K, Nasi L, Khanh NQ: „Evolution of the structure and hydrogen bonding configuration in annealed hydrogenated a-Si/a-Ge multilayers and layers", *Appl Surf Sci 262: AiP (2012), IF:2.103*
59. **Fülöp E**, Nagy N, Deák A, Bársony I: „Langmuir–Blodgett Films of Gold/silica Core/shell Nanorods", *Thin Solid Films 520: 7002-7005 (2012), IF:1.890*
60. **Fürjes P**, Fekete Z, Illés L, Tóth AL, Battistig G, Gyurcsányi RE: „Effects of the Focused Ion Beam parameters on nanopore milling in solid state membranes", *Procedia Engineering 47: 684-687 (2012)*
61. **Gasparics A**, Vértesy G, Pávó J: „Probe for detecting weakly interacting magnetic nanoparticles", *Int J Appl Electrom 39: (1-4)29-34 (2012), IF:0.122*
62. **Gouma P**, Xue R, Goldbeck CP, Perrotta P, Balázsi Cs: „Nano-hydroxyapatite—Cellulose acetate composites for growing of bone cells", *Mater Sci Eng C 32: (3)607-612 (2012), IF:2.686*
63. **Grzonka J**, Mania R, Lábár J, Morgiel J: „Effect of Silicon Additions in CrSi (10, 20, 30, 40 at% Si) Magnetron Targets on Microstructure of Reactively Deposited (Cr,Si)N Coatings", *Solid State Phenom 186: 182-187 (2012)*
64. **Hasaneen MF**, Biro D, Székely L, Nemes-Incze P, Barna PB: „Substructure in the columnar crystals of the Ti0.45O0.20N0.35 oxynitride thin film", *Vacuum 86: (12)2105-2108 (2012), IF:1.317*
65. **Hegedűs Z**, Gubicza J, Kawasaki M, Chinh NQ, Fogarassy Zs, Langdon TG: „Microstructure of low stacking fault energy silver processed by different routes of severe plastic deformation", *J Alloy Compd 536: (Suppl.1)S190-S193 (2012), IF:2.289*
66. **Horváth ZsJ**, Rakovics V, Yakovlev YP, Turmezei P: „Current transport in nanocrystalline CdS/InP heterojunction p-n diodes", In: *E Savostyanova (Eds.), 20th International Symposium Nanostructures: Physics and Technology, St. Petersburg:2012. pp.227-228. (ISBN:978-5-91326-179-3)*
67. **Horváth ZsJ**, Basa P, Jászi T, Molnár KZ, Pap AE, Molnár Gy: „Charging behavior of silicon nitride based non-volatile memory structures with embedded semiconductor nanocrystals", *Appl Surf Sci (in press) (2012), IF:2.103*
68. **Horváth ZsJ**, Molnár KZs, Molnár Gy, Basa P, Jászi T, Pap AE, Lovassy R, Turmezei P: „Charging behaviour of MNOS structures with embedded Ge nanocrystals", *Phys Status Solidi C Conf Crit Rev 9: (6)1370-1373 (2012)*
69. **Hvizdos P**, Puchy V, Duszová A, Dusza J, Balázsi Cs: „Tribological and electrical properties of ceramic matrix composites with carbon nanotubes", *Ceram Int 38: (7)5669-5676 (2012), IF:1.751*
70. **Jiang Q**, Edwards MJ, Shields PA, Allsopp DWE, Bowen CR, Wang WN, Tóth L, Pécz B, Srnanek R, Satka A, Kovac J: „Growth of crack-free GaN epitaxial thin films on composite Si(111)/polycrystalline diamond substrates by MOVPE", *Phys Status Solidi C Curr T Solid State Phys 9: (3-4)650-653 (2012)*
71. **Juhász R**, Ódor G, Castellano C, Munoz MA: „Rare-region effects in the contact process on networks", *Phys Rev E Stat Nonlin 85: (6) 066125 (2012), IF:2.255*
72. **Juhász R**, Ódor G: „Anomalous coarsening in disordered exclusion processes", J Stat Mech-Theor E 2012: (8) P08004 (2012), IF:1.727

73. **Juhász Z**: „A mathematical study of note association paradigms in different folk music cultures", *J Math Music 6: (3)169-185 (2012), IF:0.190*

74. **Juhász Z**: „Őstípusok, népzenei nyelvek elemzése egy öntanuló modell segítségével", In: *Szalay O (Ed.), Tükröződések. Ünnepi tanulmánykötet Domokos Mária népzenekutató-zenetörténész tiszteletére, Budapest: L'Harmattan, 2012. pp.21-56. (ISBN:978 963 236 629 6)*

75. **Juhász Z**: „Topograhic study of folk music using artificial intelligences", *Symmetry-Art and Science 1-2: 64-67 (2012)*

76. **Kárpáti T**, Pap AE, Ádám M, Ferencz J, Fürjes P, Battistig G, Bársony I: „Electrostatic force detection during anodic wafer bonding", *Proceedings of IEEE Sensors, art. no. 6411331 (2012)*

77. **Károly Z**, Mohai I, Klébert Sz, Balázsi Cs, Szépvölgyi J: „SiC és Si_3N_4 bevonatok kialakítása plazma szórással", *Bányászati Kohászati Lapok: Bányászat 145: (2)26 (2012)*

78. **Kee YY**, Tan SS, Yong TK, Nee CH, Yap SS, Tou TY, Sáfrán G, Horváth ZE, Moscatello JP, Yap YK: „Low-temperature synthesis of indium tin oxide nanowires as the transparent electrodes for organic light emitting devices", *Nanotechnology 23:(2) Paper 025706 (2012), IF:3.979*

79. **Kelling J**, Ódor G, Nagy MF, Schulz H, Heinig KH: „Comparison of different parallel implementations of the 2+1-dimensional KPZ model and the 3-dimensional KMC model", *Eur Phys J-Spec Top 210: (1)175-187 (2012), IF:1.562*

80. **Kertész K**, Koós AA, Murdock AT, Vértesy Z, Nemes-Incze P, Szabó PJ, Horváth ZE, Tapasztó L, Hwang C, Grobert N, Biró LP: „Polarized light microscopy of chemical-vapor-deposition-grown graphene on copper", *Appl Phys Lett 100:(21) Paper 213103 (2012), IF:3.844*

81. **Khanh NQ**, Serényi M, Csik A, Frigeri C: „Determination of hydrogen concentration in a-Si and a-Ge layers by elastic recoil detection analysis", *Vacuum 86: (6)711-713 (2012), IF:1.317*

82. **Khanh NQ**, Lukács I, Sáfrán G, Erdélyi R, Fülöp E, Deák A, Volk J: „Effect of nanosphere monolayer on the morphology of ZnO nanowires grown by hydrothermal method", *Mater Lett 79: 242-244 (2012), IF:2.307*

83. **Kirchner SR**, Ohlinger A, Pfeiffer T, Urbán AS, Stefani FD, Deák A, Lutich AA, Feldmann J: „Membrane composition of jetted lipid vesicles: a Raman spectroscopy study", *J Biophotonics 5: 40-46 (2012), IF:4.343*

84. **Klein A**, Tóth B, Jankovics H, Muskotal A, Vonderviszt F: „A polymerizable GFP variant", *Protein Eng Des Sel 25: (4)153-157 (2012), IF:2.937*

85. **Koós AA**, Nicholls RJ, Dillon F, Kertész K, Biró LP, Crossley A, Grobert N: „Tailoring gas sensing properties of multi-walled carbon nanotubes by in situ modification with Si, P, and N", *Carbon 50: (8)2816-2823 (2012), IF:5.378*

86. **Körösi L**, Papp S, Beke S, Pécz B, Horváth R, Petrik P, Agócs E, Dékány I: „Highly transparent ITO thin films on photosensitive glass: sol-gel synthesis, structure, morphology and optical properties", *Appl Phys A-Mater 1: (1)1-8 (2012), IF:1.630*

87. **Kőrösi L**, Papp S, Hornok V, Oszkó A, Petrik P, Patkó D, Horváth R, Dékány I: „Titanate nanotube thin films with enhanced thermal stability and high-transparency prepared from additive-free sols", *J Solid State Chem 192: 342-350 (2012), IF:2.159*

88. **Kovács-Kis V**, Bajnóczi B: „Cassiterite in Tin Glaze of Anabaptist Faience from Hungary: Morphological and Crystallographic Characterization by SEM and TEM", In: *Braekmans D, Honings J, Degryse P (Eds.), 39th International Symposium on Archaeometry, Belgie: &, 2012. pp.385-386. Paper V61., (ISBN:978-94-6165-043-6)*

89. **Kovalcíková A**, Balázsi Cs, Dusza J, Tapasztó O: „Mechanical properties and electrical conductivity in a carbon nanotube reinforced silicon nitride composite", *Ceram Int 38: (1)527-533 (2012), IF:1.751*

90. **Krupa I**, Cecen V, Boudenne A, Krizanová Z, Vávra I, Srnánek R, Radnóczi Gy: „Mechanical Properties and Morphology of Composites Based on the EVA Copolymer Filled with Expanded Graphite", *Polym-Plast Technol 51: (13)1388-1393 (2012), IF:1.279*

91. **Kulinyi S**, Végvári R, Pongrácz A, Nagy A, Kárpáti T, Ádám M, Battistig G, Bársony I: „Flexible packaging for tyre integrated shear force sensor", *Proceedings of IEEE Sensors, art. no. 6411326 (2012)*

92. **Kun P**, Tapasztó O, Wéber F, Balázsi Cs: „Determination of structural and mechanical properties of multilayer graphene added silicon nitride-based composites", *Ceram Int 38: (1)211-216 (2012), IF:1.751*

93. **Kurunczi S**, Hainard A, Juhász K, Patkó D, Orgován N, Truck N, Sanchez JC, Horváth R: „Polyethylene imine-based receptor immobilization for label free bioassays", *Sensor Actuat B Chem 1: (1)1-10 (2012), IF:3.898*

94. **Kvetková L**, Duszová A, Hvizdos P, Dusza J, Kun P, Balázsi Cs: „Fracture toughness and toughening mechanisms in graphene platelet reinforced Si3N4 composites", *Scripta Mater 66: (10)793-796 (2012), IF:2.699*

95. **Lábár JL**, Adamik M, Barna BP, Czigány Zs, Fogarassy Zs, Horváth ZE, Geszti O, Misjak F, Morgiel J, Radnóczi Gy, Sáfrán G, Székely L, Szűcs T: „Electron Diffraction Based Analysis of Phase Fractions and Texture in Nanocrystalline Thin Films, Part III: Application Examples", *Microsc Microanal 18: (2)406-420 (2012), IF:3.007*

96. **Lábár JL**, Kiss AK, Christiansen S, Falk F: „Characterization of Grain Boundary Geometry in the TEM, exemplified in Si thin films", *Solid State Phenom 186: 7-12 (2012)*

97. **Lábár JL**, Walker CT, Brisset F, Dugne O and Robaut F (Eds.): „IOP Conference Series: Materials Science and Engineering 32", *(2012) (ISSN 1757-8981)*

98. **Lee SW**, Kim SG, Balázsi Cs, Chae WS, Lee HO: „Comparative study of hydroxyapatite from eggshells and synthetic hydroxyapatite for bone regeneration", *Oral Surg Oral Med O 113: (3)348-355 (2012), IF:1.457*

99. **Lugomer S**, Maksimovic A, Farkas B, Geretovszky Z, Szörényi T, Tóth AL, Zolnai Zs, Bársony I: „Multipulse irradiation of silicon by femtosecond laser pulses: Variation of surface morphology", *Appl Surf Sci 258: (8)3589-3597 (2012), IF:2.103*

100. **Lugomer S**, Zolnai Zs, Tóth AL, Bársony I, Maksimovic A, Nagy N: „Reorganization of Langmuir-Blodgett layers of silica nanoparticles induced by the low energy, high fluence ion irradiation", *Thin Solid Films 520: (11)4046-4056 (2012), IF:1.890*

101. **Márk GI**, Vancsó P, Hwang C, Lambin P, Biró LP: „Anisotropic dynamics of charge carriers in graphene", *Phys Rev B Condens Matter Mater Phys 85:(12) Paper 125443 (2012), IF:3.691*

102. **Márk GI**, Vancsó P, Lambin P, Chanyong H, Biró LP: „Forming electronic waveguides from graphene grain boundaries", *J Nanophotonics 6: 061718-1-061718-6 (2012), IF:1.570*
103. **Marton G**, Fekete Z, Bakos I, Battistig G, Pongrácz A, Baracskay P, Juhász G, Bársony I: „Deep-brain silicon multielectrodes with surface-modified Pt recording sites", *Proceedings of IEEE Sensors, art. no. 6411325 (2012)*
104. **Medvegy M**, Simonyi G, Szűcs E, Szakolczai K, Bauernfeind T, Duray G, Preda I: „Body surface mapping with nitroglycerine administration in the localization of the coronary artery lesion", *Circulation 125: (19)E857-E858 (2012)*
105. **Menyhárd M**, Daróczi CsS (Eds.): „MTA MFA Yearbook 2011", *MTA MFA, Budapest, Hungary (2012)*
106. **Mező G**, Enyedi K, Szabó I, Hegedues R, Mihala N, Majer Z, Czajlik A, Lajkó E, Kohidai L, Orgován N, Horváth R, Perczel A: „Chemical stability and structure - activity relationship studies of novel cyclic NGR peptides", *J Pept Sci 18: (1)S178-S179 (2012)*
107. **Misják F**, Czigány Zs, Kovács A, Radnóczi Gy: „Nanostructure of sputtered Cu-Mn alloy films", In: *Proceedings of 15th European Microscopy CongressManchester: 2012. pp.*
108. **Molnár D**, Pongrácz A, Ádám M, Hajnal Z, Timárné V, Battistig G: „Sensitivity tuning of A 3-axial piezoresistive force sensor", *Microelectron Eng 90: 40-43 (2012), IF:1.557*
109. **Molnár Gy**, Dózsa L, Vértesy Z, Baji Zs, Pető G: „Thickness and annealing dependent morphology changes of iron silicide nanostructures on Si(001)", *Phys Status Solidi C Conf Crit Rev 9: (6)1366-1369 (2012)*
110. **Molnár KZ**, Horváth ZsJ: „Simulation of MNOS memory hysteresis - Effect of layer thicknesses", In: *Szakál A (Ed.), Proceedings of the 7th IEEE International Symposium on Applied Computational Intelligence and Informatics (SACI), 2012., New York: IEEE, 2012. pp.365-369. (ISBN:978-1-4673-1012-3 (pendrive); 978-1-4673-1011-6 (printed))*
111. **Monier G**, Bideux L, Robert-Goumet C, Gruzza B, Petit M, Lábár JL, Menyhárd M: „Passivation of GaAs(001) surface by the growth of high quality c-GaN ultra-thin film using low power glow discharge nitrogen plasma source", *Surf Sci 606: (13-14)1093-1099 (2012), IF:1.994*
112. **Murata K**, Neumann PL, Koyano T, Yasutake Y, Nittoh K, Sakamoto K, Fukatsu S, Miki K: „Characterization of Highly Concentrated Bi Donors Wire-d-Doped in Si", *Jpn J Appl Phys 51: (11PE05)1-4 (2012), IF:1.058*
113. **Nagy N**, Zolnai Zs, Deák A, Fried M, Bársony I: „Various nanostructures on macroscopically large areas prepared by tunable ion-swelling", *J Nanosci Nanotechno 12: (8)6712-6717 (2012), IF:1.563*
114. **Nagy N**, Zolnai Zs, Fülöp E, Deák A, Bársony I: „Tunable Ion-swelling for Nanopatterning of Macroscopic Surfaces: The Role of Proximity Effects", *Appl Surf Sci 259: 331-337 (2012), IF:2.103*
115. **Nemcsics Á**, Nagy Sz: „Plausible quantum-mechanical interpretaions of RHEED oscillation", *Vacuum 86: (6)620-622 (2012), IF:1.317*
116. **Nemcsics Á**, Stemmann A, Takács J: „To the understanding of the formation of the III-V based droplet epitaxial nanorings", *Microelectron Reliab 52: (2)430-433 (2012), IF:1.167*

117. **Németh A**, Attygalle D, Dahal LR, Aryal P, Huang Z, Salupo C, Petrik P, Juhász Gy, Major Cs, Polgár O, Fried M, Pécz B, Collins RW: „Wide-spectral-range, Expanded-beam Spectroscopic Ellipsometer and its Application for Imaging/Mapping of Graded Nanocrystalline Si:H Films", In: *B Yan, S Higashi, C C Tsai, Q Wang, H Gleskova (Eds.). MRS Spring Meeting and Exhibit., Cambridge: Materials Research Society, 2012. pp.267-272.*
118. **Neumann PL**, Horváth ZE, Nemes-Incze P, Molnár Gy, Vértesy G, Biró LP: „Electrical behavior of indium contacted graphene flakes", *Nanopages 7: (1)9-16 (2012)*
119. **Neumann P**L, Tóvári E, Csonka S, Kamarás K, Horváth ZE, Biró LP: „Large scale nanopatterning of graphene", *Nucl Instrum Meth B 282: 130-133 (2012), IF:1.211*
120. **Ódor G**, Liedke B, Heinig KH, Kelling J: „Ripples and dots generated by lattice gases", *Appl Surf Sci 258 (2012) 4186*
121. **Ódor G**, Pastor-Satorras R: „Slow dynamics and rare-region effects in the contact process on weighted tree networks", *Phys Rev E Stat Nonlin 86: 026117 (2012), IF:2.255*
122. **Ódor G**: „Understanding Surface Patterning By Lattice Gas Models", In: *Tapobrata Som, Dinakar Kanjilal (Eds.), Nanofabrication by Ion-Beam Sputtering - Fundamentals and Applications, Singapore: PAN, 2012. pp.259-297. (ISBN:9789814303750)*
123. **Oh S**, Nagata T, Volk J, Wakayama Y: „Nanoimprint for Fabrication of Highly Ordered Epitaxial ZnO Nanorods on Transparent Conductive Oxide Films", *Appl Phys Express 5: 095003-1-095003-3 (2012), IF:3.013*
124. **Ohlinger A**, Deák A, Lutich AA, Feldmann J: „Optically Trapped Gold Nanoparticle Enables Listening at the Microscale", *Phys Rev Lett 108: (1) (2012), IF:7.370*
125. **Pamjav H**, Juhász Z, Zalán A, Németh E, Damdin B: „A comparative phylogenetic study of genetics and folk music", *Mol Genet Genomics 287: (4)337-349 (2012), IF:2.635*
126. **Patkó D**, Cottier K, Hámori A, Horváth R: „Single beam grating coupled interferometry: high resolution miniaturized label-free sensor for plate based parallel screening", *Opt Express 20: (21)23162-23173 (2012), IF:3.587*
127. **Perc M**, Szolnoki A: „Self-organization of punishment in structured populations", *New J Phys 14: (2012) 043013, IF:4.177*
128. **Pető G**, Paszternák A, Daróczi CsS: "The valence band photoemission spectra of the nanoparticle and the bulk like silver", *MAX-lab Activity Report 2011, National Laboratory, Lund, Sweden (2012)*
129. **Petrik P**, Egger H, Eiden S, Agócs E, Fried M, Pécz B, Kolari K, Aalto T, Horváth R, Giannone D: „Ellipsometric characterization of thin nanocomposite films with tunable refractive index for biochemical sensors", In: *X Chen, M Graetzel, C Li, P D Cozzoli (Eds.), MRS Spring Meeting and Exhibit., Cambridge: Materials Research Society, 2012. pp.81-87*
130. **Petrik P**: „Characterization of Nanocrystals Using Spectroscopic Ellipsometry", In: *Sudheer Neralla, Sudheer Neralla (Eds.), Nanocrystals - Synthesis, Characterization and Applications, Rijeka: InTech, 2012. pp. 29-40 (ISBN:978-953-51-0714-9)*
131. **Petrik P**: „Optical thin film metrology for optoelectronics", *J Phys Conf Ser 398: (1)012002 (2012)*

132. **Polgári M**, Hein JR, Tóth AL, Pál-Molnár E, Vigh T, Bíró L, Fintor K: „Microbial action formed Jurassic Mn-carbonate ore deposit in only a few hundred years (Úrkút, Hungary)", *Geology 40: (10)903-906 (2012), IF:3.612*

133. **Polgári M**, Hein JR, Vigh T, Szabó-Drubina M, Fórizs I, Bíró L, Müller A, Tóth L: „Microbial processes and the origin of the Úrkút manganese deposit, Hungary", *Ore Geol Rev 47: 87-109 (2012), IF:2.159*

134. **Pongrácz A**, Fekete Z, Marton G, Fiáth R, Fürjes P, Ulbert I, Battistig G: „Deep-brain silicon multielectrodes for simultaneous neural recording and drug delivery", *Procedia Engineering 47: 281-284 (2012)*

135. **Rácz M**, Makai J, Serényi M, Hámori A, Hidasi J, Bársony I: „Mérési elrendezés és eljárás folyadékfelszínen úszó szennyeződések kimutatására, elsősorban vízügyi mérőkutakhoz", *Registration Num.: 227 761, P0900115, 2008/2012, Hungary*

136. **Ryc L**, Calcagno L, Dubecky F, Margarone D, Nowak T, Parys P, Pfeifer M, Riesz F, Torrisi L: „Application of single-crystal CVD diamond and SiC detectors for diagnostics of ion emission from laser plasmas", In: *Hascík S, Osvald J (Eds.), ASDAM 2012, The Ninth International Conference on Advanced Semiconductor Devices and Microsystems, Piscataway: IEEE, 2012. pp.255-258. (ISBN:978-1-4673-1195-3)*

137. **Saftics A**, Agócs E, Fodor B, Patkó D, Petrik P, Kolari K, Aalto T, Fürjes P, Horváth R, Kurunczi S: „Investigation of thin polymer layers for biosensor applications", *Appl Surf Sci 1: (1)1-10 (2012), IF:2.103*

138. **Schmidt S**, Czigány Zs, Greczynski G, Hultman L: „Ion Mass Spectrometry Investigations of the Discharge during Reactive High Power Pulsed and Direct Current Magnetron Sputtering of Carbon in Ar and Ar/N2", *J Appl Phys 112: (1) (2012), IF:2.168*

139. **Schronk E**, Daróczi CsS: "Kísérletek nanovastagságú hártyakondenzátorokkal", *Fizikai szemle LXII(62): (5)164-169 ISSN:0015325-7 (2012)*

140. **Sipos P**, Kovács-Kis V, Márton E, Németh T, May Z, Szalai Z: „Lead and Zinc in the suspended particualte matter and settled dust in Budapest, Hungary", *Eur Chem Bull 1: (11)449-454 (2012)*

141. **Sulyok A**, Menyhárd M, Malherbe JB: „In-depth distribution of ion beam damage in SiC", *Vacuum 86: (6)761-764 (2012), IF:1.317*

142. **Szabó G**y, Szolnoki A: „Selfishness, fraternity, and other-regarding preference in spatial evolutionary games", *J Theor Biol 299: 81-87 (2012), IF:2.208*

143. **Szabó Gy**: „Az együttműködés természete", *Magyar Tudomány 2012: (6)642-652 (2012)*

144. **Szentpáli B**, Matyi G, Fürjes P, László E, Battistig G, Bársony I, Károlyi G, Berceli T: „Thermopile-Based THz Antenna", *Microsyst Technol 18: (7)849-856 (2012), IF:0.931*

145. **Szentpáli B**: „Noise limitations of miniature thermistors and bolometers", In: *Unil Perera (Eds.) Bolometers, Rijeka: InTech, 2012. pp.53-76. (ISBN:978-953-51-0235-9)*

146. **Szilágyi IM**, Fórizs B, Rosseler O, Szegedi A, Németh P, Király P, Tárkányi G, Vajna B, Varga-Josepovits K, László K, Tóth AL, Baranyai P, Leskela M: „WO_3 photocatalysts: Influence of structure and composition", *J Catal 294: 119-127 (2012), IF:6.002*

147. **Szolnoki A**, Perc M, Szabó Gy: „Accuracy in strategy imitations promotes the evolution of fairness in the spatial ultimatum game", *Europhys Lett 100: (2) (2012) 28005, IF:2.171*

148. **Szolnoki A**, Perc M, Szabó Gy: „Defense Mechanisms of Empathetic Players in the Spatial Ultimatum Game", *Phys Rev Lett 109: (7) (2012) 078701, IF:7.370*

149. **Szolnoki A**, Perc M: „Conditional strategies and the evolution of cooperation in spatial public goods games", *Phys Rev E Stat Nonlin 85: (2) (2012) 026104, IF:2.255*

150. **Szolnoki A**, Perc M: „Evolutionary advantages of adaptive rewarding", *New J Phys 14: (2012) 093016, IF:4.177*

151. **Szolnoki A**, Wang Z, Perc M: „Wisdom of groups promotes cooperation in evolutionary social dilemmas", *Sci Rep 2: (2012) 576*

152. **Tamáska I**, Kertész K, Vértesy Z, Bálint Z, Kun A, Yen SH, Biró LP: „Color changes upon cooling of Lepidoptera scales containing photonic nanoarchitectures", In: *International Conference on Materials and Applications for Sensors and Transducers 2012. pp.*

153. **Tapasztó L**, Dumitrica T, Kim SJ, Nemes-Incze P, Hwang C, Biró LP: „Breakdown of Continuum Mechanics for Nanometre-Wavelength Rippling of Graphene", *Nat Phys 8: (10)739-742 (2012), IF:18.967*

154. **Tapasztó L**, Nemes-Incze P, Dobrik G, Yoo KJ, Hwang C, Biró LP: „Mapping the electronic properties of individual graphene grain boundaries", *Appl Phys Lett 100:(5) Paper 053114 (2012), IF:3.844*

155. **Tapasztó O**, Markó M, Balázsi Cs: „Distribution patterns of different carbon nanostructures in silicon nitride composites", *J Nanosci Nanotechno 12: (11)8775-8778 (2012), IF:1.563*

156. **Tikhonov AV**, Malin TV, Zhuravlev KS, Dobos L, Pécz B: „TEM study of defects in AlXGa1?XN layers with different polarity", *J Cryst Growth 338: (1)30-34 (2012), IF:1.726*

157. **Tomás I**, Kadlecová J, Vértesy G: „Measurement of Flat Samples With Rough Surfaces by Magnetic Adaptive Testing", *IEEE T Magn 48: (4)1441-1444 (2012), IF:1.363*

158. **Tomás I**, Vértesy G: „Magnetic Adaptive Testing", In: *Mohammad Omar (Eds.), Nondestructive Testing Methods and New Applications., Rijeka: InTech Open Access Publisher, 2012. pp.145-186. (ISBN:978-953-51-0108-6)*

159. **Tóvári E**, Neumann PL, Horváth ZE, Biró LP, S Csonka: „PhD Conference of the Doctoral School for Physics: organised by the Doctoral School of Physics of the Faculty of Natural Sciences Budapest University of Technology and Economics", *in the framework of TÁMOP-4.2.2/B-10/1-2010-0009, BME, 2012., (ISBN:978-963-313-065-0)*

160. **Tóvári E**, Neumann PL, Horváth ZE, Biró LP, S Csonka: „Transport properties of graphene-based nanocircuits", In: *Tóvári E, Neumann PL, Horváth ZE, Biró LP, S Csonka: PhD Conference of the Doctoral School for Physics: organised by the Doctoral School of Physics of the Faculty of Natural Sciences Budapest University of Technology and Economics, in the framework of TÁMOP-4.2.2/B-10/1-2010-0009., BME, 2012. pp.33-37. (ISBN:978-963-313-065-0)*

161. **Vancsó P**, Márk GI, Lambin P, Hwang C, Biró LP: „Time and energy dependent dynamics of the STM tip - graphene system", *Eur Phys J B 85:(4) Paper 142 (2012), IF:1.534*

162. **Vértesy G**, Tomás I, Gillemot F, Székely R: „Magnetic characterization of neutron irradiated reactor steel material", *J Electr Eng 63: (7s)66-70 (2012), IF:0.370*

163. **Vértesy G**, Tomás I, Uchimoto T, Takagi T: „Nondestructive investigation of wall thinning in layered ferromagnetic material by magnetic adaptive testing", *NDT&E INT 47: 51-55 (2012), IF:1.477*

164. **Vértesy G**, Tomás I, Uchimoto T, Takagi T: „Nondestructive investigation of wall thinning in doubled layer tube by Magnetic Adaptive Testing", *E-Journal of Advanced Maintenance, Vol. 4, No. 2. (2012) 96-104*

165. **Volk J**, Szabó Z, Erdélyi R, Khanh NQ: „Engineered ZnO nanowire arrays using different nanopatterning techniques", In: *Ferechteh H Teherani, David C Look, David J Rogers (Eds.), Oxide-Based Materials and Devices III., Bellingham: SPIE, 2012. pp.1-6. Paper 82631L. (Proceedings of SPIE - The International Society for Optical Engineering) 8263, (ISBN:9780819489067)*

166. **Vonderviszt F**: „A baktériumok flagelláris filamentumainak szerkezete és önszerveződése", *Magyar Tudomány 2012/9: 1064-1071 (2012)*

167. **Vukov J**, Santos FC, Pacheco JM: „Cognitive strategies take advantage of the cooperative potential of heterogeneous networks", *New J Phys 14: (2012), IF:4.177*

168. **Wang Z**, Szolnoki A, Perc M: „Evolution of public cooperation on interdependent networks: The impact of biased utility functions", *Europhys Lett 97: (4) (2012) 48001, IF:2.171*

169. **Wang Z**, Szolnoki A, Perc M: „If players are sparse social dilemmas are too: Importance of percolation for evolution of cooperation", *Sci Rep 2: (2012) 369*

170. **Wang Z**, Szolnoki A, Perc M: „Percolation threshold determines the optimal population density for public cooperation", *Phys Rev E Stat Nonlin 85: (3) (2012) 037101, IF:2.255*

171. **Yong TK**, Tan SS, Nee CH, Yap SS, Kee YY, Sáfrán G, Horváth ZE, Moscatello J, Yap YK, Tou TY: „Pulsed laser deposition of indium tin oxide nanowires in argon and helium", *Mater Lett 66: (1)280-281 (2012), IF:2.307*